Dissertation

CALCIUM REGULATION OF MITOCHONDRIAL BIOENERGETICS IN HEALTH AND DISEASE

submitted by

Zhanat KOSHENOV, MSc.

for the Academic Degree of
Doctor of Philosophy
(PhD)

at the
Medical University of Graz

Gottfried Schatz Research Center
Molecular Biology and Biochemistry

under the Supervision of
Univ.-Prof. Mag.pharm. Dr.rer.nat. Wolfgang Graier

2022

Statutory Declaration

I hereby declare that this thesis is my own original work and that I have fully acknowledged by name all of those individuals and organizations that have contributed to the research for this thesis. Due acknowledgement has been made in the text to all other material used. Throughout this thesis and in all related publications I followed the “Guidelines of the Medical University of Graz on Good Scientific Practice”.

Graz, August 12th, 2022 Zhanat Koshenov

Disclosures

Following publications are based on and are part of this dissertation:

Koshenov Z, Oflaz F.E., Hirtl M, Gottschalk B, Rost R, Malli R, Graier WF. Citrin mediated metabolic rewiring in response to altered basal subcellular Ca2+ homeostasis. Communications Biology. 2022; DOI: 10.1038/s42003-022-03019-2

Koshenov, Z., Oflaz, FE., Hirtl, M., Pilic, J., Bachkoenig, OA., Gottschalk, B., Madreiter-Sokolowski, CT., Rost, R., Malli, R., Graier, WF. 2021 Sigma-1 Receptor Promotes Mitochondrial Bioenergetics by Orchestrating ER Ca2+ Leak during Early ER Stress. Metabolites. 11, 422. https://doi.org/10.3390/metabo11070422

Koshenov, Z., Oflaz, FE., Hirtl, M., Bachkoenig, OA., Rost, R., Osibow, K., Gottschalk, B., Madreiter-Sokolowski, CT., Waldeck-Weiermair, M., Malli, R., Graier, WF. 2020. The contribution of uncoupling protein 2 to mitochondrial Ca2+ homeostasis in health and disease - A short revisit. Mitochondrion. 55, 164-173 https://doi: 10.1016/j.mito.2020.10.003

I was responsible for writing of the first drafts, incorporation of suggestions and corrections from co-authors, and preparation of the final manuscripts. Individual contributions of co-authors are specified in respective papers.

The following co-authors contributed to my first-author publications:

Furkan E. Oflaz[1], Martin Hirtl[1], Olaf A. Bachkoenig[1], Benjamin Gottschalk[1], Rene Rost[1], Corina T. Madreiter-Sokolowski[1], Johannes Pilic[1], Karin Osibow[2], Markus Waldeck-Weiermair[1], Roland Malli[1,3], Wolfgang F. Graier[1,3].

[1] Gottfried Schatz Research Center, Division of Molecular Biology and Biochemistry, Medical University of Graz, Neue Stiftingtalstraße 6/6, 8010 Graz, Austria

[2] Diagnostic and Research Institute of Pathology, Medical University of Graz, Neue Stiftingtalstrasse 6/5, 8010 Graz, Austria

[3] BioTechMed Graz, Mozartgasse 12/II, 8010 Graz, Austria

I confirm that all co-authors have agreed to the use of their data in my dissertation. I have permission from the publishers to reproduce the publications Koshenov et al. 2020, Koshenov et al. 2021, and Koshenov et al. 2022 in toto. All three papers are distributed under the terms of the Creative

During my PhD thesis I also contributed to the following publications:

Gottschalk B, Koshenov Z, Bachkoenig OA, Rost R, Malli R and Graier WF (2022), MFN2 mediates ER-mitochondrial coupling during ER stress through specialized stable contact sites. Front. Cell Dev. Biol. 10:918691. doi: 10.3389/fcell.2022.918691

Gottschalk, B., Koshenov, Z., Waldeck-Weiermair, M., Radulović, S., Oflaz, F.E., Hirtl, M., Bachkoenig, O.A., Leitinger, G., Malli, R. & Graier, W.F. MICU1 controls spatial membrane potential gradients and guides Ca2+ fluxes within mitochondrial substructures. Commun Biol 5, 649 (2022). https://doi.org/10.1038/s42003-022-03606-3

Oflaz, F.E.; Koshenov, Z.; Hirtl, M.; Rost, R.; Malli, R.; Graier, W.F. Sigma-1 Receptor Modulation by Ligands Coordinates Cancer Cell Energy Metabolism. Biomolecules 2022, 12, 762. https://doi.org/10.3390/biom12060762 (shared first authorship)

Joshi, L.; Plastira, I.; Bernhart, E.; Reicher, H.; Koshenov, Z.; Graier, W.F.; Vujic, N.; Kratky, D.; Rivera, R.; Chun, J.; Sattler, W. Lysophosphatidic Acid Receptor 5 (LPA5) Knockout Ameliorates the Neuroinflammatory Response In Vivo and Modifies the Inflammatory and Metabolic Landscape of Primary Microglia In Vitro. Cells 2022, 11, 1071. https://doi.org/10.3390/cells11071071

Oflaz, FE., Koshenov, Z., Hirtl, M., Rost, R., Bachkoenig, OA., Gottschalk, B., Madreiter-Sokolowski, CT., Malli, R., Graier, WF. 2021. Near UV light Induced ROS Production Initiates Spatial Ca2+ Spiking to Fire NFATc3 Translocation. In J Mol Sci 22, 8189. https://doi.org/10.3390/ijms22158189

Joshi, L., Plastira, I., Bernhart, E., Reicher, H., Koyani, CN., Madl, T., Madreiter-Sokolowski, CT., Koshenov, Z., Graier, WF., Hallström, S., Sattler, W. 2021. Lysophosphatidic Acid Induces Aerobic Glycolysis, Lipogenesis, and Increased Amino Acid Uptake in BV-2 Microglia. Int J Mol Sci. 22, 1968. https://doi.org/10.3390/ijms22041968

Madreiter-Sokolowski, CT., Ramadani-Muja, J., Ziomek, G., Burgstaller, S., Bischof, H., Koshenov, Z., Gottschalk, B., Malli, R., Graier, WF.,2019. Tracking intra- and inter-organelle signaling of mitochondria. FEBS J. 286, 4378-4401. https://doi.org/10.1111/febs.15103

Zutterling C, Mursalimov A, Talhaoui I, Koshenov Z, Akishev Z, Bissenbaev AK, Mazon G, Geacintov NE, Gasparutto D, Groisman R, Zharkov DO, Matkarimov BT, Saparbaev M. 2018. Aberrant repair initiated by the adenine-DNA glycosylase does not play a role in UV-induced mutagenesis in Escherichia coli. PeerJ 6:e6029 https://doi.org/10.7717/peerj.6029

Acknowledgements

As a PhD student, I received funding from the Austrian Science Fund (FWF) through Doctoral College Metabolic and Cardiovascular Disease (DK-MCD W1226 to Wolfgang F. Graier).

I would like to acknowledge all family, friends and colleagues who supported me along the way up until this point. This path would not have been possible without you.

My special thanks goes to my supervisor, Wolfgang Graier, for his undying scientific enthusiasm, mentorship, and the trust he put in me. In fast-paced scientific environment, Wolfgang taught me to question everything, to think outside the box, and to do solid work. I admire his willingness and patience to develop his students, to extensively discuss science, and, when necessary, to argue with his students, proving me wrong more often than I would like to admit. I hope to continue our joint scientific exploration and to make many more exciting discoveries.

I would like to thank my co-supervisor and thesis committee member, Roland Malli, for giving helpful advice and always being willing to assist. I also want to thank Rainer Schindl, my thesis committee member, for his valuable input on my work.

I would like to express my sincere appreciation and gratitude to my friends and colleagues from Graier & Malli group. You guys made the time in the lab pleasant and engaging. Thanks for lively scientific discussions and fun we have in the lab, especially around our lunch table. I thank Furkan for being perfect companion, and for our extensive chats on the second floor. I would like to thank Rene for being the soul of our group, I wish you to stay who you are and never change. I thank Benjamin for always offering his insights and being open for discussions. I thank Anna for her helpful advices and moral support. I thank all my past and present colleagues, you all had an impact on me and made my time in Graz colourful.

Finally, and most importantly, I want to thank my family for always being there for me, for giving me their unconditional love and support. I am grateful to my parents for my education, for their hard work and selflessness when it came to their children. I cannot thank you enough and am eternally indebted to you. I am thankful to Aigerim, my love and soulmate. Thank you for taking this journey with me, for believing in me, and for everything you have done for our family. This is as much your achievement as it is mine, since I cannot imagine having done it without you. I thank my kids for being my inspirations, for filling my life with joy and giving me strength to do the impossible.

Table of Contents

List of Abbreviations

ADP	Adenosine diphosphate
ATF6	Activating transcription factor 6
ATP	Adenosine triphosphate
CFP	Cyan fluorescent protein
cGPD	Cytosolic glycerol 3-phosphate dehydrogenases
DHAP	Dihydroxyacetone phosphate
EMRE	Essential MCU regulator
ER	Endoplasmic reticulum
ERAD	ER-associated degradation
ETC	Electron transport chain
FADH	Flavin adenine dinucleotide, reduced form
FRET	Förster resonance energy transfer
GRP75	Glucose-regulated protein 75
GRP78 (BiP)	Glucose-regulated protein 75 (binding immunoglobulin protein)
GSIS	Glucose stimulated insulin secretion
GTP	Guanosine triphosphate
IBM	Inner boundary membrane
IMM	Inner mitochondrial membrane
IMS	Intermembrane space
IP_3R	Inositol-3-phosphate receptors
IRE1	Inositol requiring enzyme 1
kDa	Kilodalton
LDH	Lactate dehydrogenase
LETM1	Leucine zipper-EF-hand containing transmembrane protein 1
MAM	Mitochondria associated ER membrane
MAS	Malate-aspartate shuttle
MCU	Mitochondrial Ca^{2+} uniporter
MCUb	Mitochondrial Ca^{2+} uniporter, dominant negative form
MCUC	Mitochondrial Ca^{2+} uniporter complex

MCUR1	Mitochondrial Ca^{2+} Uniporter Regulator 1
mGPD	Mitochondrial glycerol 3-phosphate dehydrogenases
MICU 1-3	Mitochondrial Ca^{2+} uptake 1-3
mPTP	Mitochondrial permeability transition pore
NAD^+	Nicotinamide adenine dinucleotide, oxidized form
NADH	Nicotinamide adenine dinucleotide, reduced form
NCLX	Na^+/Ca^{2+} exchanger
NOX1	NADPH Oxidase 1
OGC	Malate-α-ketoglutarate antiporter
OMM	Outer mitochondrial membrane
OXPHOS	Oxidative phosphorylation
PDH	Pyruvate dehydrogenase
PERK	Double-stranded RNA-dependent protein kinase (PRK)-like ER kinase
PM	Plasma membrane
PMCA	Plasma membrane Ca^{2+}-ATPase
PRMT1	Protein arginine N-methyltransferase 1
ROS	Reactive oxygen species
S1R	Sigma-1 receptor
SERCA	Sarco/endoplasmic reticulum Ca^{2+}-ATPase
SOCE	Store operated Ca^{2+} entry
STIM1	Stromal interaction molecule 1
UCP1-3	Uncoupling protein 1-3
UPR	Unfolded protein response
VDAC	Voltage-dependent anion channels
YFP	Yellow fluorescent protein

Abstract

Ca^{2+} is a versatile regulator of many cellular processes, including cellular and mitochondrial energy metabolism. To achieve precise control of metabolic processes, Ca^{2+} signalling events occur at specific locations and for certain duration. Main focus of the current dissertation is on differential spatial and temporal Ca^{2+} regulation of mitochondrial bioenergetics. Two main sites important for Ca^{2+} regulation of mitochondrial energy metabolism are mitochondrial matrix and mitochondrial intermembrane space (IMS). Matrix Ca^{2+} regulation of mitochondrial bioenergetics occurs through Ca^{2+} sensitive dehydrogenases of citric acid cycle. Main control spots for activation of matrix dehydrogenases are endoplasmic reticulum (ER)-mitochondria contact cites, or mitochondria associated ER membranes (MAMs), where the Ca^{2+} transfer from ER to mitochondria occurs. Ca^{2+} uptake into the matrix occurs through mitochondrial Ca^{2+} uniporter, and is regulated by a complex mechanism involving several proteins, which form MCU complex (MCUC). Composition of MCUC is altered under different pathological states and during aging. In the former case, as well as in certain cancers, mitochondrial uncoupling protein 2 (UCP2) was shown to play a major role in the regulation of matrix Ca^{2+} uptake through MCU. The first publication of the cumulative dissertation reviews the involvement of UCP2 in mitochondrial Ca^{2+} uptake in health and disease. The second regulatory site of mitochondrial bioenergetics is the IMS, which hosts Ca^{2+} sensitive NADH shuttles, malate-aspartate shuttle (MAS) and glycerol-phosphate shuttle. Since MAS forms the main shuttle in mammalian cells, it was the focus of the second publication. Ca^{2+} ions activate MAS at lower concentrations than matrix dehydrogenases, in addition to the absence of Ca^{2+} uptake threshold into the IMS, thus MAS is crucial for basal mitochondrial bioenergetics. As a result of high sensitivity of the NADH shuttle, it can respond to slight alterations in subcellular Ca^{2+} levels by rewiring cellular and mitochondrial bioenergetics. It provides a fast and reliable way to pre-emptively respond to cellular stress. The final publication of the cumulative dissertation is on Ca^{2+} mediated regulation of mitochondrial bioenergetics during early ER stress that is orchestrated by sigma-1 receptor (S1R). In this work, we have demonstrated that S1R directs the ER Ca^{2+} leak generated during early phases of ER stress towards mitochondria, which boosts mitochondrial energy production. S1R also plays a role in timely diversion of the leak away from mitochondria as the ER stress progresses, preventing mitochondrial Ca^{2+} overload. Thus, current dissertation adds new insights in spatial and time-resolved Ca^{2+} regulation of mitochondrial energy metabolism in health and disease, identifies new pathways, and open new venues for future research.

Zusammenfassung

Ca^{2+} ist ein vielseitiger Regulator vieler zellulärer Prozesse, einschließlich des zellulären und mitochondrialen Energiestoffwechsels. Um eine präzise Steuerung von Stoffwechselprozessen zu erreichen, treten Ca^{2+} Signalisierungsereignisse an bestimmten Orten und für eine bestimmte Dauer auf. Der Schwerpunkt der aktuellen Dissertation liegt auf der differentiellen räumlichen und zeitlichen Ca^{2+}-Regulation der mitochondrialen Bioenergetik. Zwei Hauptstellen, die für die Ca^{2+}-Regulation des mitochondrialen Energiestoffwechsels wichtig sind, sind die mitochondriale Matrix und der mitochondriale Intermembranraum (IMS). Matrix Ca^{2+} Regulation der mitochondrialen Bioenergetik erfolgt durch Ca^{2+} sensitive Dehydrogenasen des Zitronensäurezyklus. Hauptkontrollpunkte für die Aktivierung von Matrixdehydrogenasen sind Kontaktstellen zwischen endoplasmatischem Retikulum (ER) und Mitochondrien oder Mitochondrien-assoziierte ER-Membranen (MAMs), wo der Ca^{2+}-Transfer vom ER zu den Mitochondrien stattfindet. Die Ca^{2+}-Aufnahme in die Matrix erfolgt durch mitochondrialen Ca^{2+}-Uniporter und wird durch einen komplexen Mechanismus reguliert, an dem mehrere Proteine beteiligt sind, die den MCU-Komplex (MCUC) bilden. Die Zusammensetzung von MCUC wird unter verschiedenen pathologischen Zuständen und während des Alterns verändert. Im ersteren Fall sowie bei bestimmten Krebsarten wurde gezeigt, dass das mitochondriale Entkopplungsprotein 2 (UCP2) eine wichtige Rolle bei der Regulierung der Ca^{2+}-Aufnahme der Matrix durch MCU spielt. Die erste Veröffentlichung der kumulativen Dissertation befasst sich mit der Beteiligung von UCP2 an der mitochondrialen Ca^{2+}-Aufnahme bei Gesundheit und Krankheit. Die zweite regulatorische Stelle der mitochondrialen Bioenergetik ist das IMS, das Ca^{2+}-sensitive NADH-Shuttles, Malat-Aspartat-Shuttle (MAS) und Glycerol-Phosphat-Shuttle beherbergt. Da MAS das Hauptshuttle in Säugerzellen bildet, stand es im Mittelpunkt der zweiten Veröffentlichung. Ca^{2+}-Ionen aktivieren MAS bei niedrigeren Konzentrationen als Matrixdehydrogenasen, zusätzlich zum Fehlen einer Ca^{2+}-Aufnahmeschwelle in das IMS, daher ist MAS entscheidend für die basale mitochondriale Bioenergetik. Als Ergebnis der hohen Empfindlichkeit des NADH-Shuttles kann es auf geringfügige Veränderungen des subzellulären Ca^{2+}-Spiegels reagieren, indem es die zelluläre und mitochondriale Bioenergetik neu verdrahtet. Es bietet eine schnelle und zuverlässige Möglichkeit, präventiv auf zellulären Stress zu reagieren. Die letzte Veröffentlichung der kumulativen Dissertation befasst sich mit der Ca^{2+}-vermittelten Regulation der mitochondrialen Bioenergetik während frühem ER-Stress, die durch den Sigma-1-Rezeptor (S1R) orchestriert wird. In dieser Arbeit haben wir gezeigt, dass S1R das ER- Ca^{2+}-Leck, das während früher Phasen von ER-Stress entsteht, in Richtung Mitochondrien lenkt, was die

mitochondriale Energieproduktion ankurbelt. S1R spielt auch eine Rolle bei der rechtzeitigen Umleitung des Lecks weg von den Mitochondrien, wenn der ER-Stress fortschreitet, wodurch eine mitochondriale Ca^{2+}-Überladung verhindert wird. Somit fügt die aktuelle Dissertation neue Einblicke in die räumlich und zeitaufgelöste Ca^{2+}-Regulierung des mitochondrialen Energiestoffwechsels bei Gesundheit und Krankheit hinzu, identifiziert neue Wege und eröffnet neue Möglichkeiten für zukünftige Forschung.

1 Introduction

1.1 Cellular Ca^{2+} homeostasis

Ca^{2+} ions are ubiquitous second messengers with plethora of specific functions necessary to sustain life, development, and when necessary, to execute programmed death of a cell[1]. One might wonder how a cell can achieve such specificity when it comes to regulation of so many vital processes by an ion that on its own is not so specific and has many effector and binding proteins. It does so by controlling space and time where Ca^{2+} ions act, thus limiting any unwanted side effects[1]. Cells employs different intracellular Ca^{2+} storage units that can sequester the ions and keep their concentration in the cytosol to a minimum. While the extracellular fluids contain plenty of Ca^{2+} (about 1-2 mM), the cytosolic Ca^{2+} concentration lies around 100 nM[2,3]. In case there is a need for Ca^{2+} signalling, a cell can deploy Ca^{2+} either from its internal stores, such as endoplasmic reticulum (ER) as main intracellular Ca^{2+} store, or from outside of a cell. Ca^{2+} mobilization events occur by specialized channel proteins located either on the membranes of intracellular Ca^{2+} stores or on the plasma membrane (PM), such as Inositol 1,4,5-trisphosphate receptors (IP_3R) on the ER membrane and Orai channels on the PM. These elevations in cellular Ca^{2+} level can be decoded by many different Ca^{2+} sensitive effector proteins and elicit cellular responses. For example calmodulin is one of these proteins, and contains four Ca^{2+} binding sites[4]. Upon Ca^{2+} binding, Ca^{2+} -calmodulin complex can activate numerous downstream proteins, including kinases, phosphatases, and transcription regulators, among others[4].

Once the signalling cascade has been activated and Ca^{2+} ions are elevated in the cytosol and/or other intracellular organelles, the resting Ca^{2+} levels need to be restored to avoid unnecessary secondary effects of prolonged Ca^{2+} elevation, which can trigger programmed cell death if left unchecked[5]. Restoration of basal Ca^{2+} levels is mainly achieved by re-sequestration into ER stores by sarco/endoplasmic reticulum Ca^{2+}-ATPase (SERCA) or extrusion into extracellular space by PM Ca^{2+}-ATPase (PMCA)[1]. The SERCA pump is the main Ca^{2+} pump that keeps high ER luminal Ca^{2+} concentration (100-500 uM) and maintains a steep gradient between ER and cytosol[6]. Both SERCA and PMCA consume high amount of ATP, which is predominantly supplied to them by mitochondria as main source for cellular ATP synthesis. In addition to SERCA and PMCA, cytosolic Ca^{2+} elevations can be cleared by Ca^{2+} uptake into intracellular organelles such as mitochondria[7].

1.2 Mitochondrial Ca^{2+} homeostasis

Mitochondria are able to sequester large quantities of Ca^{2+} and buffer cytosolic Ca^{2+} elevations[7]. Mitochondrial matrix is separated from the cytosol by two mitochondrial membranes, inner mitochondrial membrane (IMM), which restricts free ion movement, and a more permeable outer mitochondrial membrane (OMM). In order to reach the mitochondrial matrix, Ca^{2+} ions pass the OMM through voltage-dependent anion channels (VDACs) that form large oligomeric, high conductance channels permeable to ions and metabolites[8]. Once Ca^{2+} ions pass OMM, they enter the mitochondrial intermembrane space (IMS), a tight opening in between the two mitochondrial membranes. From there, they need to pass the IMM, which has proven to be a sophisticated process with intricate mechanisms and several layers of regulation[9]. One important point that needs to be considered is that the ion impermeable nature of the IMM is paramount for the mitochondrial well-being. Mitochondria are known to build a highly negative membrane potential across the IMM by pumping protons out of the matrix using the so-called respiratory complexes, thus creating an overall negative charge on the inner leaflet of the IMM. This negative membrane potential serves as a driving force for positively charged Ca^{2+} ion uptake into mitochondrial matrix. A more detailed explanation of the mitochondrial sub-structure and membrane potential generation will be addressed below.

The main route Ca^{2+} ions take on their way through the IMM is the mitochondrial Ca^{2+} uniporter complex (MCUC)[10,11]. Scientist have known of the existence of an mitochondrial uniporter for a long time, but the protein itself was only recently discovered[10,11]. Early studies with isolated mitochondria have shown that a high conductance Ca^{2+} uniporter exists, and that mitochondria can uptake Ca^{2+} ions through it as long as it can maintain negative membrane potential, up to the point of “rupture”, when mitochondria burst and release all of the Ca^{2+} ions that have been taken up[12,13]. This process is known as mitochondrial permeability transition and happens via the mitochondrial permeability transition pore (mPTP). Opening of the mPTP is triggered by mitochondrial Ca^{2+} overload and the assambly of multiple proteins forming the mPTP which is permeable to molecules smaller than 1.5 kDa[14]. This transition leads to loss of mitochondrial membrane potential and subsequent cell death, which is why mitochondrial Ca^{2+} uptake needs to be tightly regulated.

One of the two pore-forming proteins of the MCUC is MCU, a 35-kDa protein with two transmembrane α-helixes that span the IMM[11]. It is predicted that MCU forms higher oligomeric structures to form the pore, with tetrameric structure being more likely[11,15]. MCU assembles with further proteins to a large complex called MCU complex (MCUC) (Figure 1), which consists of pore

forming MCU, its dominant negative form MCUb[15], and essential MCU regulator (EMRE), the second pore-forming protein of the MCUC[16]. EMRE is attributed with bridging MCU to other regulatory proteins, namely to Mitochondrial Ca^{2+} Uptake (MICU) proteins[16]. Three MICU proteins have been described so far and all are said to exert additional regulation to mitochondrial Ca^{2+} uptake by setting a threshold for Ca^{2+} uptake[17–19]. MICU1 and MICU2 were shown to be main gatekeepers of MCU in most tissues[20,21], while MICU3 is shown to be exclusively expressed in neuronal tissues[19]. MICU proteins set a certain threshold for mitochondrial Ca^{2+} uptake, below which, MCU is in its closed state and doesn't conduct Ca^{2+} [20] (Figure 1). Different tissues express MCU, MICU1, and MICU2 at varying stoichiometry, allowing to fine-tune the mitochondrial Ca^{2+} uptake threshold[22]. For example, skeletal muscle cells have lower MICU1 to MCU ratio then heart muscle cells, thus mitochondria of skeletal muscle cells take up Ca^{2+} more easily, meaning the threshold for mitochondrial Ca^{2+} uptake is lower[22]. Further to its role as a gatekeeper in MCUC, MICU1 was described to be involved in organizing inner mitochondrial membrane structure and facilitating MCU shuttling from out of cristae membrane into inner boundary membrane (IBM) upon Ca^{2+} mobilization from the ER[23]. Additionally, it was demonstrated by our group that MICU1 is responsible for spatial regulation of mitochondrial membrane potential[24]. Another component of MCUC is the Mitochondrial Ca^{2+} Uniporter Regulator 1 (MCUR1) protein, which is described to serve as a scaffold for the complex and to play an important role in the functioning of the MCUC[25].

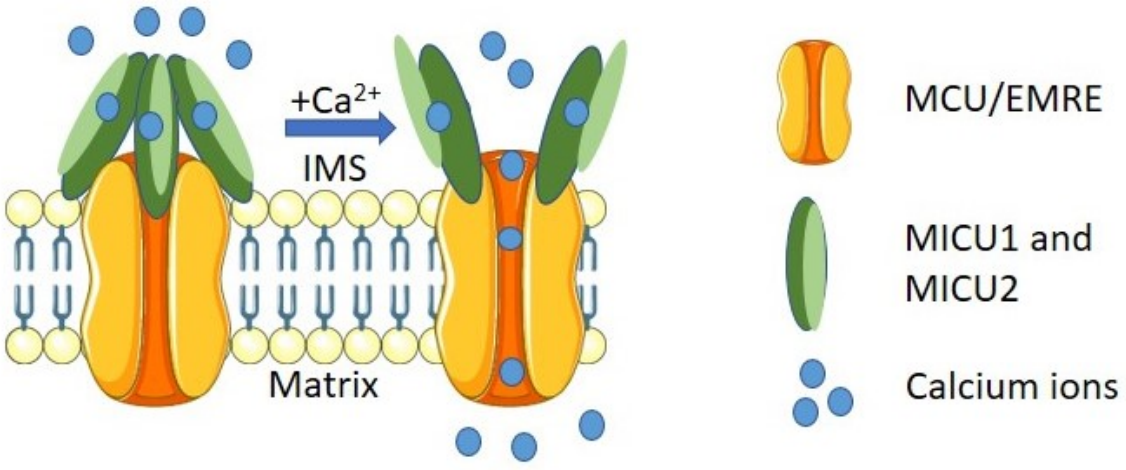

Figure 1. *Graphical illustration of the MCUC. MICU1 and MICU2 "guard" the MCU and set a Ca^{2+} uptake threshold; upon Ca^{2+} elevation in the IMS that reaches the threshold, MICU1 and MICU2 open*

and allow the Ca^{2+} ions to pass through MCU. For simplicity, other components of the MCUC were not included.

Since the mitochondrial Ca^{2+} uptake threshold set by MICU1 and MICU2 is high, sometimes reported to be in range of 2-5 uM, which is not reached in the cytosol of healthy cells, mitochondrial Ca^{2+} uptake mainly takes place at specialized contact sites between ER and mitochondria called Mitochondria Associated ER Membranes (MAMs)[26]. As ER contains 100-500 uM Ca^{2+}, ER Ca^{2+} release generates high enough Ca^{2+} concentration at MAMs that can reach the mitochondrial Ca^{2+} uptake threshold[26]. Thus, ER-mitochondria communication plays a vital role in regulation of mitochondrial fitness. In fact, many age related pathological conditions, including cancer and neurodegenerative diseases, are thought to be caused by alteration in the MAMs[27,28]. It is reported that patients with Alzheimer's disease, Parkinson's disease, and Amyotrophic Lateral Sclerosis have altered MAM structure and composition[29].

As mitochondria sequester large quantities of Ca^{2+}, it needs to balance it with an efficient extrusion mechanism. Mitochondrial Ca^{2+} extrusion is achieved through the $Na^+/(Li^+)/Ca^{2+}$ exchanger (NCLX)[30]. The stoichiometry of Ca^{2+} and Na^+ exchange by NCLX is a matter of debate, with 1:2 and 1:3 being proposed, meaning for every Ca^{2+} ion extruded, mitochondria take up two or three sodium ions, resulting in either electroneutral (in case of 1:2) or electrogenic (in case of 1:3) exchange[31]. These sodium ions in turn are extruded from the matrix by the means of sodium proton exchangers[32]. NCLX is of paramount importance for mitochondria, since matrix Ca^{2+} levels need to be kept at certain level to prevent mitochondrial Ca^{2+} overload and depolarization, a process that leads to cell death[33]. Hence, NCLX knock out (KO) animals do not survive[34], while MCU KO animal do, although only in unstressed state[35].

The latter can possibly be explained by the fact that besides MCUC, mitochondria can take up Ca^{2+} ions through other means. It was shown that leucine zipper-EF-hand containing transmembrane protein 1 (LETM1) can serve as an alternative Ca^{2+} uptake pathway[36,37]. Although it is still disputed weather LETM1 is a Ca^{2+}/H^+ or K^+/H^+ exchanger[38], it was definitively shown to be important for mitochondrial Ca^{2+} uptake of Ca^{2+} entering the cell via the store operated Ca^{2+} entry (SOCE)[37]. SOCE is characterized by cellular Ca^{2+} entry through the plasma membrane via Orai channels following ER Ca^{2+} store depletion[39]. Depletion of ER Ca^{2+} store is sensed by ER Ca^{2+} sensing protein stromal interaction molecule 1 (STIM1), which is recruited to the sub-PM region upon sensing low luminal Ca^{2+} level[40–42]. There, it recruits and activates Orai channels, which facilitate Ca^{2+} entry and refilling of

ER Ca^{2+} stores[40–42]. Some of the Ca^{2+} entering through these means can be taken up by mitochondria, but the amount of Ca^{2+} coming from this route is not as high as the one directly released from ER[7,43]. As such, Ca^{2+} concentration reaching mitochondrial during SOCE does not reach mitochondrial Ca^{2+} uptake threshold, thus does not enter mitochondrial matrix via the MCUC, but likely through other means. [37]In addition to described members of MCUC, our group has found yet another fundamental regulator of the complex, namely uncoupling protein 2 (UCP2)[44], which is indispensable for mitochondrial Ca^{2+} uptake in cancer cells and during aging[45,46]. My first publication reviews findings on UCP2 function in health and disease, and contrasts its function as a proton uncoupler versus a regulator of mitochondrial Ca^{2+} uptake[46].

1.3 The contribution of uncoupling protein 2 to mitochondrial Ca^{2+} homeostasis

Electrochemical gradient generated by the ETC is used to synthesize ATP on the IMM invaginations called cristae, a process called oxidative phosphorylation (OXPHOS)[47]. However, some part of the proton gradient is dissipated and not used to make ATP[48]. This is done, in part, to prevent hyperpolarization of the IMM, which can result in formation of reactive oxygen species (ROS)[49]. Additionally, uncoupling proteins 1 (UCP1) which represents app. 30 % of the protein mass in the brown adipose tissue, is responsible for heat generation by directly uncoupling of the proton gradient[50]. Unlike UCP1, it is appears unlikely that UCP2 and 3, which are expressed in far less amounts than UCP1, possess the same mechanism of action[51]. UCP2 was first described to be involved in mitochondrial Ca^{2+} uptake by Trenker et al. in 2007. Following years, many more publications established that UCP2 is indispensable for mitochondrial Ca^{2+} uptake, especially during aging and in cancer[45,46,52,53]. This is due to post-translational modification of MICU1, which gets asymmetrically methylated by protein arginine N-methyltransferase 1 (PRMT1)[45]. As a result of the methylation, mitochondrial Ca^{2+} uptake threshold set by MICU1 gets increased[45] (Figure 2). Madreiter-Sokolowski et al. 2016 has shown that UCP2 is able to directly interact with methylated MICU1 and lower the threshold needed for mitochondrial Ca^{2+} uptake. PRMT1 activity is known to be upregulated in certain cancers and during aging, which is mimicked by the involvement of UCP2 in mitochondrial Ca^{2+} uptake[54]. It is described that during aging, cells heavily rely on mitochondria for energy production, and in order to boost mitochondrial productivity, the communication between ER and mitochondria is increased[55]. This tight communication between the two organelles supplies mitochondria with Ca^{2+} from ER stores and in turn supplies ER with mitochondrially produced ATP. But a caveat of increased mitochondrial Ca^{2+} supply is a danger of Ca^{2+} overload, which is likely a

reason why cells have methylated MICU1 – to increase the mitochondrial Ca^{2+} uptake threshold. In this scenario, UPC2 serves as an additional layer of regulation, thus fine-tuning mitochondrial Ca^{2+} uptake during aging. Similar to aged cells, cancer cells too rely on mitochondrial bioenergetics, despite many reports showing increased glycolysis in cancer[3,56]. Healthy mitochondrial are paramount for cancer wellbeing, thus cancer cells have mechanisms to balance mitochondrial Ca^{2+} levels, like aged cells[57]. They, too have methylated MICU1-UCP2 interaction to control proper mitochondrial function[54].

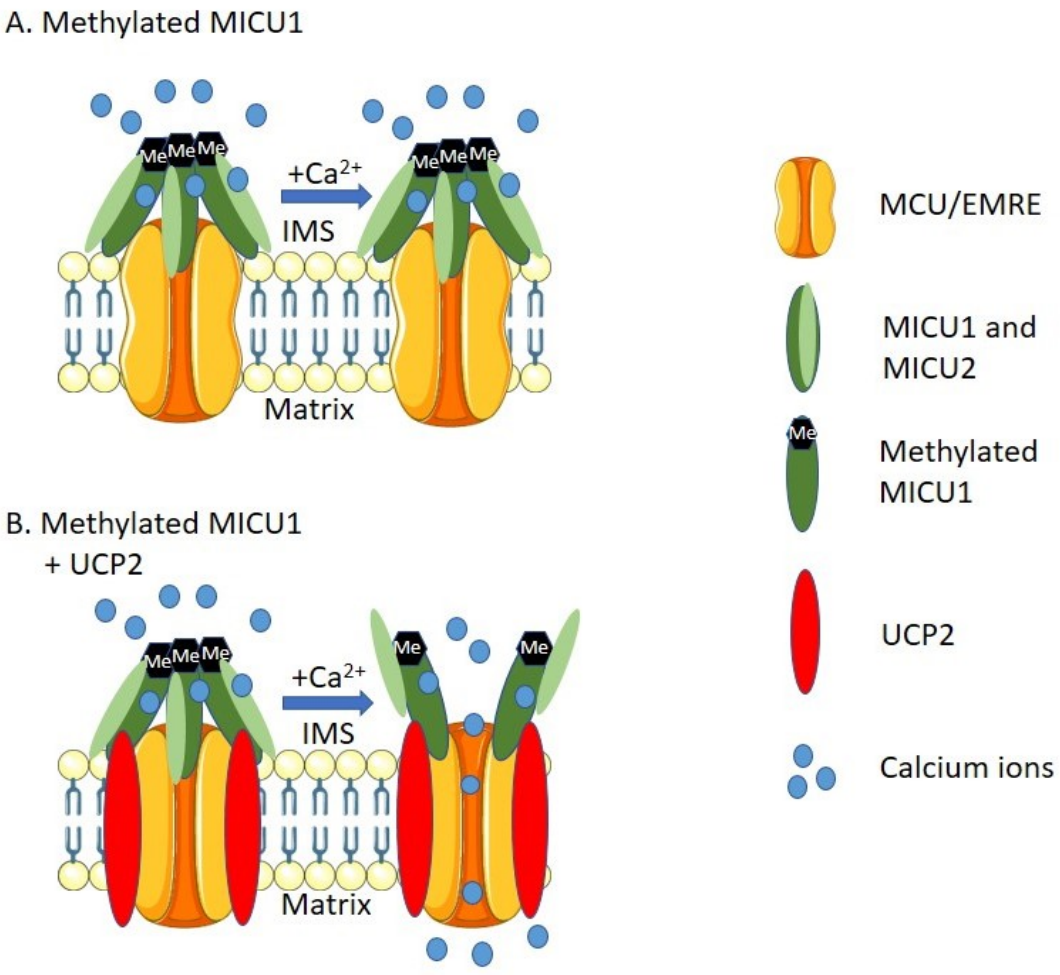

Figure 2. *Graphical representation of the effect of MICU1 methylation by PRMT1 on mitochondrial Ca^{2+} uptake. MICU1 methylation increases the MCU opening threshold, thus decreasing mitochondrial Ca^{2+} uptake. This threshold is normalized by UCP2, which interacts with methylated MICU1 and lowers the threshold.*

1.4 Matrix Ca^{2+} regulation of mitochondrial bioenergetics

Perhaps one of the reasons why cells have evolved so many regulatory mechanisms for mitochondrial Ca^{2+} homeostasis is because mitochondria critically depend on Ca^{2+} ions for their proper function and energy production[58]. Mitochondria are known as cellular powerhouses since majority of the cells rely on mitochondria to produce cellular energy bearing molecule – adenosine triphosphate (ATP). Cells use ATP to maintain their survival and function, which involves basically all processes of a living cell. Despite a general misconception that cancer cells mostly rely on aerobic glycolysis, cancer mitochondria are active and generates fair share of cellular ATP[59]. Besides, maintenance of mitochondrial membrane potential is a priority of most cancer cells[3], as collapse of mitochondrial membrane potential will activate apoptosis, thus cancer cells maintain a good balance between fast growth and mitochondrial well-being and have evolved several layers for regulation as seen in case of involvement of UCP2[60].

Mitochondrial matrix hosts crucial cellular metabolic pathways, including citric acid cycle, which is where most of the energy from nutrients is extracted[61]. After being taken up from extracellular space, glucose enters cytosolic glycolysis. During glycolysis, cells produce 2 molecules of ATP, 2 molecules of reduced nicotinamide adenine dinucleotide (NADH), and 2 molecules of pyruvate. After exiting glycolysis, pyruvate is transported into mitochondrial matrix, where it enters citric acid cycle. There, it undergoes series of enzymatic reactions to extract energy bearing molecules (GTP, ATP) and electron donors (NADH, FADH). The latter reaction is catalysed by mitochondrial dehydrogenases, two of which, isocitrate dehydrogenase and a-ketoglutarate dehydrogenase, are directly regulated by matrix Ca^{2+} concentration[62,63]. Additionally, pyruvate dehydrogenase (PDH) is indirectly regulated by Ca^{2+} ions through phosphorylation[64,65]. PDH kinase phosphorylates and inactivates PDH, while PDH phosphatase dephosphorylates it in a Ca^{2+} dependent manner, removing inhibitory phosphate group and activating the dehydrogenase[62,65]. Thus, matrix Ca^{2+} can regulate mitochondrial NADH generation. Subsequently, NADH molecules produced by the citric acid cycle donate their electrons to the electron transport chain (ETC). ETC is composed of large protein supercomplexes embedded in the mitochondrial inner membrane, particularly on specialized cristae membranes[66,67]. ETC consists of 4 complexes. Complex I is NADH:ubiquinone oxidoreductase and is a complex where NADH molecules donate their electrons, that are passed along the ETC onto molecular oxygen, forming water molecule in the end. FADH on the other hand donates its electron at complex II - succinate dehydrogenase. Electrons from complex II join the ones from complex I at complex III, cytochrome bc_1 complex, and go on to complex IV - cytochrome c oxidase, where the electrons get transferred to

molecular oxygen. Using the energy from electron transfer down the ETC, complexes I, III, and IV shuttle protons from the mitochondrial matrix into cristae lumen, creating a negative membrane potential and a proton gradient across the IMM, which is then used for ATP synthesis[47].

1.5 IMS Ca^{2+} regulation of cellular and mitochondrial bioenergetics

In addition to regulation of mitochondrial bioenergetics by matrix Ca^{2+} through the activation of mitochondrial dehydrogenases, Ca^{2+} ions can influence mitochondrial and cellular energy production from the mitochondrial intermembrane space (IMS)[3,68–70]. Mitochondrial IMS is a tightly packed space in between the two mitochondrial membranes, which houses many structural and functional proteins and protein complexes. Malate-aspartate shuttle (MAS) is one of these complexes that resides in the IMS. MAS is attributed with transferring NADH equivalents, in form of solute metabolites, in and out of mitochondria[71,72]. It is a major component of cytosolic NADH recycling machinery of mammalian cells[69]. MAS consists of two solute carrier antiports that shuttle metabolites in and out of mitochondrial matrix. Additionally, the antiporters are complemented by malate dehydrogenase and aspartate aminotransferase, both of which are present in the cytosol/IMS and in mitochondrial matrix[69]. First antiporter component of MAS is aralar1, or in case of non-excitable cells, citrin[73,74]. Aralar and citrin are glutamate and aspartate antiporters, which transport aspartate out of the mitochondria and glutamate in. Importantly, both carriers need Ca^{2+} ions for their activity[68]. Aralar has a half maximal activation at Ca^{2+} concentration of around 300 nM, while citrin's half maximal activation by Ca^{2+} is achieved at 100 nM[68,75]. Activation concentrations of the two proteins fit to the cell types they are expressed in. Aralar is the main MAS component in excitable cells that frequently have basal cytosolic Ca^{2+} oscillations that can translate to the IMS, reach the 300 nM range and keep aralar active. On the other hand, citrin is activated at lower Ca^{2+} levels and is expressed mainly in non-excitable cells that don't have spontaneous cytosolic Ca^{2+} oscillations. Aralar and citrin are complemented by the second antiporter of the MAS – malate- α-ketoglutarate antiporter (OGC), which transports malate into the matrix and α-ketoglutarate out of the matrix[76]. In contrast to aralar and citrin, malate- α-ketoglutarate antiporter is not Ca^{2+} sensitive. The metabolites transported by the solute carriers are interconverted and form two anti-parallel cycles. After leaving the mitochondrial matrix, aspartate and α-ketoglutarate are processed by aspartate aminotransferase, which transfers the amine group of aspartate to α-ketoglutarate, forming glutamate and oxaloacetate. Glutamate can be transferred back into the matrix via aralar/citrin, while oxaloacetate is oxidized by malate dehydrogenase in the IMS to form malate[77]. Malate is then transported into the

matrix against another molecule of α-ketoglutarate. The reverse reactions then happen in the matrix, with the same two enzymes present there as well. The schematic representation of the MAS is shown Figure 3.

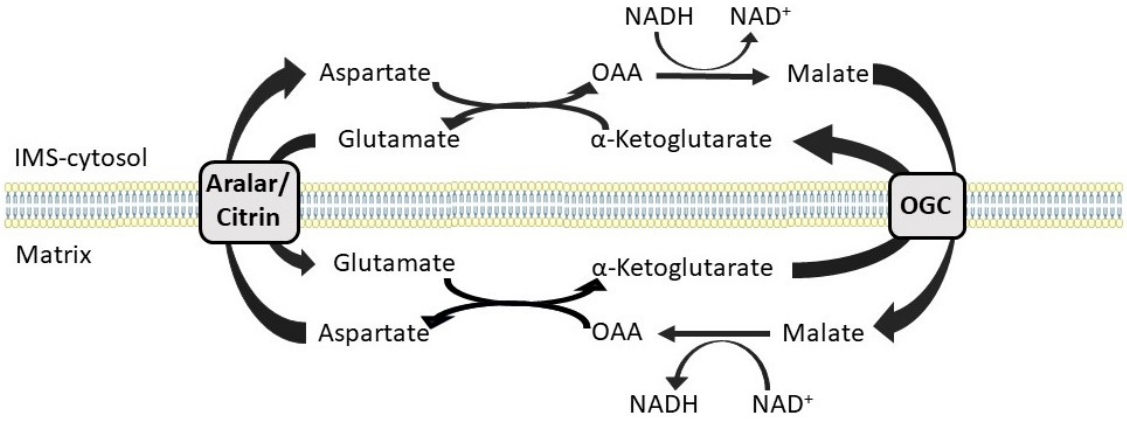

Figure 3. *Schematic representation of malate-aspartate shuttle. MAS connects cytosolic and mitochondrial energy pathways by interconverting and shuttling of substrates, in the process recycling NADH and transferring its equivalents from cytosol to mitochondria. OAA – oxaloacetate, OGC – malate- α-ketoglutarate antiporter. OAA to malate is catalysed by cytosolic MDH, while the reverse reaction is catalysed by mitochondrial MDH. Similarly, aspartate aminotransferase is present in both IMS/cytosol and matrix, where it interconverts aspartate, OAA, α-ketoglutarate and glutamate*

Glycerol phosphate shuttle is another Ca^{2+} sensitive NADH shuttle located at IMS of many cell types, but the contribution of glycerol phosphate shuttle to the transfer of NADH equivalents into mitochondria is far less than that of MAS in mammalian cells[78,79]. Glycerol phosphate shuttle consists of cytosolic and mitochondrial inner membrane residing glycerol 3-phosphate dehydrogenases, cGPD and mGPD, respectively (Figure 4). cGPD transfers electrons from NADH to dihydroxyacetone phosphate (DHAP), as a result forming glycerol-3-phosphate and recycling NADH back to NAD^+. In IMS, mGDP oxidizes glycerol-3-phosphate to regenerate DHAP and in the process forms $FADH_2$ molecule. mGPD can facilitate or directly be involved in transfer of electrons to coenzyme Q of the electron transport chain. Of the two enzymes involved in glycerol phosphate shuttle, only the mGPD is reported to be Ca^{2+} sensitive[69,78–80].

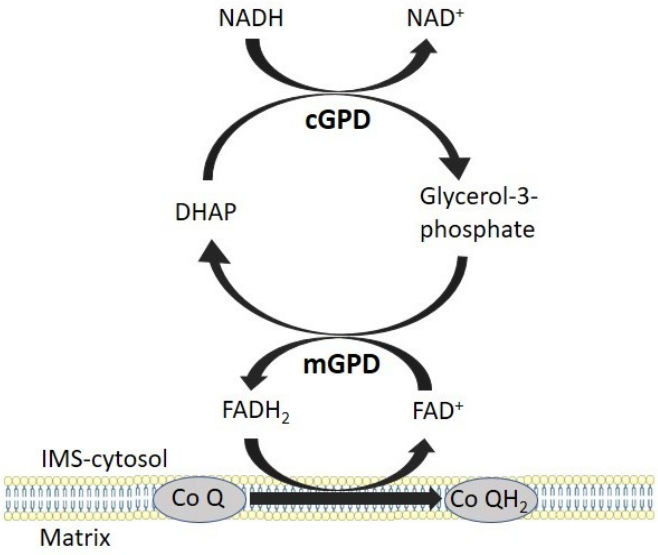

Figure 4. *Schematic representation of glycerol phosphate shuttle. Cytosolic glycerol 3-phosphate dehydrogenases converts glycolytic intermediate DHAP to glycerol-3-phosphate, which is converted back to DHAP by IMS residing, Ca^{2+} sensitive glycerol 3-phosphate dehydrogenases. The former also generates $FADH_2$ and assists in its oxidation and electron donation to coenzyme Q of the ETC.*

Both NADH shuttles control glycolysis, through recycling NADH and making NAD^+ available, and OXPHOS, through substrate supply, giving IMS Ca^{2+} a major function in regulating mitochondrial bioenergetics and in linking cytosolic and mitochondrial energy pathways. Low Ca^{2+} activation concentrations of IMS residing shuttles compared to matrix dehydrogenases makes IMS regulation of mitochondrial bioenergetics more subtle and easier to manipulate. In my second first author publication, I have studied the importance of basal sub-cellular Ca^{2+} homeostasis, with an emphasis on IMS Ca^{2+} as a regulator of mitochondrial bioenergetics[3]. We have described how alteration in IMS Ca^{2+} level can reversibly rewire cellular metabolism of non-excitable cells in citrin dependent manner. Nevertheless, IMS and matrix regulation mechanisms of mitochondrial function often go hand to hand, as one cannot function without the other.

1.6 Mitochondrial bioenergetics and ER stress

Mitochondrial bioenergetics are adjusted to cellular energy demand under normal and pathological conditions. ER stress represent a hallmark of cancer as well as many metabolic and neurodegenerative disease[81–83] and serves as an important example for the regulation of mitochondrial bioenergetics in response to cellular stress. ER is multifunctional organelle and is primarily responsible for processing, folding, and trafficking of nearly 1/3 of all proteins in eukaryotic cells. Once proteins are co-translationally targeted into the ER, they are handled by many chaperones and foldase enzymes that facilitate proper protein folding and posttranslational modifications[84]. Misfolded proteins are recognized in the ER lumen and are removed and degraded by a system called ER-associated degradation (ERAD)[85]. As it can be anticipated, all these processes require energy in form of ATP, thus ER also benefits from keeping close contact with mitochondria[86]. Additionally, as it was already mentioned above, ER is the main intracellular Ca^{2+} storage unit and many of the processes and enzymes in the ER lumen depend on Ca^{2+} ions. The main Ca^{2+} binding ER chaperone is calreticulin, which is responsible for folding and post-translational modification of nearly all glycosylated proteins[87]. Together with calnexin, another Ca^{2+} binding ER chaperone, calreticulin is responsible for the lifecycle of glycoproteins[87–89]. Another ER luminal Ca^{2+} binding protein is the main ER chaperone – heat shock protein A5, also known as glucose-regulated protein 78 (GRP78) or binding immunoglobulin protein (BiP). BiP is responsible for folding and post-translational modification of non-glycosylated proteins and plays a crucial role in ER stress response[90].

ER stress is a condition that is characterized as an inability of ER to properly fold and process proteins in its lumen, resulting in excessive accumulation of misfolded proteins and disruption of ER functions. ER stress triggers ER unfolded protein response (UPR), which senses and responds to ER stress by halting general protein synthesis, while increasing expression of ER chaperones. Three main pathways of ER UPR include double-stranded RNA-dependent protein kinase (PRK)-like ER kinase (PERK), activating transcription factor 6 (ATF6), and inositol requiring enzyme 1 (IRE1)[91].

It was reported that during early stages of ER stress, ER-mitochondrial contact sites increase, leading to increased ER-mitochondria Ca^{2+} crosstalk and boosted mitochondrial bioenergetics[92]. This is thought to be due to increased ER ATP demand to sustain UPR and to deal with unfolded proteins. It is suggested that ER increases Ca^{2+} supply of mitochondria, which in turn supply the ATP for the UPR[86,93]. At first glance, it appears to be a beneficial exchange, but if the ER stress persist, mitochondrial will run into a danger of Ca^{2+} overload, which is known to happen in many pathologies involving prolonged ER stress[94]. Thus, the timing of the ER-mitochondrial crosstalk is of upmost

importance, hence cells have developed adaptive mechanisms to prevent mitochondrial Ca^{2+} overload and still maintain elevated ATP production. During my studies, I have worked on the function of Sigma 1 receptor in ER stress and found that it plays a role in timely activation of mitochondria during early phases of ER stress response[93].

1.7 Role of sigma-1 receptor in regulation of mitochondrial bioenergetics in health and disease

We have identified Sigma-1 receptor (S1R) as an orchestrator of ER-mitochondria interaction during early ER stress[93]. S1R is an ER chaperone, located primarily in the ER-mitochondria contact sites[95]. It is a transmembrane protein and is expressed in various tissue types, although it is dramatically concentrated in cells of the central nervous system[95,96]. S1R has plethora of reported functions and interaction partners, but the large body of research suggests its main role is to regulate ER-mitochondrial communication[95,97]. S1R was shown to interact with inositol 1,4,5-trisphosphate receptor 3 (IP3R3), and to stabilize it at the mitochondria associated ER membranes[95,98]. Additionally, S1R interacts with IRE1 and assists in sustaining prolonged UPR by IRE1[99]. As both IP3R3 and IRE1 are resident MAM proteins, S1R boosts ER-mitochondria crosstalk by concentrating these proteins to the MAMs. In addition, one study identified S1R's role in store operated Ca^{2+} entry. It was shown that S1R interferes with STIM1 and Orai interaction upon ER store depletion and thus reduces Ca^{2+} entry[100]. Numerous studies have reported the involvement of S1R deficiency in various neurodegenerative diseases and cancer, emphasizing the importance of S1R in health and disease[101,102].

We have uncovered a crucial role of S1R in directing the ER Ca^{2+} leak towards mitochondria during early ER stress. We have confirmed the existence of ER Ca^{2+} leak directed towards mitochondria during early ER stress, and discovered that as the ER stress persists longer, the leak is redirected towards global cytosol and no longer directed only at mitochondria[93]. It was already shown that S1R can redistribute from the MAM area towards other parts of the ER as ER stress progresses[95], which supports the time dependence of the phenomenon that we describe. As S1R has many described ligands that can modulate its action, targeting S1R in diseases involving ER stress can be an attractive therapeutic approach.

In line with this, we have demonstrated that S1R modulation by its ligands can serve as an effective tool to manipulate cancer cell bioenergetics[103]. We uncovered that S1R activation can boost

mitochondrial bioenergetics by enhancing mitochondrial Ca^{2+} uptake, thus mimicking the early stages of ER stress[103]. This finding identifies S1R as an important target for cancer therapy as well.

1.8 Fluorescence microscopy as a potent method to study mitochondrial bioenergetics

As a final note, it is worth mentioning that recent advances in fluorescence imaging and development of genetically encoded fluorescent sensors has pushed the field of bioenergetics research forward immeasurably. During my studies, the majority of the experiments were performed using fluorescence microscopy. Many of the cellular metabolites that were undetectable before, or were only detectable in cell lysates, can now be studied within living cells. Since bioenergetics is a dynamic concept that only makes sense in regards to living cells, these new methods allow to image real time fluctuations of key ions and metabolites that define the cellular bioenergetics. An illustrative example is given in Figure 5, where mitochondrial ATP dynamics are imaged with mitochondrial matrix targeted ATP biosensor AT1.03[104]. The sensor consists of ATP binding domain flanked on both sides by two fluorescent proteins, cyan fluorescent protein (CFP) and yellow fluorescent protein (YFP)[104]. Binding of ATP to the sensor results in a conformational change, which moves the two fluorescent proteins closer to each other. Upon excitation of the CFP, part of the excitation energy is transferred to the YFP, the Förster resonance energy transfer (FRET), which is proportional to the distance between fluorescent proteins. This gives dual emission from both CFP and YFP upon single excitation of a CFP, providing an advantage of ratiometric readout of ATP concentration, which is not dependant on expression level of the sensor. Dynamic measurement of mitochondrial ATP level before and after application of ATP synthase inhibitor is depicted in Figure 5, which shows the difference in basal mitochondrial ATP levels between two adjacent cells and highlights the advantages of single cell fluorescent imaging technique for bioenergetics research. In a similar manner, many cellular metabolites, including, but not limited to, Ca^{2+}, pyruvate, lactate, NAD/NADH, and citrate can be investigated with high spatio-temporal resolution in single living cells. Some of the most important genetically encoded biosensors that made my work possible are presented in Table 1.

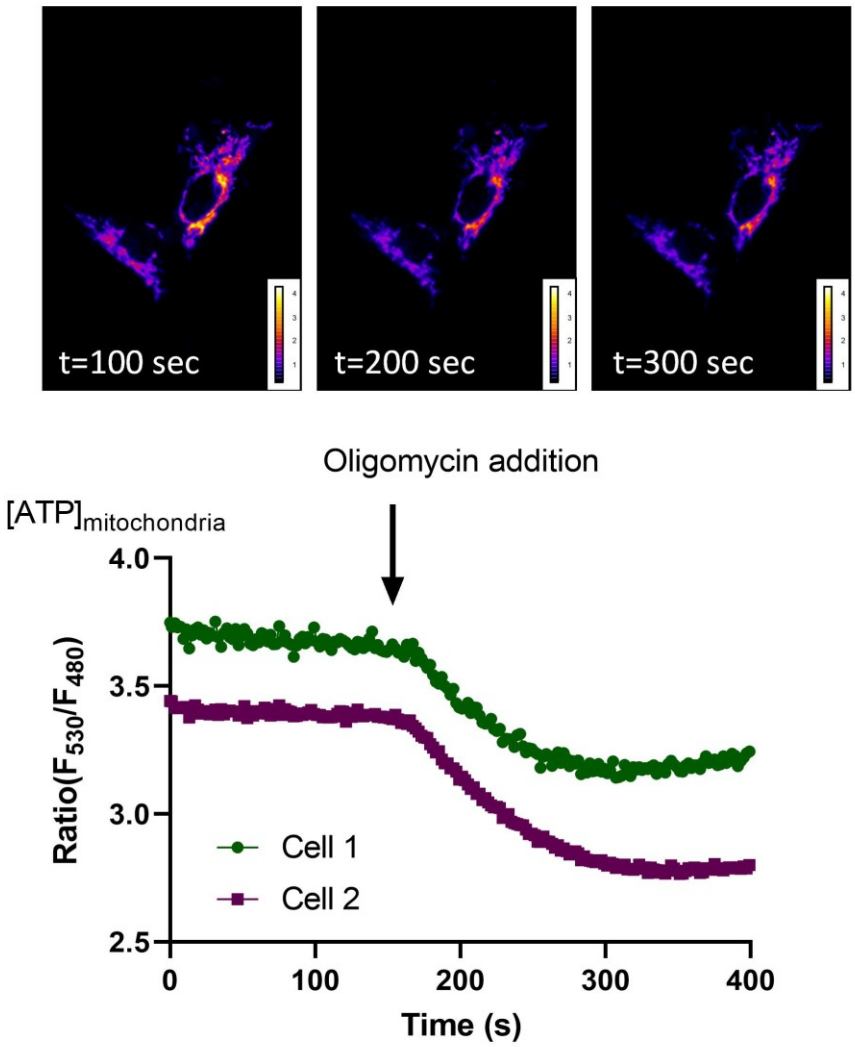

Figure 5. *Representative pseudocolored images of live cell mitochondrial ATP measurement using matrix targeted ATP biosensor AT1.03 in EA.hy926 cells. The graph below shows respective mitochondrial ATP dynamics. Basal level was recorded for 2 minutes, followed by addition of mitochondrial ATP synthase inhibitor oligomycin in real time.*

Table 1. List of genetically encoded biosensors used during the studies

Name of the sensor	**What it detects**	**Characteristics**	**References**
AT1.03 and mtAT1.03	ATP	FRET based ratiometric biosensors targeted to cytosol or mitochondria	[104]
Pyronic	Pyruvate	Cytosolic FRET based ratiometric biosensor	[105]
mtPyronicSF	Pyruvate	Mitochondrial single FP based biosensor	[106]
Peredox	NAD/NADH ratio	Cytosolic ratiometric biosensor	[107]
D3Cpv and 4mtD3cpv	Ca^{2+}	Cytosolic and mitochondrial FRET based ratiometric biosensors	[108]
D1ER	Ca^{2+}	ER targeted FRET based ratiometric biosensors	[109]
GEM-GECO (cyto, IMS, cristae, matrix)	Ca^{2+}	Ratiometric biosensors targeted to various subcellular and submitochondrial compartments	[110,111]
Laconic	lactate	Cytosolic FRET based biosensor	[112]
Hyper7	H_2O_2	Cytosolic ratiometric biosensor	[113]
mtCitrON	citrate	Mitochondrial intensiometric biosensor	[114]

2 First author publications:

Mitochondrion 55 (2020) 164–173

Contents lists available at ScienceDirect

Mitochondrion

journal homepage: www.elsevier.com/locate/mito

The contribution of uncoupling protein 2 to mitochondrial Ca^{2+} homeostasis in health and disease – *A short revisit*

Zhanat Koshenov[a], Furkan E. Oflaz[a], Martin Hirtl[a], Olaf A. Bachkoenig[a], Rene Rost[a], Karin Osibow[b,c], Benjamin Gottschalk[a], Corina T. Madreiter-Sokolowski[a,b], Markus Waldeck-Weiermair[a,d], Roland Malli[a,e], Wolfgang F. Graier[a,e,*]

[a] *Molecular Biology and Biochemistry, Gottfried Schatz Research Center, Medical University of Graz, Neue Stiftingtalstraße 6/6, 8010 Graz, Austria*
[b] *Diagnostic and Research Institute for Pathology, Medical University of Graz, Neue Stiftingtalstraße 6, 8010 Graz, Austria*
[c] *Department of Health Sciences and Technology, ETH Zurich, Schorenstraße 16, 8603 Schwerzenbach, Switzerland*
[d] *Division of Cardiovascular Medicine, Department of Medicine, Brigham and Women's Hospital, Harvard Medical School, 75 Francis Street, Boston, MA 02115, USA*
[e] *BioTechMed, Graz, Austria*

ARTICLE INFO

Keywords:
Mitochondrial calcium homeostasis
UCP2
MICU1
PRMT1
MCU

ABSTRACT

Considering the versatile functions attributed to uncoupling protein 2 (UCP2) in health and disease, a profound understanding of the protein's molecular actions under physiological and pathophysiological conditions is indispensable. This review aims to revisit and shed light on the fundamental molecular functions of UCP2 in mitochondria, with particular emphasis on its intricate role in regulating mitochondrial calcium (Ca^{2+}) uptake. UCP2's modulating effect on various vital processes in mitochondria makes it a crucial regulator of mitochondrial homeostasis in health and disease.

1. Uncoupling proteins – *General understanding*

Besides their involvement in various signaling cascades (Groschner et al., 2012; Madreiter-Sokolowski, 2019), mitochondria are cell's powerhouse, thereby accounting for the final steps in nutrient metabolism and the synthesis of the high-energy compound adenosine trisphosphate (ATP) (Mitchell, 1961) from adenosine diphosphate (ADP) and free phosphate at invaginations of the mitochondrial inner membrane (IMM) (Golic, 2016) called cristae. The F_0F_1-ATP synthase, a multi-enzyme complex in the cristae membrane, utilizes the proton gradient across the IMM to synthesize ATP (Mitchell, 1961; Golic, 2016). The proton gradient is generated by the mitochondrial electron transport chain (ETC). This multi-enzyme complex locates in the cristae membrane, where it oxidizes its substrates, the reduced forms of nicotinamide adenine dinucleotide (NADH) and flavin adenine dinucleotide ($FADH_2$), to reduce molecular oxygen and to form H_2O (Mitchell, 1961; Golic, 2016). Energy gained by this process empowers the complexes of the ETC to pump protons from the mitochondrial matrix into the cristae lumen, thereby generating an electrochemical gradient across the IMM, which enables oxidative phosphorylation (OXPHOS). However, the proton gradient is not entirely spent on the synthesis of ATP as a fraction is dissipated by so-called uncoupling proteins (UCPs) (Brand, 1999; Ricquier and Bouillaud, 2000; Ježek et al., 2018).

According to their structure, UCPs belong to the family of mitochondrial anion carrier proteins localized in the IMM (Ricquier and Bouillaud, 2000). They are proposed to transport protons along the electrochemical gradient across the IMM, thereby uncoupling the proton gradient from ATP production (Brand, 1999; Ježek et al., 2018). This uncoupling process might seem counterproductive at first, but it serves several physiological functions. In brown adipose tissue, uncoupling protein 1 (UCP1) constitutes approximately one-third of the entire mitochondrial protein mass and uncouples the proton gradient to generate heat (Palou et al., 1998). Further functions of uncouplers are reducing the formation of reactive oxygen species (ROS) and maintaining the NAD + /NADH ratio (Ježek et al., 2018; Jabůrek et al., 2018; Su, 2017).

Five members of the mammalian UCP family (UCP1 − 5) that are differentially expressed in tissues and organs (Ricquier and Bouillaud, 2000) have been identified so far. While UCP1 is primarily expressed in brown adipose tissue as already mentioned, UCP2 is ubiquitously expressed and highly abundant in the liver, kidney, pancreas, spleen, neurons, and skeletal muscle (Fleury, 1997). UCP3 can be

* Corresponding author at: Molecular Biology and Biochemistry, Gottfried Schatz Research Center, Medical University of Graz, Neue Stiftingtalstraße 6/6, 8010 Graz, Austria.
E-mail address: wolfgang.graier@medunigraz.at (W.F. Graier).

https://doi.org/10.1016/j.mito.2020.10.003
Received 23 July 2020; Received in revised form 30 September 2020; Accepted 12 October 2020
Available online 15 October 2020

predominantly found in skeletal and heart muscle cells (Boss, 1997), whereas UCP4 and UCP5 are most common in neurons (Mao, 1999; Ramsden, 2012; Sanchis, 1998). Although the UCP family has been known for decades and the uncoupling effect of UCP1 has been thoroughly studied, the functions of other UCPs, particularly of UCP2 and UCP3, is still under debate (Carmona, 1998; Trenker et al., 2007, 2008; Žáčkova and Ježek, 2002; Jabůrek, 1999; Couplan, 2002; Kukat, 2014; Brookes, 2008). Interestingly, while UCP2 and UCP3 are approximately 73% homologous (Mailloux, 2011), they share only about 58% homology with UCP1 (Ricquier and Bouillaud, 2000) and even less with UCP4 (Mao, 1999) and UCP5 (Mao, 1999; Sanchis, 1998), thus rendering a functional homology is highly questionable. However, the implication of UCP2 and UCP3 in diverse physiological and pathophysiological conditions (Donadelli et al., 2013) indicates highly versatile roles within mitochondria and makes it of utmost importance to determine the protein's s respective molecular functions.

2. Early findings in mitochondria

By screening for UCP1 homologs, researchers discovered UCP2 in the late 1990s (Fleury, 1997; Gimeno, 1997). Those early studies described UCP2 as being expressed in small amounts in a wide variety of tissues and organs, and to exhibit effects in obesity, hyperinsulinemia, and in the regulation of mitochondrial membrane potential (Fleury, 1997; Sanchis, 1998; Žáčkova and Ježek, 2002; Jabůrek, 1999). Further studies in isolated mitochondria and reconstituted liposomes revealed that UCP2 can facilitate a proton flux only under certain conditions, such as in the presence of ROS, explained as a feedback mechanism to reduce mitochondrial ROS formation (Rial, 1999; Echtay et al., 2002). UCP2 was also shown to enable uncoupling by fatty acid (FA) transport across the mitochondrial inner membrane (Žáčkova and Ježek, 2002; Jabůrek, 1999; Berardi and Chou, 2014; Garlid et al., 1998). It is proposed that UCP2 transports the anionic FAs from the matrix into the inter-membrane space (IMS), where they get protonated and can slip back, attributing a flippase function to UCP2 (Berardi and Chou, 2014; Garlid et al., 1998). The result of this action is creation of a net proton gain for the matrix and uncoupling of the proton gradient from ATP synthesis. In contrast to UCP2, UCP3 was discovered to be primarily expressed in skeletal muscle and brown adipose tissue (Boss, 1997; Vidal-Puig et al., 1997). Hence, UCP3 was suggested to be involved in thermogenesis (Vidal-Puig et al., 1997) and fatty acid beta-oxidation (Hilse, 2018). The proposed uncoupling mechanism of action of UCP3 is fatty acid-mediated uncoupling, similar as for UCP2 (Žáčková et al., 2003; Macher, 2018). Since the scope of this review is to discuss the contribution of UCP2 and UCP3 in the mitochondrial Ca^{2+} regulation, we would like to refer the reader to excellent reviews for general overview of UCP2 and UCP3 (Ježek et al., 2018; Donadelli et al., 2013; Pohl et al., 2019). A short summary of differences and similarities of UCP2 and UCP3 is presented in Table 1.

3. UCP2/3′s role in mitochondrial Ca^{2+} uptake routes

The physiological significance of UCP2 and UCP3 was first challenged by Trenker et al. (Trenker et al., 2007), demonstrating by overexpression, knock-down and mutagenesis that they are fundamentally required for mitochondrial Ca^{2+} uptake in intact cells (Trenker et al., 2007). Since the identity of the mitochondrial Ca^{2+} uniporter (MCU) complex was still unknown at that time, the work attracted a lot of attention and controversy in the field (Brookes, 2008; Marchi et al., 2011; Jiang et al., 2009). Basically, the study demonstrated that overexpression of UCP2 or UCP3 significantly increased the Ca^{2+} sequestration by mitochondria, whereas their knockdown drastically reduced it. The cell line-derived data were substantiated in isolated hepatic mitochondria of UCP2 knockout ($UCP2^{-/-}$) mice that showed no Ruthenium Red-sensitive mitochondrial Ca^{2+} uptake. The authors also demonstrated that the intermembrane loop 2 (IML2) of UCP2 and UCP3, which is highly homologous within these UCPs but largely differs from that of UCP1 or other UCPs, plays a critical role in the involvement of UCP2 and UCP3 in the mitochondrial Ca^{2+} uptake. Accordingly, chimeric constructs of UCP2 or UCP3 containing the IML2 of UCP1 elicited a decreased mitochondrial Ca^{2+} uptake compared to control HeLa cells and thus mimicked a dominant negative effect. Later publications by Waldeck-Weiermair *et al.* (2010) added further insights into the involvement of UCP2 and UCP3 in mitochondrial Ca^{2+} homeostasis (Waldeck-Weiermair, 2010a, 2010b). The knockdown of UCP2 and UCP3 only diminished mitochondrial Ca^{2+} uptake of intracellularly released Ca^{2+} upon treatment with the inositol-1,4,5-triphosphate (IP_3) mobilizing agonist histamine but remained unchanged during store-operated calcium entry (SOCE) (Waldeck-Weiermair, 2010). These data point to a distinct contribution of UCP2 and UCP3 to mitochondrial Ca^{2+} uptake depending on the source and route of intracellular Ca^{2+} rise (Waldeck-Weiermair, 2013). Ca^{2+} release from the endoplasmic reticulum (ER) results in local Ca^{2+} hotspots at so-called mitochondria-associated ER membranes (MAMs). Within these subcellular compartments shaped by ER membranes, high Ca^{2+} levels (approximately 15–20 μM) are rapidly reached (Giacomello, 2010; Csordás, 2010). In contrast, SOCE proceeds with rather slow kinetics, and mitochondrial Ca^{2+} uptake via this Ca^{2+} source occurs in a different mode (Giacomello, 2010). However, overexpression of UCP2 or UCP3 increased mitochondrial Ca^{2+} sequestration from both Ca^{2+} sources, the intracellular ER Ca^{2+} store and the extracellular Ca^{2+} entry, pointing towards their role in increasing the mitochondria's capability for Ca^{2+} sequestration (Waldeck-Weiermair, 2010). Using site-directed mutagenesis of UCP3′s IML2, key amino acid residues were identified for preferential mitochondrial Ca^{2+} sequestration from either low or high Ca^{2+} levels (Waldeck-Weiermair, 2010).

Subsequent electrophysiological analysis demonstrated that UCP2 and UCP3 regulate MCU-dependent Ca^{2+} current in mitoplasts and thus, confirmed the initially hypothesized regulatory role of UCP2 and UCP3 in mitochondrial Ca^{2+} uptake (Bondarenko, 2015). These findings were further supported by electrophysiological studies of other

Table 1
Summary of differences, similarities, and proposed mechanisms of action of UCP2 and UCP3.

	UCP2	UCP3
Structure	309 amino acids, 6 transmembrane domains, 3 intermembrane loops (Trenker et al., 2007)	312 amino acids, 6 transmembrane domains, 3 intermembrane loops (Trenker et al., 2007)
Homology to UCP1	59% (Fleury, 1997)	54% (Boss, 1997; Vidal-Puig et al., 1997)
Shared homology	71–73% (Boss, 1997; Trenker et al., 2007; Vidal-Puig et al., 1997)	
Expression pattern/tissues	Ubiquitously expressed, incl. liver, kidney, pancreas, spleen, neurons and skeletal muscle (Fleury, 1997)	Primarily in skeletal muscle, heart and BAT (Boss, 1997; Vidal-Puig et al., 1997; Pohl et al., 2019)
Proposed uncoupling mechanism	FA mediated flippase-like mechanism (Jabůrek, 1999; Berardi and Chou, 2014; Žáčková et al., 2003; Macher, 2018); Direct uncoupling in the presence of ROS (UCP2) (Rial, 1999; Echtay et al., 2002)	
Proposed regulatory role in mitochondrial Ca^{2+} uptake	Regulates mitochondrial Ca^{2+} uptake threshold upon MICU1 methylation (Trenker et al., 2007; Madreiter-Sokolowski, 2016)	

research groups that showed involvement of UCP2 in the mitochondrial Ca^{2+} uptake current in mitoplasts of mouse cardiac myocytes (Motloch, 2016a, 2016b). In summary, all these early studies at least indicated a crucial contribution of UCP2 and UCP3 on the mitochondrial Ca^{2+} uptake mechanism. However, the functional conditions and a possible participation within the entire mitochondrial Ca^{2+} pore remained to be clarified.

4. Conflicting studies

The findings of Trenker et al. (Trenker et al., 2007) considering the involvement of UCP2 and UCP3 on mitochondrial Ca^{2+} uptake, were initially questioned by the scientific community. Concerning their denotation and function as 'uncoupling proteins' two groups independently expressed concerns in follow-up works (Brookes, 2008). Brookes *et al.* studied the role of UCP2 and UCP3 in isolated mitochondria from various tissues of wildtype, $UCP2^{-/-}$ and $UCP3^{-/-}$ mice, but failed to reproduce the results of Trenker *et al.* Moreover, the work had also been criticized concerning the kinetics of Ca^{2+} uptake in overexpression models, tissue selection for mitochondria isolation, and the use of compounds to inhibit UCP2 and UCP3. An additional work by Trenker *et al.* addressed these reservations by a set of new experiments and conclusions, revealing that the kinetics of mitochondrial Ca^{2+} uptake in overexpressing and knockdown cells differ from controls (Trenker et al., 2008). The results therein also demonstrated that the experimental procedure of mitochondria isolation plays a crucial role in their subsequent functional readout. Brookes *et al.* (Brookes, 2008) and Trenker *et al.* (Trenker et al., 2007, 2008) used different procedures for mitochondrial preparations, which resulted in varying size distribution of mitochondria as well as in discrepancies in staining and in the levels of mitochondrial marker proteins (Trenker et al., 2008). Comparatively crude isolation of mitochondria by differential centrifugation, as performed by Brookes *et al.,* yielded more fragmented mitochondria with reduced levels of mitochondrial marker proteins, exhibiting UCP2/UCP3-independent Ca^{2+} uptake. Isolation of mitochondria by gradient centrifugation, as done by Trenker *et al.*, resulted in mitochondrial Ca^{2+}sequestration modulated by UCP2 and UCP3 (Trenker et al., 2008). We assume the comparatively gentle isolation procedure yielded less fragmented, more intact mitochondria. The preservation of the mitochondrial ultrastructure, in particular the cristae junction, separating the cristae lumen from the intermembrane space might be of utmost importance for the intact functionality of UCP2 Ca^{2+} regulation. Although the correspondence between the authors of Brookes *et al.* and Trenker *et al.* resolved some of the discrepancies related to the initial findings, reports from other groups raised additional concerns regarding the role of UCP2 in Ca^{2+} homeostasis. Work by Jiang et al. (Jiang et al., 2009) using a high-throughput approach identified LETM1 as the mitochondrial Ca^{2+}/H^{+} exchanger while failing to find any involvement of UCP2 and UCP3 in mitochondrial Ca^{2+} uptake (Jiang et al., 2009). The approach of Jiang *et al.* was based on permeabilized cells and the use of thapsigargin to deplete the ER Ca^{2+} store that for instance also activates SOCE. Nonetheless, at the same time it had been found that mitochondrial Ca^{2+} uptake from capacitative Ca^{2+} entry is insensitive of UCP2 and UCP3 in knockdown experiments (Waldeck-Weiermair, 2010a, 2010b).

In 2011 De Marchi *et al.* proposed an indirect modulation of the mitochondrial Ca^{2+} uptake by UCP2 and UCP3 via regulation of tarco/endoplasmic reticulum C activity a^{2+}-ATPase (SERCA) (Marchi et al., 2011). The authors claimed that a diminished mitochondrial Ca^{2+} uptake in UCP3 knockdown cells upon ER Ca^{2+} depletion is due to increased ATP-consuming SERCA pump activity, which shuffles Ca^{2+} back into the ER (Marchi et al., 2011). The authors explained this hypothesis by increased mitochondrial ATP levels in UCP3 knockdown cells, thereby boosting SERCA activity that competes with mitochondria for the Ca^{2+} released from the ER. They further supported their claims by showing reduced cytosolic Ca^{2+} signals during stimulation with histamine, reduced SOCE as well as the normalization of both cytosolic and mitochondrial Ca^{2+} elevations upon ER Ca^{2+} release upon combined application of the SERCA inhibitor thapsigargin and the IP_3-generating agonist histamine (Marchi et al., 2011). Notably, while this report confirmed several findings of Trenker *et al.*, e.g. that UCPs are not involved in mitochondrial Ca^{2+} uptake due to SERCA inhibition (Trenker et al., 2007), other data and interpretations differed from Trenker et al. (Trenker et al., 2007) and Waldeck-Weiermair *et al.* (2010). De Marchi *et al.* found increased basal ATP level as well as a further increase after histamine stimulation under conditions of UCP3 knockdown and assumed that this was a primary effect of UCP3 depletion. In contrast, Trenker *et al.* have shown increased ATP levels upon histamine treatment in cells with UCP2 and UCP3 overexpression (Trenker et al., 2007), which is in line with increased Ca^{2+} sequestration and a subsequent increase in the activity of the mitochondrial dehydrogenases (Hajnóczky et al., 1995; Denton, 2009). This result also serves as proof against an uncoupling function of UCP2 or UCP3 since the overexpression of uncoupling proteins would rather decrease ATP levels. As mentioned above, Waldeck-Weiermair *et al.* (2010) reported that mitochondrial Ca^{2+} uptake upon SERCA inhibition utilizes an alternate Ca^{2+} uptake route or, at least, a distinctly regulated Ca^{2+} uptake mechanism in comparison to ER Ca^{2+} release by an IP_3-generating agonist (Waldeck-Weiermair, 2010). In subsequent work, Waldeck-Weiermair *et al.* showed that modulation of Ca^{2+} release from the ER by inhibition of SERCA modifies cytosolic Ca^{2+} signals and consequently alters the mode of mitochondrial Ca^{2+} uptake from a UCP2- and UCP3-dependent to an independent pathway (Waldeck-Weiermair, 2013). Interestingly, mitochondrial Ca^{2+} uptake upon SERCA inhibition by thapsigargin became independent of UCP2 and UCP3 but shifted to a LETM1 dependency under this condition (Waldeck-Weiermair, 2013). These data indicate that SERCA affects the mode of mitochondrial Ca^{2+} sequestration and determines the MCU-dependent pathway by which mitochondria take up Ca^{2+}.

These reports indicate that the contribution of UCP2 or UCP3 to the regulation of mitochondrial Ca^{2+} uptake depends on various parameters, including the localization (MAM vs. non-MAM areas), the Ca^{2+} source as well as the kinetic and the amount of Ca^{2+} floating towards the mitochondrial surface. However, the discussion on the role of UCP2 and UCP3 in mitochondrial Ca^{2+} uptake was overcome by the discoveries leading to identifying the actual components forming the mitochondrial Ca^{2+} uniporter complex.

5. The mitochondrial Ca^{2+} uniporter complex

Following the discovery of an essential regulator of mitochondrial Ca^{2+} uptake, the so-called mitochondrial calcium uptake 1 (MICU1) (Perocchi, 2010), the mitochondrial calcium uniporter (MCU) itself was identified as the pore-forming protein responsible for shuttling Ca^{2+} from the IMS into the matrix (Stefani et al., 2011; Baughman, 2011). These findings hallmarked the beginning of a new era in mitochondrial research. In the following years, many other components and regulators of the mitochondrial Ca^{2+} uptake machinery were revealed and characterized, leading to a better understanding of the MCU complex (MCUC) as follows: MCU, along with its dominant-negative form mitochondrial Ca^{2+} uptake b (MCUb) (Raffaello, 2013) and the essential MCU regulator (EMRE) (Sancak, 2013), forms the basis of the functional uniporter. MICU1, MICU2, and in some tissues MICU3, act as gatekeepers and set the Ca^{2+} concentration threshold for the channel opening (Patron, 2014; Kamer and Mootha, 2014; Plovanich, 2013; Patron et al., 2018). Furthermore, mitochondrial calcium uniporter regulator 1 (MCUR1) serves as an important scaffold and regulator protein of the MCUC (Tomar, 2016). Based on this considerable progress in the understanding of the molecular constituents and function of the MCUC as well as in the techniques available to investigate these subcellular processes (Madreiter-Sokolowski, 2019), the molecular function of UCP2 and UCP3 within the MCUC was further elaborated

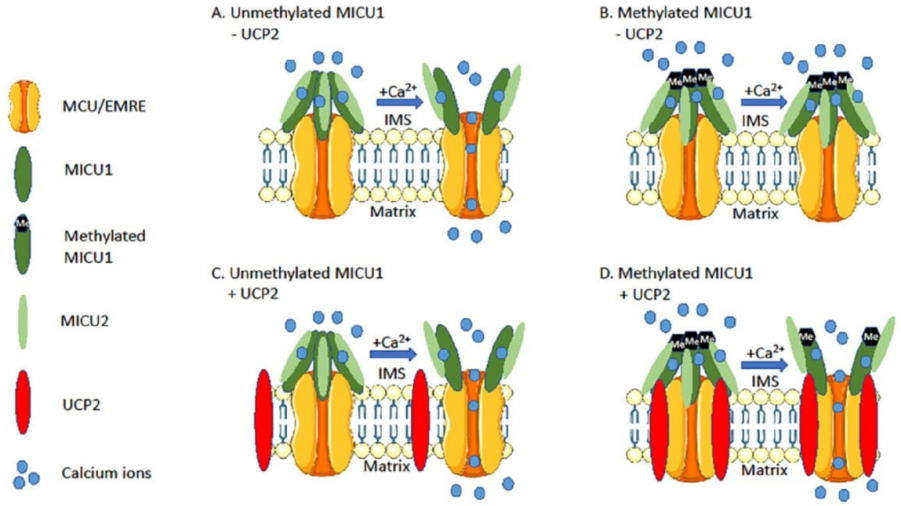

Fig. 1. Schematic illustration of mitochondrial Ca^{2+} uptake regulated by UCP2. **A.** In case of un-methylated MICU1, proper mitochondrial Ca^{2+} uptake occurs upon a certain threshold. **B.** The threshold for mitochondrial Ca^{2+} uptake is increased as soon as MICU1 gets methylated, resulting in reduced uptake in the absence of UCP2. **C.** In case of un-methylated MICU1, mitochondrial Ca^{2+} uptake is independent of UCP2. **D.** In case MICU1 is methylated, mitochondrial Ca^{2+} uptake threshold gets normalized by UCP2, resulting in proper Ca^{2+} uptake.

(Fig. 1). Knowing the actual proteins establishing the MCUC offered the chance to investigate a potentially modulatory role of UCP2 and UCP3 in MCUC regulation.

6. Solving the contradiction in UCP2/3's contribution to mitochondrial Ca^{2+} uptake and more

Trenker *et al.* suggested that UCP2 and UPC3 do not form the mitochondrial Ca^{2+} uptake pore themselves, but rather exhibit a regulatory function on the activity of the respective protein(s). This claim was finally solved by publications of Madreiter-Sokolowski *et al.* (2016) and Gottschalk et al. (Gottschalk, 2019). The former demonstrated cell type-specific differences in the dependence of the mitochondrial Ca^{2+} uptake on UCP2 and UCP3, which correlates with the activity of protein arginine methyl transferase 1 (PRMT1) (Madreiter-Sokolowski, 2016). PRMT1's transferase activity is particularly high during development, aging and in cancer and was found to yield asymmetric arginine dimethylation of MICU1 at position 455 (Madreiter-Sokolowski, 2016, 2017; Yoshimatsu, 2011; Mathioudaki, 2008). The methyl transferase activity of PRMT1 also positively correlates with a respective cell type dependence on UCP2 or UCP3 for mitochondrial Ca^{2+} uptake (Madreiter-Sokolowski, 2016). Knockdown of PRMT1 rescued the effect of UCP2 and UCP3 knockdown on mitochondrial Ca^{2+} uptake. The authors demonstrated that asymmetrical arginine dimethylation of MICU1 by PRMT1 reduces MICU1's Ca^{2+} sensitivity and, thereby, increases the threshold of Ca^{2+} for MCU activation, while the interaction of methylated MICU1 with UCP2 or UCP3 normalizes the sensitivity and lowers the Ca^{2+} threshold (Fig. 1). Overexpression of PRMT1 or a MICU1-mutant, which mimics arginine demethylation, turn cells from former UCP2-independent to UCP2-dependent cells. Hence, overexpression of mutants that mimic unmethylated MICU1, rescues mitochondrial Ca^{2+} uptake in UCP2 and UCP3 knockdown cells. Using an approach based on Foerster resonance energy transfer (FRET) to study MICU1 multimerization (Waldeck-Weiermair, 2015), Madreiter-Sokolowski *et al.* demonstrated that methylation of MICU1 yields a reduced Ca^{2+} sensitivity to trigger the rearrangement of MICU1 oligomers and, thus the activation of a MICU1 rearrangement (Madreiter-Sokolowski, 2016) (Fig. 1). Furthermore, using super-resolution microscopy, Gottschalk *et al.* reported specific association of UCP2 exclusively with PRMT1-methylated MICU1 and demonstrated that UCP2 facilitates anchoring of MCU at the inner boundary membrane (IBM) upon histamine-stimulated ER Ca^{2+} release (Gottschalk, 2019).

Notably, it has been shown that MICU1 regulates cristae junctions (Gottschalk, 2019; Tomar, 2019) and UCP2 was recently found to essentially contribute to Ca^{2+}-induced reorganization of cristae junctions in case of MICU1 methylation (Gottschalk, 2019). These recent findings may solve the discrepancy between decreased mitochondrial Ca^{2+} uptake but increased ATP levels in cells depleted of UCP2/UCP3 after histamine-induced ER Ca^{2+} release (Trenker et al., 2007). Coupling IMM and cristae morphology with the Ca^{2+} uptake machinery and the sub-mitochondrial organization of F_0F_1ATPase and ETC-complexes I, II and IV within the cristae membrane might give a comprehensive model to explain the manifold roles of UCP2 in mitochondria. Both mechanisms of action proposed for UCP2, Ca^{2+} uptake regulation and uncoupling, might be combined in a model including cristae junction modulation by UCP2. UCP2 might disrupt the stability of the cristae junction that is maintained by oligomerized MICU1 (Gottschalk, 2019), leading to a leakage of protons out of the cristae lumen into the IMS space, which could explain the uncoupling function of UCP2. Additionally, a cristae junction leakage would lead to an increased mitochondrial Ca^{2+} uptake due to an easier access of Ca^{2+} to the cristae and MCU residing in it.

7. Potential roles of UCP2 in health and disease

7.1. UCP2 in cancer

In recent years, mitochondrial activity and metabolism in cancer cells have come into the spotlight. Mitochondria are implicated in crucial cellular events such as Ca^{2+} homeostasis, cell death, tumor anabolism, and growth. In line with this, mitochondria play an important role in cancer metabolism by influencing the initiation, development, and progression of cancer (Porporato et al., 2018). Reliance of cancer cells on glycolysis as the primary energy source even in the presence of oxygen, known as Warburg effect (Porporato et al., 2018), is an established hallmark of cancer metabolism. Nevertheless, *Fantin*

Table 2
Disorders accompanied with upregulated UCP2 expression levels.

Disease		Impact of UCP2	Associated Ca^{2+}-related mechanism(s)	Reference
Cancer	Breast cancer Colon cancer Bladder cancer Lung cancer Prostate cancer	Increased cancer viability, reduced ROS level, decreased mitochondrial membrane potential, inhibition of apoptosis	UCP2 and PRMT1 levels are upregulated in cancer, thus, normalizing Ca^{2+} entry to mitochondria, avoiding Ca^{2+} overload and regulating OXPHOS levels. Thereby, cells are protected from apoptosis and increased ROS production and the viability and proliferation of cancer cells is enhanced	(Pons, 2015; Romancer et al., 2010) (Mathioudaki, 2008) (Yoshimatsu, 2011; Pozza, 2012) (Yoshimatsu, 2011; Madreiter-Sokolowski, 2017; Ayyasamy, 2011) (Ayyasamy, 2011; Majumder et al., 2006)
Cardiovascular diseases	Atherosclerosis	Compensatory mechanism to counteract preeminent oxidative stress	Modulation of mitochondrial Ca^{2+} uptake in macrophages to fuel ATP production and push polarization towards M2 phenotype	(Blanc, 2003; Moukdar, 2009)
	Ischemia reperfusion injury Arrhythmia		Cardioprotective function by induction of mitophagy and modulation of mitochondrial Ca^{2+} uptake Modulating of mitochondrial Ca^{2+} uptake protects mitochondria from Ca^{2+} overload or propagation of arrhythmic initiation of CICR	(Wu, 2019; Motloch et al., 2015) (Motloch, 2016; Larbig, 2017)
Aging and neurodegeneration	Parkinson's disease Amyotrophic lateral sclerosis Alzheimer's disease	Decreased mitochondrial membrane potential, increased oxygen consumption, reduced ROS levels, increased Ca^{2+} uptake in mitochondrial matrix	Oxidative stress is one of the major factors for development of neurodegeneration and aging. UCP2 and PRMT1 are highly expressed under these conditions, pointing towards a role of UCP2 in intricate regulation of mitochondrial Ca^{2+} uptake upon PRMT1 overexpression.	(Papkovskaia, 2012) (Peixoto, 2013; Ikenaka, 2019) (Jun, 2015; McKetney, 2019)
	Aging	Decreased ROS production, decreased lipid peroxidation, increased lifespan compared to knockout animals		(Hirose, 2016; Rose et al., 2011; Andrews and Horvath, 2009)

et al. showed that tumor cells can still switch back to mitochondrial respiration upon transient knockdown of lactate dehydrogenase, indicating that cancer cells do not always depend on glycolysis for energy production (Fantin et al., 2006). Also, it has been shown that the activity of the pyruvate kinase isoenzyme M2 (PKM2) affects a metabolic switch between glycolysis and OXPHOS by converting phosphoenolpyruvate into pyruvate (Mazurek, 2011). Other studies suggest that cancer cells can expend ATP to maintain mitochondrial membrane potential by the F_0F_1-ATP synthase operating in reverse mode (Depaoli, 2018). Overall, it is evident that cancer cells need to balance glycolysis and OXPHOS and keep polarized mitochondria functional.

Numerous reports describe the upregulation of UCP2 protein levels in diverse cancers, such as leukemia and lung, kidney, pancreas, prostate, ovarian, bladder, esophagus, testicular and colorectal cancer (Baffy et al., 2011; Ayyasamy, 2011) (Table 2). Given the necessity to maintain mitochondrial function, the upregulation of UCP2 can be attributed to attempts within cancer cells to boost mitochondrial dehydrogenases by increasing Ca^{2+} sequestration towards mitochondria. Overexpression of an uncoupler in cancer mitochondria that sometimes uses ATP to maintain IMM polarization (Depaoli, 2018) seems counterproductive, hence hinting on UCP2's Ca^{2+}-related mechanisms of action in these cancer cells (Fig. 2).

A recent study revealed increased expression of UCP2 in clinical samples of gallbladder cancer (Yu et al., 2019). Notably, UCP2 knockdown in cancerous gallbladder cells significantly reduces their proliferation rates (Yu et al., 2019). This concept is also supported by an *in vivo* study on UCP2's contribution to tumor formation, revealing a suppression of skin carcinogenesis in $UCP2^{-/-}$ mice (Li, 2015). These studies indicate the notion of a UCP2 upregulation as an adaptive mechanism in cancer cells.

Several research groups have attributed UCP2's function in cancer as dissipating the proton gradient and, thereby, modulating ROS production (Baffy et al., 2011) (Fig. 2). Cells depleted of mitochondrial DNA (rho^0) were used as a Warburg effect model system to investigate the involvement of UCP2 in cancer formation and metabolic handling (Ayyasamy, 2011). Thus, UCP2 expression was significantly higher in rho^0 cells compared to control epithelial cells and suggested that the uncoupling function of UCP2 may protect cells from excessive ROS production caused by mitochondrial defects. However, evidence of uncoupling function of UCP2 under physiological conditions is still largely lacking. It rather seems that uncoupling by UCP2 is mostly mediated under certain conditions, such as in the presence of superoxides (Couplan, 2002; Echtay et al., 2002), or indirectly by mediating fatty acid transport (Ježek et al., 2018). Therefore, it appears likely that the impact of UCP2 in cancer cells is mostly due to the regulation of mitochondrial Ca^{2+} levels. Since UCP2 normalizes the Ca^{2+} sensitivity of PRMT1-methylated MICU1 (Madreiter-Sokolowski, 2016) (Fig. 1), it is tempting to speculate that modulation of UCP2 expression levels in cancer cells may control the activity of Ca^{2+}-dependent dehydrogenases of the TCA cycle, which crucially impacts the ETC by producing FADH and NADH (Fig. 2).

This claim is further supported by the study of Chakraborty *et al.* reporting the impact of MICU1 on the glycolytic phenotype by regulating pyruvate dehydrogenase (PDH) activity (Chakraborty, 2017). By modulating mitochondrial Ca^{2+} levels, MICU1 can regulate PDH-phosphatase activity to activate PDH (Chakraborty, 2017). Moreover, downregulation of MICU1 induced overproduction of ROS (Chakraborty, 2017), which implies regulation of ROS as well as ATP production by MICU1 and mitochondrial Ca^{2+} levels, emphasizing the importance of UCP2 as a modulator of MICU1 and mitochondrial Ca^{2+} uptake in cancer cells (Fig. 2).

Madreiter et al. (2017) identified UCP2 and PRMT1 as key prognostic markers for lung carcinoma in patients and showed that they crucially affect mitochondrial ATP production, thus, highlighting that a proper mitochondrial Ca^{2+} uptake is essential for cancer cells (Madreiter-Sokolowski, 2017). This is in line with findings showing an

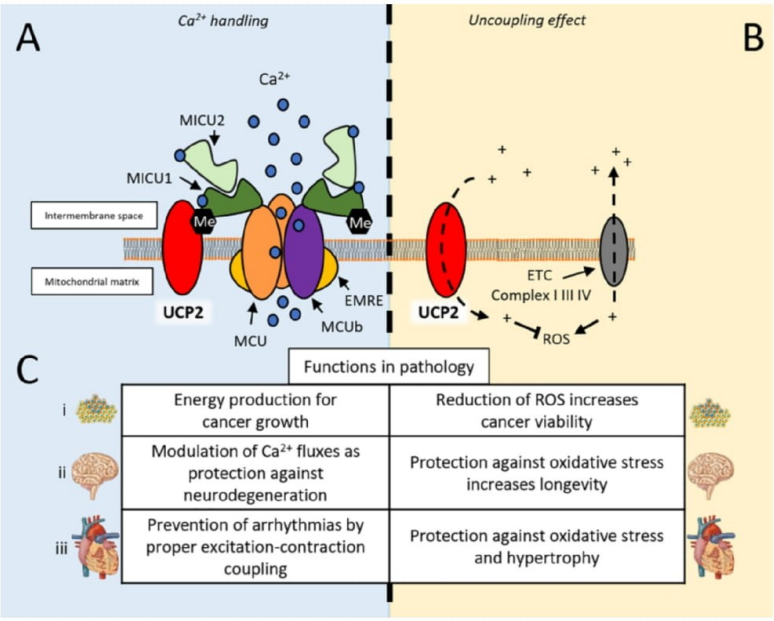

Fig. 2. Schematic illustration of UCP2UCP2′s proposed functions under various pathophysiological conditions. **A.** UCP2 as a regulator of mitochondrial calcium uptake under condition of MICU1 methylation by PRMT1. **B.** UCP2 as an uncoupler; different uncoupling modes were not depicted for the reasons of simplicity, such as fatty acid-facilitated uncoupling. **C.** Various functions of UCP2, dependent on its action as regulator of mitochondrial Ca^{2+} (left side) or as uncoupler (right side), in cancer (i), aging and neurodegenerative diseases (ii) and in cardiovascular diseases (iii).

increased ER-mitochondria tethering in HeLa and EA.hy926 cancer cell lines compared to noncancerous endothelial cell lines (HUVEC), which establishes a direct route of Ca^{2+} flux from ER to mitochondria (Madreiter-Sokolowski, 2016). However, enhanced mitochondrial Ca^{2+} uptake comes along with a risk of mitochondrial Ca^{2+} overload, which may cause the opening of the mitochondrial permeability transition pore (MPTP), release of cytochrome *C* and, eventually, apoptosis and cell death (Kwong and Molkentin, 2015). In this regard, cancer cells obviously found a way to protect themselves from Ca^{2+} overload by methylation and desensitization of MICU1 upon PRMT1 methylation (Madreiter-Sokolowski, 2016) (Fig. 1). Consistently, PRMT1 levels are also increased in most types of cancer (Yoshimatsu, 2011; Mathioudaki, 2008; Madreiter-Sokolowski, 2017), pointing to a possible adaptive mechanism of UCP2 upregulation in response to PRMT1 activity. Overall, cancer cells need to maintain a tight control of mitochondrial Ca^{2+} levels, which is fine-tuned by the balance between PRMT1-mediated MICU1 methylation and UPC2 expression (Madreiter-Sokolowski, 2016a, 2016b).

In line with this findings, Madreiter-Sokolowski *et al.* showed that simultaneous overexpression of UCP2 and PRMT1 increases cell proliferation and viability of human lung cancer cells (A549, Calu-3 and H1299) (Madreiter-Sokolowski, 2017). In addition, lung carcinoma patients with higher mRNA expression level of PRMT1 and UCP2 exhibited a reduced survival probability (Madreiter-Sokolowski, 2017). Until now, impact of UCP2 expression level alone on patients' survival probability was not shown for lung and gastric cancer. Analysis by the kmplot tool (Nagy et al., 2018) revealed significantly reduced survival probability of lung cancer (Fig. 3**A**) and gastric cancer (Fig. 3**B**) patients with high mRNA expression levels of UCP2. These findings support the rationale to test UCP2 as therapeutic target in order to treat patients suffering from cancer.

While the molecular mechanism of UCP2 in cancer cells is still under intensive investigation, targeting of UCP2 in cancer therapy is already intensively discussed. A very recent study about the effect of UCP2 on radiosensitivity of cervical cancer cells indicated that irradiation caused UCP2 upregulation (Liu, 2020). A combination of irradiation and UCP2 silencing enhanced mitochondrial ROS production, restricted cell survival and induced apoptosis and cell cycle arrest. UCP2 silencing in two different breast cancer cell lines (MCF-7 and T47D) increased mitochondrial membrane potential, ROS production, apoptosis and autophagy, resulting in sensitization of cancer cells to cisplatin and tamoxifen (Pons, 2015). Additionally, a strong correlation between UCP2 expression and a poor prognosis for the survival of breast cancer patient was revealed (Pons, 2015). Moreover, ovarian serous carcinoma patients with lower UCP2 expression levels exhibited higher sensitivity to platinum-based chemotherapy with longer overall survival rate and a negative correlation between the UCP2 level and effectiveness of platinum-based chemotherapy (Kawanishi, 2018). A similar approach of UCP2 silencing as therapeutic target elicited enhanced gemcitabine-induced mitochondrial ROS generation and apoptosis in a hepatocellular carcinoma (HCC) cell line (Yu et al., 2015). In line with this report, a Genipin-treated breast cancer cell line (MCF7) showed downregulated UCP2 levels, decreased cell proliferation and clonogenic survival (Ayyasamy, 2011). Since silencing of UCP2 in combination with conventional chemotherapy showed promising results, but the available UCP2 targeting drugs lack specificity (Kreiter, 2018), it is of great importance to design new drugs that specifically target UCP2 protein.

7.2. Cardiovascular diseases and type 2 diabetes

Mitochondrial Ca^{2+} signals strictly following cytosolic and nuclear Ca^{2+} changes in cardiomyocytes are essential for proper cardiovascular function (Robert, 2001). Alterations in the tightly controlled mitochondrial Ca^{2+} uptake can lead to atrial fibrillation (Wiersma, 2019), arrhythmia (Larbig, 2017) and heart failure (Santulli et al., 2015).

Due to its role in mitochondrial Ca^{2+} homeostasis (Trenker et al., 2007; Waldeck-Weiermair, 2010a, 2010b), UCP2 has come under scrutiny regarding its impact on the pathogenesis of cardiovascular and metabolic diseases (Larbig, 2017; Li et al., 2017; McLeod et al., 2005; Blanc, 2003; Moukdar, 2009; Wu, 2019; Motloch et al., 2015) (Table 2). Modulation of mitochondrial ATP and ROS production (McLeod et al., 2005; Blanc, 2003; Moukdar, 2009) are discussed as possible cause, whereas it is once again questionable whether UCP2 evokes these

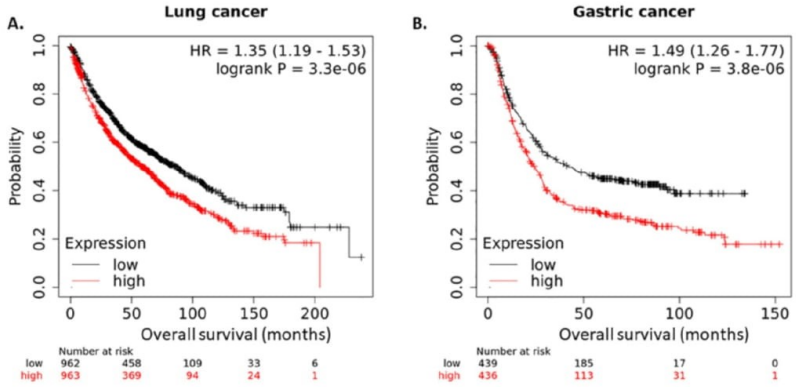

Fig. 3. Survival analysis of lung (A) and gastric (B) cancer patients was analyzed depending on UCP2 mRNA expression level and presented as Kaplan-Meier survival plot. Median expression value was used as a cutoff.

effects by modulation of mitochondrial Ca^{2+} homeostasis (Larbig, 2017; Motloch et al., 2015) or by an uncoupling function (McLeod et al., 2005) (Fig. 2).

Atherosclerosis is the main cause of cardiovascular diseases. It is caused by amalgamation of immune cells and lipids into lipid-containing plaques and leads to blood vessel blockage, potentially resulting in myocardial infarction (Hansson and Hermansson, 2011). Within atherosclerotic plaques, macrophages are exposed to sustained pro-inflammatory stimuli and oxidative stress that furthers cell adhesion and migration (Moore and Tabas, 2011). Notably, upon exposure to pro-inflammatory signals macrophages increasingly depend on glycolysis for ATP production (Vats, 2006), while mitochondrial respiration is reduced in favor of ROS production (West, 2011). This is caused by the toll like receptor (TLR)-induced expression of HIF-1α, leading to enhanced production of lactate from pyruvate (Imtiyaz and Simon, 2010; Kim et al., 2006). Overexpression of UCP2 was shown to reduce intracellular ROS levels and macrophages' adhesion downregulating β2 integrin expression (Je-Won, 2004). Additionally, increased abundance of UCP2 may alleviate inflammation induced ER-stress (Schaftenaar et al., 2016) in macrophages by boosting mitochondrial ATP production. This counteracts ER stress by providing ATP for protein folding, protein translocation, ER-associated protein degradation (ERAD), and ER Ca^{2+} homeostasis (Depaoli et al., 2019). Microglia, the resident macrophages of the brain, were shown to upregulate UCP2 when activated by high-fat diet in wildtype mice (Kim et al., 2019). As already described, UCP2 has been wildly accepted as an uncoupler of the proton gradient from ATP production, but no proton leakage was detected under these conditions. Instead, enhanced UCP2 expression was associated with an increase in basal and maximum respiration levels and ATP production as compared to conditional UCP2 knockout microglia (Kim et al., 2019). This would suggest an increased UCP2-dependent mitochondrial Ca^{2+} uptake that fuels the TCA cycle and thereby enhancing mitochondrial respiratory chain activity and ATP production (Kim et al., 2019). Accordingly, these data strongly argue against an uncoupling function of UCP2 and hint at an important role of UCP2 in mitochondrial Ca^{2+} uptake (Kim et al., 2019).

Notably, mitochondria account for approximately 30% of a cardiomyocyte's volume (Lukyanenko et al., 2009). Therefore, appropriate handling of mitochondrial ROS and Ca^{2+} homeostasis while maintaining proper ATP production is pivotal for the function of cardiomyocytes. According to current reports, adult cardiomyocytes largely rely on OXPHOS to meet > 95% of their energy demand in form of ATP (Stanley et al., 2005; Qiancong et al., 2019). Remarkably, their ATP supply was found to switch towards glycolysis during compensatory hypertrophy (Allard et al., 1994). Interestingly, UCP2 was upregulated in the myocardium under pathological conditions like atherosclerosis, ischemia reperfusion injury and arrhythmia, evoking to the hypothesis that upregulation of UCP2 protects the cells from oxidative stress and cardiac ischemia (Wu, 2019). However, UCP2 upregulation also leads to a prolonged decay phase of cytosolic Ca^{2+} transients during EC-coupling and has been observed to trigger so called Ca^{2+}-sparks, which potentially initiate an arrhythmic initiation of the EC-coupling and thus might worsen disease progression (Jay et al., 2010).

UCP2 knockout did not affect the viability of cardiomyocytes upon induction of hypoxia but counteracted the cardioprotective effect of the MCU inhibitor Ru360, thus, pointing to UCP2′s capacity to foster MCU activity even in the presence of Ru360 (Motloch et al., 2015). Notably, ventricular cardiomyocytes from $UCP2^{-/-}$ mice exhibited slower and reduced mitochondrial Ca^{2+} uptake while cytosolic Ca^{2+} levels remained unchanged under physiological conditions (Motloch, 2016). However, UCP2 knockout cardiomyocytes had a higher susceptibility to arrhythmias after treatment with the L-type calcium channel (LTCC) activator Bay K 8644 (Larbig, 2017), pointing to disturbed Ca^{2+} homeostasis. Interestingly, UCP2 knockout cardiomyocytes counteracted cytosolic Ca^{2+} overload under basal conditions by upregulating the expression of PRMT1 and exhibited reduced Ca^{2+} entry through LTCCs, leading to decreased calcium-induced calcium release (CICR) and diminished EC coupling (Larbig, 2017).

Glucotoxicity and enhanced ROS formation are known hallmarks in the pathogenesis of type 2 diabetes. In this regard, overexpression of UCP2 was reported to rescue pancreatic β-cells from glucotoxic effects without affecting basal mitochondrial membrane potential, ATP generation, and cytosolic Ca^{2+} responses (Li et al., 2017). This observation could be explained by the recent discovery of increased Ca^{2+} leak from the ER to the mitochondria in pancreatic beta-cells, which is dependent on GSK3-beta-mediated phosphorylation of presenilin-1 (Klec, 2019a, 2019b). Continuous Ca^{2+} leak from the ER to the mitochondria increases mitochondrial Ca^{2+} levels, respiration and ATP levels under basal conditions in wildtype β-cells. This mechanism might prime β-cells to respond quick and accurately as soon as blood glucose levels raise. Consequently, this might implicate an important role of UCP2 in β-cells. Involvement of UCP2 in diabetes and metabolic diseases is further supported by studies that showed an association of UCP2 single nucleotide polymorphisms (SNPs) with diabetes mellitus and obesity (Kosuge, 2008; Yu, 2005).

Changes in cellular metabolism, raise of oxidative stress and mitochondrial dysfunction are common issues in various cardiac and metabolic diseases. Due to its described function as a mitochondrial Ca^{2+} uptake regulator, UCP2 might thus represent a potential target for

the treatment of cardiac dysfunction.

7.3. Aging and neurodegeneration

Cellular aging is associated with multiple manifestations such as loss of proteostasis, mitochondrial dysfunction and cellular senescence (López-Otín et al., 2013), which need to be tackled to preserve the homeostasis of the organism. Compensatory processes elevate cellular energy requirements and induce changes in mitochondrial function (Sun et al., 2016), and interplay between mitochondria and other organelles (Madreiter-Sokolowski, 2019). Madreiter-Sokolowski *et al. 2019* showed that tethering between ER and mitochondria is increased in senescence, leading to enhanced mitochondrial respiration, augmented ROS levels, hence elevated SOD2 expression, and Resveratrol susceptibility (Madreiter-Sokolowski, 2019). Recent reports suggest a biphasic model of mitochondrial aging. A first phase of elevated ETC activity, ROS production and antioxidant defense is followed by a second phase, in which ROS levels remain high while the antioxidant defense descends (Madreiter-Sokolowski et al., 2018). Boosted metabolism in the first phase presumably meets the urge to compensate the initial signs of senescence but builds the basis for subsequent deterioration by increased ROS levels that damage proteins and DNA.

Since one of UCP2's multiple function is the regulation of Ca^{2+} uptake into mitochondria (Trenker et al., 2007), the involvement of UCP2 in the protection against aging-related health conditions becomes evident (Fig. 2; Table 2). $UCP2^{-/-}$ mice show reduced lifespan and body weight, while respiratory exchange rate and energy expenditure are increased (Hirose, 2016). Although this appears to be contradictory, since a decreased metabolism due to reduced Ca^{2+} import into the mitochondrial matrix would rather be expected, it can be explained by inefficient energy production. Furthermore, the increased superoxide levels in three-month-old $UCP2^{-/-}$ animals (Hirose, 2016) further support the role of UCP2 in aging protection. Rose *et al.* showed that several SNPs in UCP2-4 correlate with longevity (Rose et al., 2011), adding an extra line of evidence that individual regions of UCPs may have specific function (Waldeck-Weiermair, 2010a, 2010b). Two SNPs in the UCP2 gene were detected in a cohort of people aged between 64 and 105, who were born in Calabria (Rose et al., 2011). While SNP rs659366 showed no significance in any form, the wildtype of rs660339 seems to be correlated with longevity (Rose et al., 2011). In a study on the impact of UCP2 genotypes, interleukin 6 and ciliary neurotrophic factor on weight gain, significant effects of both UCP2 polymorphisms were observed depending on the genotypes of the other two proteins (Heidema, 2010). Although these data demonstrate that UCP2 polymorphisms and their effects on an organism depend on diverse factors, it is conclusive that the functionality of the protein is important to protect from aging and age-related morbidities.

In aging rats, a decrease of UCP3 in skeletal muscle has been observed (Kerner et al., 2001; Barazzoni and Nair, 2001), correlating with a decline in muscle mass and strength during aging (Yamada, 2018). This indicates that muscle atrophy occurs due to a shift in energy supply in order to uphold the organism's homeostasis, restricting skeletal muscle growth just enough to maintain mobility (Manini, 2010). Notably, age-related muscle atrophy can be counteracted by aerobic physical exercise which elevates UCP3 expression in skeletal muscle and other tissues (Gu, 2014; Morales, 2017).

Although few studies on the involvement of UCPs in neurodegenerative diseases have been conducted, the existing data indicate that these proteins might play a role in their progression and have a neuroprotective role in some cases. Primary hippocampal neurons challenged with β-amyloid peptide showed increased UCP2 expression levels (Jun, 2015), presumably to compensate protein misfolding by increasing the mitochondrial Ca^{2+} levels and, thus, ATP production. Brain samples of 26 months-old rats showed increased UCP2 expression (Mizuno et al., 2000), whereas, in brain biopsies of Alzheimer's disease patients all three brain-specific UCPs (UCP2, UCP4 and UCP5) were decreased (de la Monte and Wands, 2006). This shows that the expression of UCPs in neurons is highly regulated and may have a distinct role in the adaptation to neurodegenerative diseases.

Upregulated UCP2 expression levels have been linked to amyotrophic lateral sclerosis (ALS) progression (Peixoto, 2013) and metabolic reprogramming during ALS (Szelechowski, 2018). This concept was further supported by the finding that challenging SH-SY5Y cells with ROS leads to an increase in the expression of UCP2 and UCP4, resulting in elevated Ca^{2+} levels in the mitochondrial matrix (Wu et al., 2009). Notably, cells stably expressing wildtype or mutated β-amyloid precursor proteins showed reduced UCP2 expression in response to increased oxidative stress (Wu et al., 2009), hinting towards a more Ca^{2+}-related function of UCP2 in them. As these cells are already challenged with unfolded proteins, they lack the ability to respond to further stress factors, resulting in accelerated progression towards a phenotype of reduced metabolic activity, comparable to the late phase in the biphasic model of mitochondrial aging.

These studies indicate that UCP2 can have various roles and further research is required to unveil its complex molecular functions during aging and in neurodegenerative diseases.

8. Conclusions and future perspectives

In conclusion, UCP2 represents a viable target for the treatment of various age-related diseases such as cancer, neurodegenerative, metabolic and cardiovascular disorders. Consequently, further studies are required to consider the protein's wide range of functions and their potential implications. The involvement of UCP2 in the regulation of mitochondrial Ca^{2+} uptake is firmly established, and many effects attributed to UCP2 in health and disease could be explained by its involvement in mitochondrial Ca^{2+} homeostasis, while its uncoupling activity under physiological conditions is still under debate. With many new techniques available to us today, including super-resolution microscopy of live cells and a plethora of genetically encoded biosensors for different ions and metabolites that can be targeted to specific subcellular locations, we may expand our knowledge on the functional mechanism of UCP2 under various physiological and pathophysiological conditions.

Acknowledgements

FUNDING: Work in the WFG lab has been supported by the Austrian Science Fund (FWF), in particular by the Doctoral Program Metabolic and Cardiovascular Disease (DK-MCD W1226 to WFG), by Nikon Austria within the Nikon Center of Excellence, Graz, and MEFO-Graz. CMS is supported by an FWF-funded Erwin Schroedinger Abroad Fellowship (J4205-B27 to CMS). ZK, FEO MH, and OAB are supported by the Austrian Science Funds (DK-MCD W1226 to WFG), the Medical University of Graz and MEFO-Graz.

References

Groschner, L.N., Waldeck-Weiermair, M., Malli, R., Graier, W.F., 2012. Endothelial mitochondria–less respiration, more integration. Pflügers Arch. Eur. J. Physiol. 464, 63–76.
Madreiter-Sokolowski, C.T., et al., 2019. Tracking intra- and inter-organelle signaling of mitochondria. FEBS J. 286, 4378–4401.
Mitchell, P., 1961. Coupling of phosphorylation to electron and hydrogen transfer by a chemi-osmotic type of mechanism. Nature 191, 144–148.
Golic, I., et al., 2016. Methods for studying the localization of mitochondrial complexes III and IV by immunofluorescent and immunogold microscopy. Arch. Biol. Sci. 68, 767–772.
Brand, M.D., et al., 1999. The significance and mechanism of mitochondrial proton conductance. Int. J. Obes. 23, S4–S11.
Ricquier, D., Bouillaud, F., 2000. The uncoupling protein homologues: UCP1, UCP2, UCP3. StUCP and AtUCP. *Biochem. J.* 345, 161–179.
Ježek, P., Holendová, B., Garlid, K.D., Jabůrek, M., 2018. Mitochondrial Uncoupling Proteins: Subtle Regulators of Cellular Redox Signaling. Antioxid. Redox Signal. 29, 667–714.
Palou, A., Picó, C., Bonet, M.L., Oliver, P., 1998. The uncoupling protein, thermogenin.

Int. J. Biochem. Cell Biol. https://doi.org/10.1016/S1357-2725(97)00065-4.
Jabůrek, M., Ježek, J., Ježek, P., 2018. Cytoprotective activity of mitochondrial uncoupling protein-2 in lung and spleen. FEBS Open Bio 8, 692–701.
Su, J., et al., 2017. Cytoprotective Effect of the UCP2-SIRT3 Signaling Pathway by Decreasing Mitochondrial Oxidative Stress on Cerebral Ischemia-Reperfusion Injury. Int. J. Mol. Sci. 18, 1599.
Fleury, C., et al., 1997. Uncoupling protein-2: a novel gene linked to obesity and hyperinsulinemia. Nat. Genet. 15, 269–272.
Boss, O., et al., 1997. Uncoupling protein-3: A new member of the mitochondrial carrier family with tissue-specific expression. FEBS Lett. https://doi.org/10.1016/S0014-5793(97)00384-0.
Mao, W., et al., 1999. UCP4, a novel brain-specific mitochondrial protein that reduces membrane potential in mammalian cells. FEBS Lett. https://doi.org/10.1016/S0014-5793(98)01713-X.
Ramsden, D.B., et al., 2012. Human neuronal uncoupling proteins 4 and 5 (UCP4 and UCP5): structural properties, regulation, and physiological role in protection against oxidative stress and mitochondrial dysfunction. Brain Behav. 2, 468–478.
Sanchis, D., et al., 1998. BMCP1, a Novel Mitochondrial Carrier with High Expression in the Central Nervous System of Humans and Rodents, and Respiration Uncoupling Activity in Recombinant Yeast. J. Biol. Chem. 273, 34611–34615.
Carmona, M.C., et al., 1998. 9-cis Retinoic acid induces the expression of the uncoupling protein-2 gene in brown adipocytes. FEBS Lett. https://doi.org/10.1016/S0014-5793(98)01598-1.
Trenker, M., Malli, R., Fertschai, I., Levak-Frank, S., Graier, W.F., 2007. Uncoupling proteins 2 and 3 are fundamental for mitochondrial Ca^{2+} uniport. Nat. Cell Biol. 9, 445–452.
Žáčkova, M., Ježek, P., 2002. Reconstitution of Novel Mitochondrial Uncoupling Proteins UCP2 and UCP3. Biosci. Rep. 22, 33–46.
Jabůrek, M., et al., 1999. Transport Function and Regulation of Mitochondrial Uncoupling Proteins 2 and 3. J. Biol. Chem. 274, 26003–26007.
Couplan, E., et al., 2002. No Evidence for a Basal, Retinoic, or Superoxide-induced Uncoupling Activity of the Uncoupling Protein 2 Present in Spleen or Lung Mitochondria. J. Biol. Chem. 277, 26268–26275.
Kukat, A., et al., 2014. Loss of UCP2 attenuates mitochondrial dysfunction without altering ROS production and uncoupling activity. PLoS Genet. 10, e1004385.
Brookes, P.S., et al., 2008. UCPs–unlikely calcium porters. Nat. Cell Biol. 10, 1235–1240.
Trenker, M., Fertschai, I., Malli, R., Graier, W.F., 2008. UCP2/3 — likely to be fundamental for mitochondrial Ca^{2+} uniport. Nat. Cell Biol. 10, 1237–1240.
Mailloux, R.J., et al., 2011. Glutathionylation acts as a control switch for uncoupling proteins UCP2 and UCP3. J. Biol. Chem. 286, 21865–21875.
Donadelli, M., Dando, I., Fiorini, C., Palmieri, M., 2013. UCP2, a mitochondrial protein regulated at multiple levels. Cell. Mol. Life Sci. 71, 1171–1190.
Gimeno, R.E., et al., 1997. Cloning and Characterization of an Uncoupling Protein Homolog: A Potential Molecular Mediator of Human Thermogenesis. Diabetes 46, 900–906.
Rial, E., et al., 1999. Retinoids activate proton transport by the uncoupling proteins UCP1 and UCP2. EMBO J. https://doi.org/10.1093/emboj/18.21.5827.
Echtay, K.S., Murphy, M.P., Smith, R.A.J., Talbot, D.A., Brand, M.D., 2002. Superoxide Activates Mitochondrial Uncoupling Protein 2 from the Matrix Side: STUDIES USING TARGETED ANTIOXIDANTS. J. Biol. Chem. 277, 47129–47135.
Berardi, M.J., Chou, J.J., 2014. Fatty acid flippase activity of UCP2 is essential for its proton transport in mitochondria. Cell Metab. https://doi.org/10.1016/j.cmet.2014.07.004.
Garlid, K.D., Jabůrek, M., Ježek, P., 1998. The mechanism of proton transport mediated by mitochondrial uncoupling proteins. FEBS Letters. https://doi.org/10.1016/S0014-5793(98)01246-0.
Vidal-Puig, A., Solanes, G., Grujic, D., Flier, J.S., Lowell, B.B., 1997. UCP3: An uncoupling protein homologue expressed preferentially and abundantly in skeletal muscle and brown adipose tissue. Biochem. Biophys. Res. Commun. https://doi.org/10.1006/bbrc.1997.6740.
Hilse, K.E., et al., 2018. The expression of uncoupling protein 3 coincides with the fatty acid oxidation type of metabolism in adult murine heart. Front. Physiol. https://doi.org/10.3389/fphys.2018.00747.
Žáčková, M., Škobisová, E., Urbánková, E., Ježek, P., 2003. Activating ω-6 polyunsaturated fatty acids and inhibitory purine nucleotides are high affinity ligands for novel mitochondrial uncoupling proteins UCP2 and UCP3. J. Biol. Chem. https://doi.org/10.1074/jbc.M212850200.
Macher, G., et al., 2018. Inhibition of mitochondrial UCP1 and UCP3 by purine nucleotides and phosphate. Biochim. Biophys. Acta - Biomembr. https://doi.org/10.1016/j.bbamem.2017.12.001.
Pohl, E.E., Rupprecht, A., Macher, G., Hilse, K.E., 2019. Important trends in UCP3 investigation. Frontiers in Physiology. https://doi.org/10.3389/fphys.2019.00470.
Madreiter-Sokolowski, C.T., et al., 2016a. PRMT1-mediated methylation of MICU1 determines the UCP2/3 dependency of mitochondrial Ca^{2+} uptake in immortalized cells. Nat. Commun. 7, 12897.
Marchi, U. De, Castelbou, C., Demaurex, N., 2011. Uncoupling protein 3 (UCP3) modulates the activity of Sarco/endoplasmic reticulum Ca^{2+}-ATPase (SERCA) by decreasing mitochondrial ATP production. J. Biol. Chem. 286, 32533–32541.
Jiang, D., Zhao, L., Clapham, D.E., 2009. Genome-wide RNAi screen identifies Letm1 as a mitochondrial Ca^{2+}/H^{+} antiporter. Science 326, 144–147.
Waldeck-Weiermair, M., et al., 2010aaaa. Uncoupling protein 3 adjusts mitochondrial Ca^{2+} uptake to high and low Ca^{2+} signals. Cell Calcium 48, 288–301.
Waldeck-Weiermair, M., et al., 2010bbbb. The contribution of UCP2 and UCP3 to mitochondrial Ca^{2+} uptake is differentially determined by the source of supplied Ca^{2+}. Cell Calcium 47, 433–440.
Waldeck-Weiermair, M., et al., 2013. Molecularly Distinct Routes of Mitochondrial Ca^{2+} Uptake Are Activated Depending on the Activity of the Sarco/Endoplasmic Reticulum Ca^{2+} ATPase (SERCA). J. Biol. Chem. 288, 15367–15379.
Giacomello, M., et al., 2010. Ca^{2+} Hot Spots on the Mitochondrial Surface Are Generated by Ca^{2+} Mobilization from Stores, but Not by Activation of Store-Operated Ca^{2+} Channels. Mol. Cell 38, 280–290.
Csordás, G., et al., 2010. Imaging interorganelle contacts and local calcium dynamics at the ER-mitochondrial interface. Mol. Cell 39, 121–132.
Bondarenko, A.I., et al., 2015. UCP2 modulates single-channel properties of a MCU-dependent Ca^{2+} inward current in mitochondria. Pflügers Arch. Eur. J. Physiol. 467, 2509–2518.
Motloch, L.J., et al., 2016a. By Regulating Mitochondrial Ca^{2+}-Uptake UCP2 Modulates Intracellular Ca^{2+}. PLoS One 11, e0148359.
Motloch, L.J., et al., 2016b. UCP3 Regulates Single-Channel Activity of the Cardiac mCa1. J. Membr. Biol. 249, 577–584.
Hajnóczky, G., Robb-Gaspers, L.D., Seitz, M.B., Thomas, A.P., 1995. Decoding of cytosolic calcium oscillations in the mitochondria. Cell. https://doi.org/10.1016/0092-8674(95)90430-1.
Denton, R.M., 2009. Regulation of mitochondrial dehydrogenases by calcium ions. Biochim. Biophys. Acta - Bioenerg. 1787, 1309–1316.
Perocchi, F., et al., 2010. MICU1 encodes a mitochondrial EF hand protein required for Ca(2+) uptake. Nature 467, 291–296.
Stefani, D. De, Raffaello, A., Teardo, E., Szabò, I., Rizzuto, R., 2011. A forty-kilodalton protein of the inner membrane is the mitochondrial calcium uniporter. Nature 476, 336–340.
Baughman, J.M., et al., 2011. Integrative genomics identifies MCU as an essential component of the mitochondrial calcium uniporter. Nature 476, 341–345.
Raffaello, A., et al., 2013. The mitochondrial calcium uniporter is a multimer that can include a dominant-negative pore-forming subunit. EMBO J. 32, 2362–2376.
Sancak, Y., et al., 2013. EMRE is an essential component of the mitochondrial calcium uniporter complex. Science 342, 1379–1382.
Patron, M., et al., 2014. MICU1 and MICU2 finely tune the mitochondrial Ca^{2+} uniporter by exerting opposite effects on MCU activity. Mol. Cell 53, 726–737.
Kamer, K.J., Mootha, V.K., 2014. MICU1 and MICU2 play nonredundant roles in the regulation of the mitochondrial calcium uniporter. EMBO Rep. 15, 299–307.
Plovanich, M., et al., 2013. MICU2, a paralog of MICU1, resides within the mitochondrial uniporter complex to regulate calcium handling. PLoS One 8, e55785.
Patron, M., Granatiero, V., Espino, J., Rizzuto, R., Stefani, D. De., 2018. MICU3 is a tissue-specific enhancer of mitochondrial calcium uptake. Cell Death Differ. 26, 179–195.
Tomar, D., et al., 2016. MCUR1 Is a Scaffold Factor for the MCU Complex Function and Promotes Mitochondrial Bioenergetics. Cell Rep. 15, 1673–1685.
Yoshimatsu, M., et al., 2011. Dysregulation of PRMT1 and PRMT6, Type I arginine methyltransferases, is involved in various types of human cancers. Int. J. Cancer 128, 562–573.
Mathioudaki, K., et al., 2008. The PRMT1 gene expression pattern in colon cancer. Br. J. Cancer 99, 2094–2099.
Madreiter-Sokolowski, C.T., et al., 2017. UCP2 and PRMT1 are key prognostic markers for lung carcinoma patients. Oncotarget 8, 80278–80285.
Waldeck-Weiermair, M., et al., 2015. Rearrangement of MICU1 multimers for activation of MCU is solely controlled by cytosolic Ca(2.). Sci. Rep. 5, 15602.
Gottschalk, B., et al., 2019. MICU1 controls cristae junction and spatially anchors mitochondrial Ca^{2+} uniporter complex. Nat. Commun. 10, 3732.
Tomar, D., et al., 2019. MICU1 regulates mitochondrial cristae structure and function independent of the mitochondrial calcium uniporter channel. bioRxiv 803213. https://doi.org/10.1101/803213.
Porporato, P.E., Filigheddu, N., Pedro, J.M.B.-S., Kroemer, G., Galluzzi, L., 2018. Mitochondrial metabolism and cancer. Cell Res. 28, 265–280.
Fantin, V.R., St-Pierre, J., Leder, P., 2006. Attenuation of LDH-A expression uncovers a link between glycolysis, mitochondrial physiology, and tumor maintenance. Cancer Cell 9, 425–434.
Mazurek, S., 2011. Pyruvate kinase type M2: A key regulator of the metabolic budget system in tumor cells. Int. J. Biochem. Cell Biol. 43, 969–980.
Depaoli, M.R., et al., 2018. Real-Time Imaging of Mitochondrial ATP Dynamics Reveals the Metabolic Setting of Single Cells. Cell Rep. 25, 501–512.e3.
Baffy, G., Derdak, Z., Robson, S.C., 2011. Mitochondrial recoupling: a novel therapeutic strategy for cancer? Br. J. Cancer 105, 469–474.
Ayyasamy, V., et al., 2011. Cellular Model of Warburg Effect Identifies Tumor Promoting Function of UCP2 in Breast Cancer and Its Suppression by Genipin. PLoS One 6, e24792.
Yu, J., Shi, L., Lin, W., Lu, B., Zhao, Y., 2019. UCP2 promotes proliferation and chemoresistance through regulating the NF-κB/β-catenin axis and mitochondrial ROS in gallbladder cancer. Biochem. Pharmacol. 172, 113745.
Li, W., et al., 2015. UCP2 Knockout Suppresses Mouse Skin Carcinogenesis. Cancer Prev. Res. 8, 487–491.
Chakraborty, P.K., et al., 2017. MICU1 drives glycolysis and chemoresistance in ovarian cancer. Nat. Commun. 8, 14634.
Madreiter-Sokolowski, C.T., et al., 2016b. Resveratrol Specifically Kills Cancer Cells by a Devastating Increase in the Ca^{2+} Coupling Between the Greatly Tethered Endoplasmic Reticulum and Mitochondria. Cell. Physiol. Biochem. 39, 1404–1420.
Kwong, J.Q., Molkentin, J.D., 2015. Physiological and pathological roles of the mitochondrial permeability transition pore in the heart. Cell Metab. 21, 206–214.
Nagy, Á., Lánczky, A., Menyhárt, O., Gyorffy, B., 2018. Validation of miRNA prognostic power in hepatocellular carcinoma using expression data of independent datasets. Sci. Rep. https://doi.org/10.1038/s41598-018-27521-y.
Liu, C.H., et al., 2020. Inhibition of Uncoupling Protein 2 Enhances the Radiosensitivity of Cervical Cancer Cells by Promoting the Production of Reactive Oxygen Species. Oxid. Med. Cell. Longev. 2020, 1–13.

Pons, D.G., et al., 2015. UCP2 inhibition sensitizes breast cancer cells to therapeutic agents by increasing oxidative stress. Free Radic. Biol. Med. 86, 67–77.
Kawanishi, M., et al., 2018. Expression of UCP2 is associated with sensitivity to platinum-based chemotherapy for ovarian serous carcinoma. Oncol. Lett. 15, 9923–9928.
Yu, G., Liu, J., Xu, K., Dong, J., 2015. Uncoupling protein 2 mediates resistance to gemcitabine-induced apoptosis in hepatocellular carcinoma cell lines. Biosci. Rep. 35, e00231.
Kreiter, J., et al., 2018. Genipin Lacks the Specificity for UCP2 Inhibition. Biophys. J. https://doi.org/10.1016/j.bpj.2017.11.3556.
Robert, V., et al., 2001. Beat-to-beat oscillations of mitochondrial [Ca^{2+}] in cardiac cells. EMBO J. 20, 4998–5007.
Wiersma, M., et al., 2019. Mitochondrial Dysfunction Underlies Cardiomyocyte Remodeling in Experimental and Clinical Atrial Fibrillation. Cells 8, 1202.
Larbig, R., et al., 2017. Through modulation of cardiac Ca^{2+} handling, UCP2 affects cardiac electrophysiology and influences the susceptibility for Ca^{2+}-mediated arrhythmias. Exp Physiol 102, 650–662.
Santulli, G., Xie, W., Reiken, S.R., Marks, A.R., 2015. Mitochondrial calcium overload is a key determinant in heart failure. Proc Natl Acad Sci USA 112, 11389.
Li, N., Karaca, M., Maechler, P., 2017. Upregulation of UCP2 in beta-cells confers partial protection against both oxidative stress and glucotoxicity. Redox Biol. 13, 541–549.
McLeod, C.J., Aziz, A., Hoyt, R.F., McCoy, J.P., Sack, M.N., 2005. Uncoupling Proteins 2 and 3 Function in Concert to Augment Tolerance to Cardiac Ischemia. J. Biol. Chem. 280, 33470–33476.
Blanc, J., et al., 2003. Protective Role of Uncoupling Protein 2 in Atherosclerosis. Circulation 107, 388–390.
Moukdar, F., et al., 2009. Reduced antioxidant capacity and diet-induced atherosclerosis in uncoupling protein-2-deficient mice. J. Lipid Res. 50, 59–70.
Wu, H., et al., 2019. UCP2 protect the heart from myocardial ischemia/reperfusion injury via induction of mitochondrial autophagy. J Cell Biochem 120, 15455–15466.
Motloch, L.J., Reda, S., Wolny, M., Hoppe, U.C., 2015. UCP2 Modulates Cardioprotective Effects of Ru360 in Isolated Cardiomyocytes during Ischemia. Pharmaceuticals 8, 474–482.
Hansson, G.K., Hermansson, A., 2011. The immune system in atherosclerosis. Nat. Immunol. 12, 204–212.
Moore, K.J., Tabas, I., 2011. Macrophages in the Pathogenesis of Atherosclerosis. Cell 145, 341–355.
Vats, D., et al., 2006. Oxidative metabolism and PGC-1beta attenuate macrophage-mediated inflammation. Cell Metab. 4, 13–24.
West, A.P., et al., 2011. TLR signalling augments macrophage bactericidal activity through mitochondrial ROS. Nature 472, 476–480.
Imtiyaz, H.Z., Simon, M.C., 2010. Hypoxia-inducible factors as essential regulators of inflammation. Curr. Top. Microbiol. Immunol. 345, 105–120.
Kim, J., Tchernyshyov, I., Semenza, G.L., Dang, C.V., 2006. HIF-1-mediated expression of pyruvate dehydrogenase kinase: A metabolic switch required for cellular adaptation to hypoxia. Cell Metab. 3, 177–185.
Je-Won, R., et al., 2004. Overexpression of Uncoupling Protein 2 in THP1 Monocytes Inhibits β2 Integrin-Mediated Firm Adhesion and Transendothelial Migration. Arterioscler. Thromb. Vasc. Biol. 24, 864–870.
Schaftenaar, F., Frodermann, V., Kuiper, J., Lutgens, E., 2016. Atherosclerosis: the interplay between lipids and immune cells. Curr. Opin. Lipidol. 27.
Depaoli, M.R., Hay, J.C., Graier, W.F., Malli, R., 2019. The enigmatic ATP supply of the endoplasmic reticulum. Biol. Rev. Camb. Philos. Soc. 94, 610–628.
Kim, J.D., Yoon, N.A., Jin, S., Diano, S., 2019. Microglial UCP2 Mediates Inflammation and Obesity Induced by High-Fat Feeding. Cell Metab. 30, 952–962.e5.
Lukyanenko, V., Chikando, A., Lederer, W.J., 2009. Mitochondria in cardiomyocyte Ca^{2+} signaling. International Journal of Biochemistry and Cell Biology. https://doi.org/10.1016/j.biocel.2009.03.011.
Stanley, W.C., Recchia, F.A., Lopaschuk, G.D., 2005. Myocardial Substrate Metabolism in the Normal and Failing Heart. Physiol. Rev. 85, 1093–1129.
Qiancong, Z., Qianchuang, S., Lufang, Z., Kexiang, L., Kai, J., 2019. Complex Regulation of Mitochondrial Function During Cardiac Development. J. Am. Heart Assoc. 8, e012731.
Allard, M.F., Schonekess, B.O., Henning, S.L., English, D.R., Lopaschuk, G.D., 1994. Contribution of oxidative metabolism and glycolysis to ATP production in hypertrophied hearts. Am. J. Physiol. Circ. Physiol. 267, H742–H750.
Jay, D.T., Lawrence, D.G., Guoqiang, W., Andrew, P.T., 2010. Uncoupling Protein-2 Modulates Myocardial Excitation-Contraction Coupling. Circ. Res. 106, 730–738.
Klec, C., et al., 2019a. Glycogen synthase kinase 3 beta controls presenilin-1-mediated endoplasmic reticulum Ca^{2+} leak directed to mitochondria in pancreatic islets and β-cells. Cell. Physiol. Biochem. https://doi.org/10.33594/000000005.
Klec, C., et al., 2019b. Presenilin-1 Established ER-Ca^{2+} Leak: a Follow Up on Its Importance for the Initial Insulin Secretion in Pancreatic Islets and beta-Cells upon Elevated Glucose. Cell. Physiol. Biochem. 53, 573–586.
Kosuge, K., et al., 2008. Human uncoupling protein 2 and 3 genes are associated with obesity in Japanese. Endocrine. https://doi.org/10.1007/s12020-008-9111-9.
Yu, X., et al., 2005. The uncoupling protein 2 Ala55Val polymorphism is associated with diabetes mellitus: The CARDIA study. Clin. Chem. https://doi.org/10.1373/clinchem.2004.044859.
López-Otín, C., Blasco, M.A., Partridge, L., Serrano, M., Kroemer, G., 2013. The hallmarks of aging. Cell 153, 1194–1217.
Sun, N., Youle, R.J., Finkel, T., 2016. The Mitochondrial Basis of Aging. Molecular Cell. https://doi.org/10.1016/j.molcel.2016.01.028.
Madreiter-Sokolowski, C.T., et al., 2019. Enhanced inter-compartmental Ca^{2+} flux modulates mitochondrial metabolism and apoptotic threshold during aging. Redox Biol. 20, 458–466.
Madreiter-Sokolowski, C.T., Sokolowski, A.A., Waldeck-Weiermair, M., Malli, R., Graier, W.F., 2018. Targeting mitochondria to counteract age-related cellular dysfunction. Genes. https://doi.org/10.3390/genes9030165.
Hirose, M., et al., 2016. Uncoupling protein 2 protects mice from aging. Mitochondrion 30, 42–50.
Rose, G., Crocco, P., Rango, F. De, Montesanto, A., Passarino, G., 2011. Further support to the uncoupling-to-survive theory: the genetic variation of human UCP genes is associated with longevity. PLoS One 6, e29650.
Heidema, A.G., et al., 2010. Sex-specific effects of CNTF, IL6 and UCP2 polymorphisms on weight gain. Physiol. Behav. https://doi.org/10.1016/j.physbeh.2009.10.002.
Kerner, J., Turkaly, P.J., Minkler, P.E., Hoppel, C.L., 2001. Aging skeletal muscle mitochondria in the rat: decreased uncoupling protein-3 content. Am. J. Physiol. Metab. 281, E1054–E1062.
Barazzoni, R., Nair, K.S., 2001. Changes in uncoupling protein-2 and -3 expression in aging rat skeletal muscle, liver, and heart. Am. J. Physiol. Metab. 280, E413–E419.
Yamada, Y., 2018. Muscle Mass, Quality, and Composition Changes During Atrophy and Sarcopenia. Adv. Exp. Med. Biol. 1088, 47–72.
Manini, T.M., 2010. Energy expenditure and aging. Ageing Research Reviews. https://doi.org/10.1016/j.arr.2009.08.002.
Gu, Q., et al., 2014. Chronic aerobic exercise training attenuates aortic stiffening and endothelial dysfunction through preserving aortic mitochondrial function in aged rats. Exp. Gerontol. 56, 37–44.
Morales, F.E., et al., 2017. BAIBA Does Not Regulate UCP-3 Expression in Human Skeletal Muscle as a Response to Aerobic Exercise. J. Am. Coll. Nutr. 36, 1–10.
Jun, Z., et al., 2015. UCP2 protects against amyloid beta toxicity and oxidative stress in primary neuronal culture. Biomed. Pharmacother. = Biomédecine pharmacothérapie 74, 211–214.
Mizuno, T., Miura-Suzuki, T., Yamashita, H., Mori, N., 2000. Distinct Regulation of Brain Mitochondrial Carrier Protein-1 and Uncoupling Protein-2 Genes in the Rat Brain during Cold Exposure and Aging. Biochem. Biophys. Res. Commun. 278, 691–697.
de la Monte, Suzanne M., Wands, Jack R., 2006. Molecular indices of oxidative stress and mitochondrial dysfunction occur early and often progress with severity of Alzheimer's disease. *J. Alzheimer's Dis.* 9, 167–181.
Peixoto, P.M., et al., 2013. UCP2 overexpression worsens mitochondrial dysfunction and accelerates disease progression in a mouse model of amyotrophic lateral sclerosis. Mol. Cell. Neurosci. 57, 104–110.
Szelechowski, M., et al., 2018. Metabolic Reprogramming in Amyotrophic Lateral Sclerosis. Sci. Rep. 8, 3953.
Wu, Z., Zhang, J., Zhao, B., 2009. Superoxide anion regulates the mitochondrial free ca 2+ through uncoupling proteins. Antioxidants Redox Signal. https://doi.org/10.1089/ars.2009.2427.
Romancer, M. Le, Treilleux, I., Bouchekioua-Bouzaghou, K., Sentis, S., Corbo, L., 2010. Methylation, a key step for nongenomic estrogen signaling in breast tumors. Steroids 75, 560–564.
Pozza, E.D., et al., 2012. Role of mitochondrial uncoupling protein 2 in cancer cell resistance to gemcitabine. Biochim. Biophys. Acta 1823, 1856–1863.
Majumder, S., Liu, Y., Ford, O.H., Mohler, J.L., Whang, Y.E., 2006. Involvement of arginine methyltransferase CARM1 in androgen receptor function and prostate cancer cell viability. Prostate 66, 1292–1301.
Papkovskaia, T.D., et al., 2012. G2019s leucine-rich repeat kinase 2 causes uncoupling protein-mediated mitochondrial depolarization. Hum. Mol. Genet. https://doi.org/10.1093/hmg/dds244.
Ikenaka, K., et al., 2019. Increase of arginine dimethylation correlates with the progression and prognosis of ALS. Neurology. https://doi.org/10.1212/WNL.0000000000007311.
McKetney, J., et al., 2019. Proteomic Atlas of the Human Brain in Alzheimer's Disease. J. Proteome Res. https://doi.org/10.1021/acs.jproteome.9b00004.
Andrews, Z.B., Horvath, T.L., 2009. Uncoupling protein-2 regulates lifespan in mice. Am. J. Physiol. - Endocrinol. Metab. https://doi.org/10.1152/ajpendo.90903.2008.

communications biology

ARTICLE

Check for updates

OPEN

Citrin mediated metabolic rewiring in response to altered basal subcellular Ca^{2+} homeostasis

Zhanat Koshenov[1], Furkan E. Oflaz[1], Martin Hirtl[1], Benjamin Gottschalk[1], Rene Rost[1], Roland Malli[1,2] & Wolfgang F. Graier[1,2]✉

In contrast to long-term metabolic reprogramming, metabolic rewiring represents an instant and reversible cellular adaptation to physiological or pathological stress. Ca^{2+} signals of distinct spatio-temporal patterns control a plethora of signaling processes and can determine basal cellular metabolic setting, however, Ca^{2+} signals that define metabolic rewiring have not been conclusively identified and characterized. Here, we reveal the existence of a basal Ca^{2+} flux originating from extracellular space and delivered to mitochondria by Ca^{2+} leakage from inositol triphosphate receptors in mitochondria-associated membranes. This Ca^{2+} flux primes mitochondrial metabolism by maintaining glycolysis and keeping mitochondria energized for ATP production. We identified citrin, a well-defined Ca^{2+}-binding component of malate-aspartate shuttle in the mitochondrial intermembrane space, as predominant target of this basal Ca^{2+} regulation. Our data emphasize that any manipulation of this ubiquitous Ca^{2+} system has the potency to initiate metabolic rewiring as an instant and reversible cellular adaptation to physiological or pathological stress.

[1] Molecular Biology and Biochemistry, Gottfried Schatz Research Center, Medical University of Graz, Neue Stiftingtalstraße 6/6, 8010 Graz, Austria. [2] BioTechMed Graz, 8010 Graz, Austria. ✉email: wolfgang.graier@medunigraz.at

etabolic rewiring represents a hallmark in cellular adaptations to physiological (e.g. anaerobic glycolysis upon lack of oxygen during exercise)[1] and pathological stress (e.g. metabolic overflow or cancer)[2–4]. To achieve an instant and reversible adaptation, such processes particularly require minimal effort to yield maximal effect when affecting basic settings of cellular metabolism. It is tempting to speculate that Ca^{2+}, a ubiquitous second messenger with a plethora of effector proteins[5], is involved in such control of basal metabolic setting of a cell. Notably, for a cell's survival and wellbeing, the cellular Ca^{2+} homeostasis has to function correctly despite all kinds of physiological and pathological challenges the cell may face[6]. Mitochondria, the powerhouses of cells, are known to be tightly regulated by Ca^{2+} ions[7,8], and understanding the basic regulation processes of mitochondrial bioenergetics represents an important task considering the fundamental role of this organelle in the cell's energy metabolism and involvements in multiple signaling cascades[9].

The foremost source of Ca^{2+} for mitochondria is the endoplasmic reticulum (ER)[10]. Upon cell stimulation with an inositol 1,4,5-trisphosphate- (IP_3-) generating agonist, the transfer of Ca^{2+} from ER to mitochondria occurs predominantly in specialized regions called Mitochondria Associated ER membranes (MAMs)[10]. Thereby Ca^{2+} passes the outer mitochondrial membrane (OMM) through voltage-dependent anion channels (VDACs)[11] into the mitochondrial inter-membrane space (IMS), where it needs to surpass a certain threshold to finally be taken up to mitochondrial matrix by mitochondrial calcium uniporter complex (MCUC)[12–15]. This flux of Ca^{2+} from ER to mitochondria is known to regulate vital processes in the mitochondrial matrix, including the activity of Ca^{2+} sensitive mitochondrial dehydrogenases[16].

Alteration in ER-mitochondria communication is reported to be involved in numerous pathological conditions, including ER stress[17], age-related diseases, such as cancer[18] and neurodegeneration[19], and metabolic and cardiovascular disorders[20]. During early stages of ER stress, cells develop a small ER Ca^{2+} leak that is sensed by mitochondria, which boosts mitochondrial ATP production to ensure proper energy support counteracting hampered ER protein folding[17,21]. Progression of ER stress triggers significant Ca^{2+} loss from the ER yielding long-term mitochondrial Ca^{2+} overload resulting in mitochondrial dysfunction and, eventually, the initiation of apoptotic cell death[22]. Accordingly, ER Unfolded Protein Response (UPR) during aging is associated with enforced ER-mitochondria tethering[23,24], which may eventually result in mitochondrial Ca^{2+} overload and, thus, can explain aging-associated oxidative stress[23] and apoptotic cell death[25]. Notably, mitochondrial bioenergetics and regulation of mitochondrial Ca^{2+} uptake are also greatly changed in cancer[26,27], where alterations in mitochondrial Ca^{2+} signaling play a role in cancer resistance to chemotherapy and increased metastasis[28,29]. Hence, in many metabolic and neurodegenerative diseases, mitochondrial Ca^{2+} signaling and ER-mitochondria crosstalk are altered, resulting in changes in mitochondrial bioenergetics that add to the disease progression and outcome[20], pointing to fundamental importance of ER to mitochondrion Ca^{2+} crosstalk and its alterations in cellular physiology and pathology.

Although it is widely assumed that the mitochondrial matrix residing Ca^{2+}-sensitive dehydrogenases are the end-point receivers of changes in mitochondrial Ca^{2+} signaling, an in-depth analysis of the contribution of basal Ca^{2+} homeostasis on mitochondrial bioenergetics and other possible players being involved in the putative Ca^{2+} control of the cell's resting metabolic settings has not been performed so far. In order to understand how basal Ca^{2+} homeostasis affects mitochondrial wellbeing, especially regarding their main attribute, energy production, we sought to study the regulation of basal mitochondrial bioenergetics by resting Ca^{2+} homeostasis. A clear understanding of this fundamental process of basal Ca^{2+} regulation of mitochondrial bioenergetics will help us to tackle many pathologies involving altered mitochondrial Ca^{2+} signaling and inter-organellar communication and would shed light on metabolic rewiring capability of resting Ca^{2+} homeostasis.

We have adapted a simple model to address this question that enabled us to slightly reduce basal Ca^{2+} level in the cytosol, ER, IMS, and matrix. Consequently, we distinguished between two main mechanisms of Ca^{2+} regulation of basal mitochondrial bioenergetics, the mitochondrial surface Ca^{2+}-controlled citrin in the IMS, and the MCU-dependent matrix Ca^{2+}-sensitive dehydrogenases. We also studied Ca^{2+} dependent mitochondrial pyruvate utilization and explored the importance of MAM vs. cytosolic Ca^{2+} for the regulation of basal mitochondrial bioenergetics. Notably, we have shown that a small decrease in IMS Ca^{2+} level strongly affects the cell's metabolism by switching it to a state of pseudo hypoxia, whereupon the cell relies less on mitochondria and more on glycolysis for energy production despite the presence of oxygen.

Results

Short-term removal of extracellular Ca^{2+} controls mitochondrial bioenergetics despite minor effects on matrix Ca^{2+} level. To establish a protocol that minimally perturbs basal subcellular Ca^{2+} homeostasis affecting the mitochondria and sub-mitochondrial compartments, we implemented a seemingly easy and widely used method of removing extracellular Ca^{2+}. Removal of extracellular Ca^{2+} yielded a very small drop in basal cytosolic Ca^{2+} level (Fig. 1a, i) that was accompanied with similar attenuations in the ER (Fig. 1a, ii), IMS (Fig. 1, iii) and the mitochondrial matrix (Fig. 1a, iv) within the first 5–7 min (Supplementary Fig. 1a–i) in cells of the human endothelial cell line EA.hy926.

Short-term removal of extracellular Ca^{2+} did not change the number of ER-mitochondria contacts sites (MAMs) (Fig. 1b, c), and that of ER-Plasma Membrane (PM) contacts (Fig. 1d, e, left panel). However, removal of extracellular Ca^{2+} decreased the average size of ER-PM contact sites (Fig. 1e, middle panel) and the total area of ER in the PM proximity (Fig. 1e, right panel).

In order to reveal the effect of disturbance in the cell's basal Ca^{2+} homeostasis on mitochondrial bioenergetics, we tested the main attribute the mitochondria are known for, the ATP synthesis. Mitochondrial ATP producing capability was assessed by administering ATP synthase inhibitor oligomycin while measuring mitochondrial ATP level ($[ATP]_{mito}$) using genetically encoded ATP sensor mtAT1.03[30]. The drop in $[ATP]_{mito}$ upon the administration of oligomycin reflects the actual ATP production by mitochondria (Fig. 2a, c). Disturbing basal mitochondrial Ca^{2+} level by the means of extracellular Ca^{2+} removal prior to oligomycin addition resulted in an increase of $[ATP]_{mito}$ in response to oligomycin in app. 35% of the cells (Fig. 2b, c). This increase in mitochondrial ATP in response to oligomycin indicates that in one-third of all cells tested in the absence of extracellular Ca^{2+} the ATP synthase switched its direction and started to consume ATP instead of producing it. In the remaining two-thirds of the cells perfused with Ca^{2+} free buffer, mitochondrial ATP production was significantly diminished (Fig. 2c). The reversal of mitochondrial ATP synthase and reduction of ATP production in response to Ca^{2+} imbalance were rescued by returning to nutrient supplemented Ca^{2+} containing buffer for 10 min after Ca^{2+} removal (Fig. 2c), pointing to a dynamic regulation and versatility of this Ca^{2+} dependent phenomenon. In almost all of the measured cells, switching to

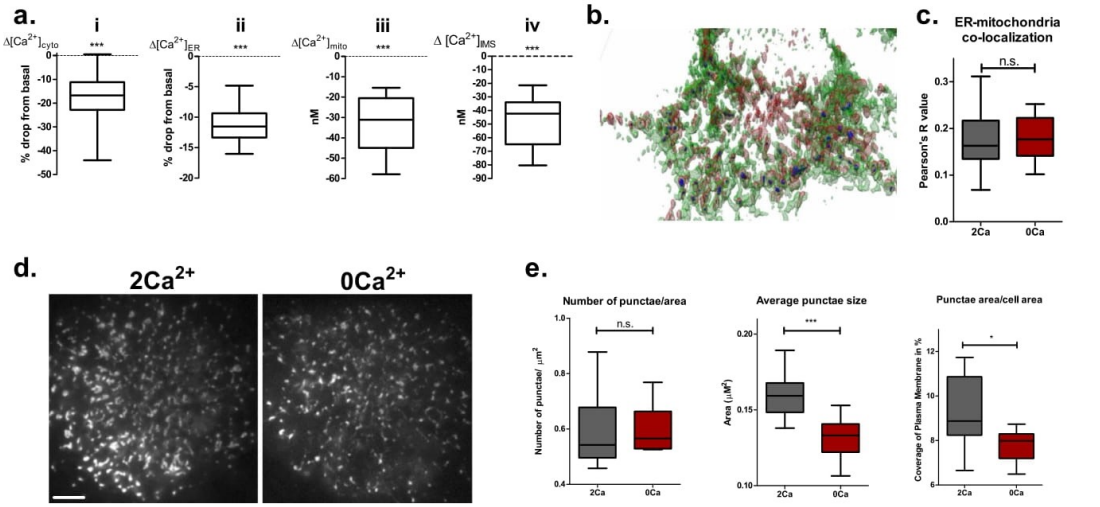

Fig. 1 Removal of extracellular Ca^{2+} triggers basal Ca^{2+} drop in intracellular compartments and affects ER-PM contact cites. a Removal of extracellular Ca^{2+} reduces basal Ca^{2+} levels in cytosol ($n = 64$), ER ($n = 17$), IMS ($n = 13$), and mitochondria ($n = 21$). **b** Exemplary 3D reconstruction of EA.hy926 cell with pseudo- colored ER (green) and mitochondria (red) used for analysis of ER-mitochondria contacts (dark blue). **c** Analysis of ER-mitochondria contacts ($n = 22$, unpaired *t*-test; n.s.; $p = 0.68$). **d** Exemplary TIRF images of ER in the plasma membrane proximity in 2 Ca^{2+} (left) and 0 Ca^{2+} (right) conditions, scale bar (left bottom corner) is 5 µm. **e** Statistical analysis of ER-PM contacts (unpaired *t*-test, $n = 9$; n.s. $p = 0.92$,; $^{*}p = 0.018$; $^{***}p = 0.004$).

Ca^{2+} free buffer is followed by a slow reduction of $[ATP]_{mito}$, suggesting that the reduced activity of the ATP synthase precedes its reversal (Fig. 2b, d).

Simultaneous measurement of mitochondrial membrane potential (Ψ_{mito}) and $[ATP]_{mito}$ allowed us to monitor the contribution of the reversed mode of ATP synthase to maintaining Ψ_{mito} under the condition of reduced basal Ca^{2+}. In cells with intact basal subcellular Ca^{2+} homeostasis, Ψ_{mito} remained stable even upon the addition of oligomycin (Fig. 2a). In contrast, in cells with perturbed basal subcellular Ca^{2+} homeostasis (i.e., in the absence of extracellular Ca^{2+}), oligomycin initiated a strong and continuous decrease in Ψ_{mito} (Fig. 2b).

To clarify the effect of the perturbed basal Ca^{2+} homeostasis achieved by removal of extracellular Ca^{2+} on mitochondrial bioenergetics, mitochondrial NADH production, which is regulated by Ca^{2+}[31,32] was measured. While basal NADH levels were comparable, maximum NADH production was strongly reduced under condition of perturbed basal Ca^{2+} homeostasis (Fig. 2e, f). This points to insufficient mitochondrial NADH production and inability to fuel electron transport chain (ETC) in the absence of extracellular Ca^{2+}. Hence, the reduced ETC activity also provides a potential reason for the reduced ATP production and reversal of ATP synthase, whereupon ATP synthase is reversed in order to prevent the total collapse of Ψ_{mito}. Similar to mitochondrial ATP, NADH production in cells with disturbed subcellular Ca^{2+} homeostasis can be rescued by Ca^{2+} re-addition (Supplementary Fig. 2a, b).

To further test our assumptions, mitochondrial respiration was measured. In the absence of extracellular Ca^{2+}, basal, maximal, and ATP-coupled oxygen consumption rates (OCR) were reduced in cell populations (Fig. 2g, h), thus, confirming the results obtained with single-cell ATP and NADH measurements mentioned above. Accordingly, our data indicate that besides the fundamental role of Ca^{2+} as a crucial mediator during cell stimulation, basal subcellular Ca^{2+} homeostasis greatly controls resting mitochondrial bioenergetics. Additionally, the findings point to a pivotal role of extracellular Ca^{2+} in maintaining basal subcellular Ca^{2+} homeostasis.

Acute perturbation of subcellular Ca^{2+} homeostasis only minimally affects mitochondrial NADH production by Ca^{2+} sensitive dehydrogenases. To test whether the drop in basal matrix Ca^{2+} upon transient removal of extracellular Ca^{2+} and the subsequent reduction in basal activity of matrix dehydrogenases are responsible for altered mitochondrial metabolism, we performed NADH measurements in the presence of pyruvate (1 mM) to overcome potential substrate limitations due to subcellular Ca^{2+} misbalance. Pyruvate supplementation resulted in elevated basal NADH level (Fig. 3a) and showed no difference in NADH production between control and 0 Ca^{2+} conditions (Fig. 3b, c), thus, indicating that the diminished NADH production upon removal of extracellular Ca^{2+} was unlikely to be due to reduced mitochondrial dehydrogenase activity. To further test this assumption, the activity of pyruvate dehydrogenase (PDH), which is known to be indirectly regulated by Ca^{2+}[33,34], was assessed by measuring mitochondrial citrate production under extracellularly added pyruvate (1 mM) using the mitochondrial-targeted genetically encoded citrate sensor CitrON[35]. Mitochondrial PDH activity was not affected by alterations in the basal subcellular Ca^{2+} homeostasis as indicated by the identical increase in mitochondrial citrate upon pyruvate administration under control and absence of extracellular Ca^{2+} conditions (Fig. 3d, e). Additionally, by measuring mitochondrial pyruvate with matrix targeted PyronicSF[36], we showed that mitochondrial pyruvate uptake was also not affected by acute Ca^{2+} deprivation (Fig. 3f, g). But, as it is known that pyruvate itself, as well as NADH and ATP/ADP ratio, can affect PDH phosphorylation and thus its activity[37], we assessed the phosphorylation status of PDH under our experimental conditions (Fig. 3h, i, Supplementary fig. 3). Short-term removal of extracellular Ca^{2+} only slightly increased the phosphorylation of PDH,

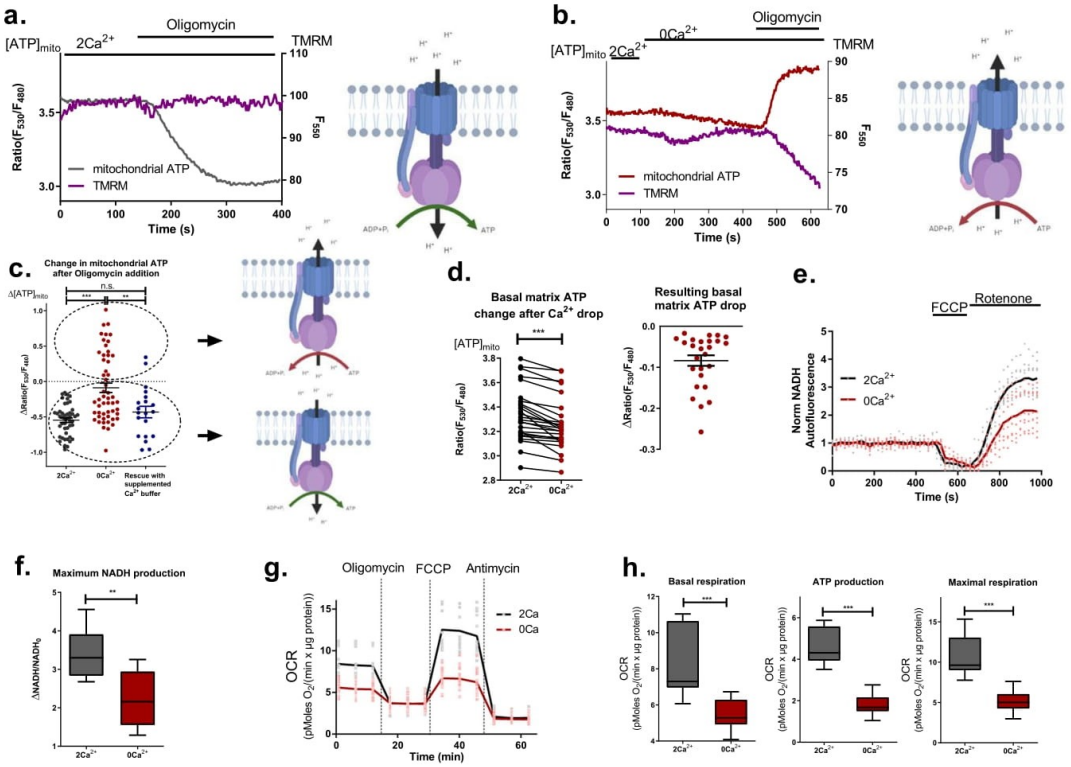

Fig. 2 Perturbance of basal Ca^{2+} homeostasis alters mitochondrial bioenergetics. a Representative control traces of simultaneous measurements of $[ATP]_{mito}$ and Ψ_{mito} using mtAT1.03 and TMRM, respectively. On the right, a graphical illustration of the ATP synthase mode is depicted (Created with BioRender.com.). **b** Representative traces of $[ATP]_{mito}$ and Ψ_{mito} in 0 extracellular Ca^{2+}. Graphical representation of the ATP synthase mode is depicted on the right (Created with BioRender.com.). **c** Statistical analysis of the change in $[ATP]_{mito}$ after 2 µM oligomycin with graphical illustration of ATP synthase modes on the right (Created with BioRender.com.) (One-way ANOVA with Tukey's multiple comparison test, $n = 46$ for 2 Ca^{2+}, $n = 53$ for 0 Ca^{2+}, $n = 20$ for the rescue experiment; $^{***}p < 0.001$, $^{**}p < 0.01$). **d** Statistical analysis of the change in $[ATP]_{mito}$ after 5 min in 0 Ca^{2+} buffer (on the left) (paired *t*-test, $n = 26$; $^{***}p < 0.0001$). **e** Average traces (solid lines) and single data points of mitochondrial NADH autofluorescence measurements. **f** Respective statistical analysis of maximal NADH production (unpaired *t*-test, $n = 8$; $^{**}p = 0.004$). **g** Average traces (solid lines) and single data points of OCR measurements. **h** Respective statistical analysis of OCR data from **g** (unpaired *t*-test, $n = 17$ for 2 Ca^{2+}, $n = 25$ for 0 Ca^{2+}; $^{***}p < 0.0001$).

with much greater increase after 1 h (Fig. 3h, i), indicating that there might be an additional effect of short-term removal of extracellular Ca^{2+} beside its influence on PDH phosphorylation.

Perturbance in basal subcellular Ca^{2+} homeostasis induces metabolic rewiring. Interestingly, while OCR data did not clarify the mechanism of how perturbation in intracellular Ca^{2+} homeostasis affects mitochondrial bioenergetics despite the differences observed (Fig. 2g), the elevation of extracellular acidification rate (ECAR) upon the removal of extracellular Ca^{2+} (Fig. 4a) points at a possible increased lactate production and, thus, metabolic rewiring caused by the disturbed subcellular Ca^{2+} homeostasis.

To further explore the observed metabolic changes upon perturbations in basal subcellular Ca^{2+} homeostasis, cytosolic lactate level was assessed. Notably, removal of extracellular Ca^{2+} yielded instant accumulation of cytosolic lactate (Fig. 4b, c), which is in line with increased ECAR (Fig. 4a). To understand if this lactate accumulation was metabolically relevant, we measured lactate under glucose-free conditions and observed that lactate accumulation in response to Ca^{2+} removal was gone in the absence of glucose (Fig. 4d). Glucose utilization and uptake were not affected by the removal of Ca^{2+} (Fig. 4e). Because cellular lactate level is tightly correlated with cytosolic $NADH/NAD^+$ balance, we tested the cytosolic redox state in order to better understand the mechanism behind lactate accumulation. By measuring cytosolic $NADH/NAD^+$ ratio with genetically encoded sensor Peredox[38] we observed an increase in the $NADH/NAD^+$ ratio under the condition of disturbed subcellular Ca^{2+} homeostasis (Fig. 4f–h). This observation provides a possible link between redox misbalance and lactate accumulation, since upon increase of cytosolic $NADH/NAD^+$ ratio lactate dehydrogenase (LDH) may convert pyruvate to lactate in order to restore the redox balance, which, in turn, would result in increased lactate production[39] and metabolic rewiring. Excitingly, the metabolic rewiring achieved by perturbed basal subcellular Ca^{2+} homeostasis was reversible by Ca^{2+} re-addition (Supplementary Fig. 4a–c).

Citrin is responsible for cytosolic and mitochondrial metabolic rewiring during disturbed subcellular Ca^{2+} homeostasis. Among several Ca^{2+}-sensitive proteins involved in cytosolic and mitochondrial redox balance and metabolism, the calcium-binding mitochondrial carrier protein citrin, which resides in

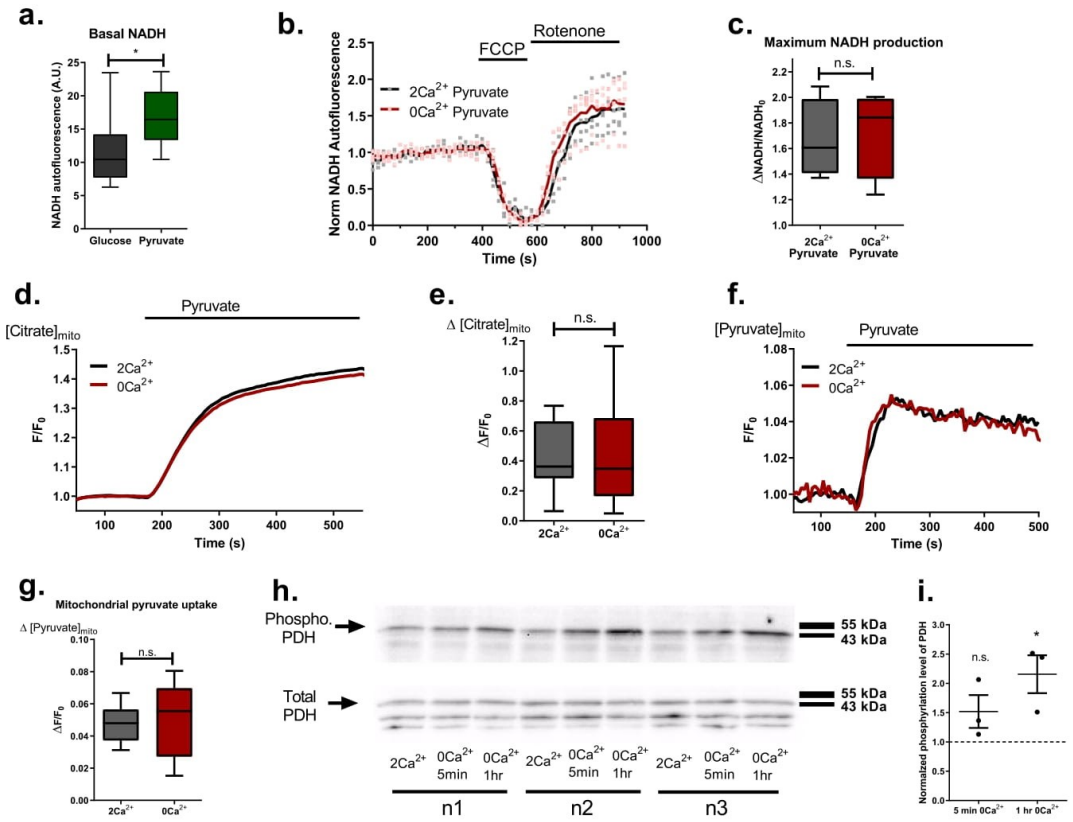

Fig. 3 Mitochondrial pyruvate uptake and utilization are not affected under reduced basal Ca^{2+} condition. a Basal mitochondrial NADH autofluorescence of cells in either glucose or glucose and pyruvate supplemented buffers (unpaired *t*-test, $n = 16$ for glucose, $n = 8$ for pyruvate supplementation, $^*p = 0.0168$). **b** Average traces (solid lines) and single data points of mitochondrial NADH autofluorescence measurements with pyruvate supplementation. **c** Statistical analysis of **b** (unpaired *t*-test, $n = 4$; n.s., $p = 0.788$). **d** Representative traces of mitochondrial citrate measurements with mito-CitrON. **e** Statistical analysis of mitochondrial citrate production measurements as shown in **d** (unpaired *t*-test, $n = 21$; n.s., $p = 0.875$). **f** Representative traces of mitochondrial pyruvate measurements with mito-PyronicSF. **g** Statistical analysis of mitochondrial pyruvate uptake as shown in **f** (unpaired *t*-test, $n = 8$; n.s., $p = 0.819$). **h** Western blot analysis of phosphorylation status of PDH; cells were incubated in 2 Ca^{2+}, 0 Ca^{2+} for 5 min and 0 Ca^{2+} for 1 hr, then harvested on ice and blotted for phosphorylated PDH at Ser293 (upper blot); total PDH was blotted after mild stripping of phospho. PDH antibody (lower blot). **i** Statistical analysis of **h**, total PDH was used as loading control; horizontal dotted line represents control level (Repeated Measures ANOVA with Tukey's multiple comparison test, $n = 3$, $^*p < 0.05$).

the mitochondrial inter-membrane space (IMS) and serves as part of the malate-aspartate shuttle (MAS)[40,41] is a good candidate for the role of a translator of the disturbed subcellular Ca^{2+} homeostasis to cellular and mitochondrial metabolic setting in our model. To elucidate whether the metabolic changes upon disturbed subcellular Ca^{2+} homeostasis were due to perturbation of IMS Ca^{2+}-controlled citrin activity, we measured cytosolic lactate (Fig. 5a, b), NADH/NAD^+ ratio (Fig. 5c, d), mitochondrial NADH (Fig. 5e–g) and ATP levels (Fig. 6a, b) under transient knockdown of citrin (Supplementary Fig. 5 a–d). Basal lactate level (Fig. 5a) and NADH/NAD^+ ratio (Fig. 5c) were elevated in citrin-depleted cells. Notably, the increase of lactate (Fig. 4b) and NADH/NAD^+ ratio (Fig. 4e, f) in response to perturbation of subcellular Ca^{2+} homeostasis were both prevented by knockdown of citrin (Fig. 5b, d). Hence, the knockdown of citrin reduced mitochondrial basal NADH level and maximum NADH production (Fig. 5e–g) as well as basal mitochondrial ATP level (Fig. 6a). These results indicate that the disturbance of subcellular Ca^{2+} homeostasis upon removal of extracellular Ca^{2+} and subsequently, the decrease in IMS Ca^{2+} (Fig. 1a), mimics the effects of citrin knockdown. Importantly, citrin KD didn't have a drastic effect on cell viability and apoptosis in the timeframe of our experiments (Supplementary Fig. 6a, b).

Differential regulation of mitochondrial bioenergetics by IMS Ca^{2+} dependent citrin and MCU dependent matrix Ca^{2+} and dehydrogenases. In order to verify the individual importance of IMS Ca^{2+} and Citrin versus matrix Ca^{2+} and dehydrogenases in regulation of resting mitochondrial bioenergetics, we compared the effect of citrin knockdown with that of MCU (Supplementary Fig. 5a–d). Basal mitochondrial ATP level was reduced under both citrin and MCU knockdown conditions, while the reduction was more pronounced in citrin-depleted cells (Fig. 6a). In line with these findings, the shift of ATP synthase towards its reverse mode and reduced ATP production in control cells with perturbed subcellular Ca^{2+} homeostasis was comparable with that found in citrin-depleted cells in both normal and 0 Ca^{2+}

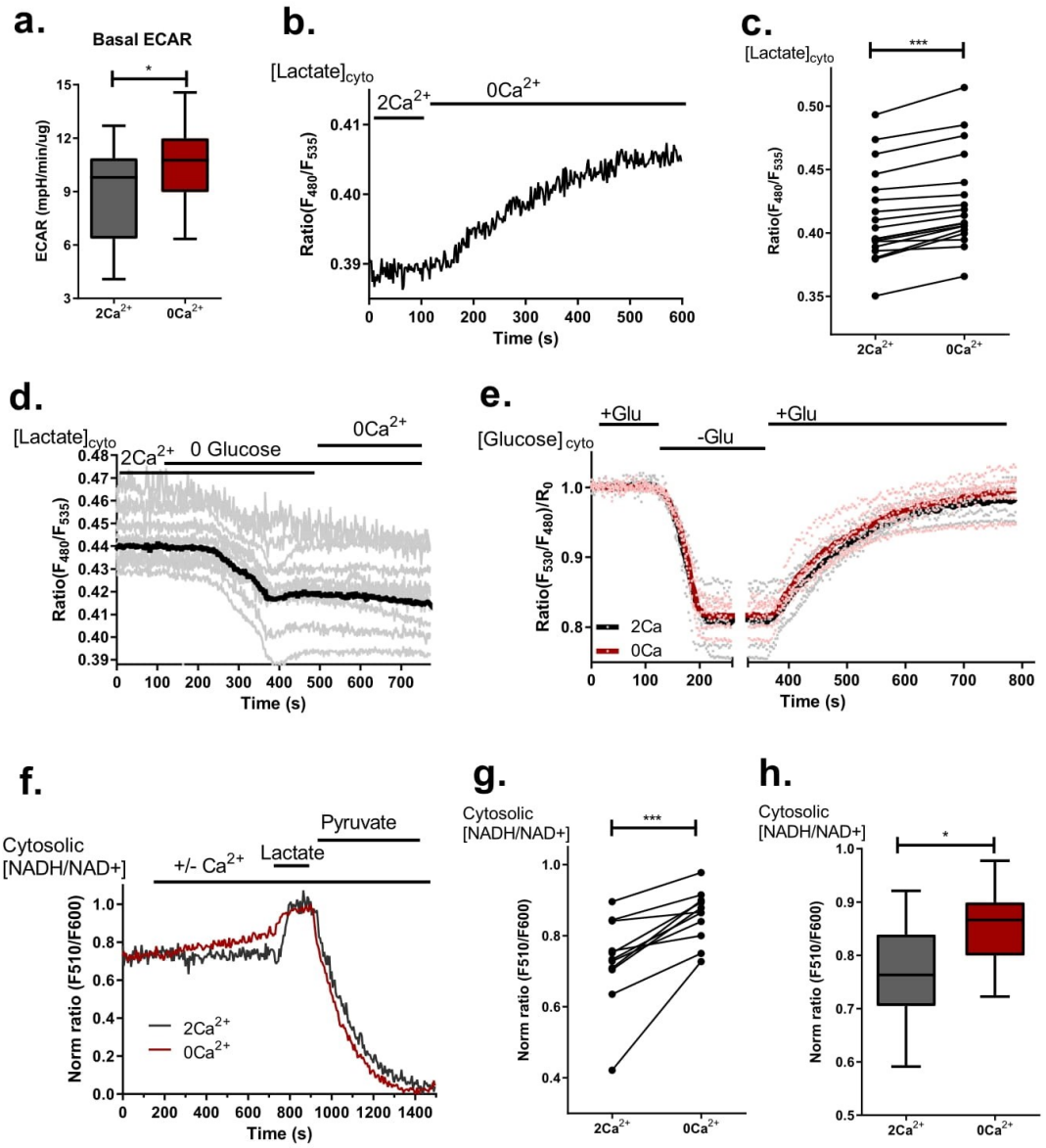

Fig. 4 ECAR, cytosolic lactate and NADH/NAD$^+$ ratio increase in response to Ca^{2+} deprivation. a Statistical analysis of ECAR (unpaired *t*-test, $n = 17$ for 2 Ca^{2+}, $n = 25$ for 0 Ca^{2+}; $^*p = 0.0414$). **b** Representative trace of cytosolic lactate accumulation measured with Laconic after perfusion with 0 Ca^{2+} buffer. **c** Statistical analysis of cytosolic lactate levels before and after 6 min of Ca^{2+} removal (paired *t*-test, $n = 18$; $^{***}p < 0.0001$). **d** Average trace (solid black line) and single cell traces (grey lines) of cytosolic lactate measurements with glucose removal ($n = 12$). **e** Average traces (solid lines) and single data points of cytosolic glucose measurements using FLII12Pglu-700μδ6 with glucose removal and re-addition ($n = 5$ for 2 Ca^{2+}, $n = 6$ for 0 Ca^{2+}). **f** Representative traces of cytosolic NADH/NAD$^+$ measurements with Peredox and subsequent calibration with 10 mM lactate and pyruvate. **g** Statistical analysis of cytosolic NADH/NAD$^+$ ratio of cells before and after 6 min of Ca^{2+} removal (paired *t*-test, $n = 11$; $^{***}p = 0.0003$). **h** Comparison of cytosolic NADH/NAD$^+$ ratio after 6 min in 2 Ca^{2+} or 0 Ca^{2+} buffer (unpaired *t*-test, $n = 9$ for 2 Ca^{2+}, $n = 11$ for 0 Ca^{2+}; $^*p = 0.0258$).

conditions (Fig. 6b). In contrast to citrin knockdown, MCU depletion showed a less drastic reversal of ATP synthase and ATP production under normal Ca^{2+} condition, while a clear additive effect of Ca^{2+} removal was present (Fig. 6b). Similar results were obtained in HeLa cells, pointing to uniformity of the findings (Supplementary Fig. 7a–c). OCR measurements further corroborated these results as citrin KD significantly reduced ATP production linked respiration, while MCU KD did not (Supplementary Fig. 8a–c). In addition, citrin KD resulted in increased ECAR (Supplementary Fig. 8d), thus supporting the findings

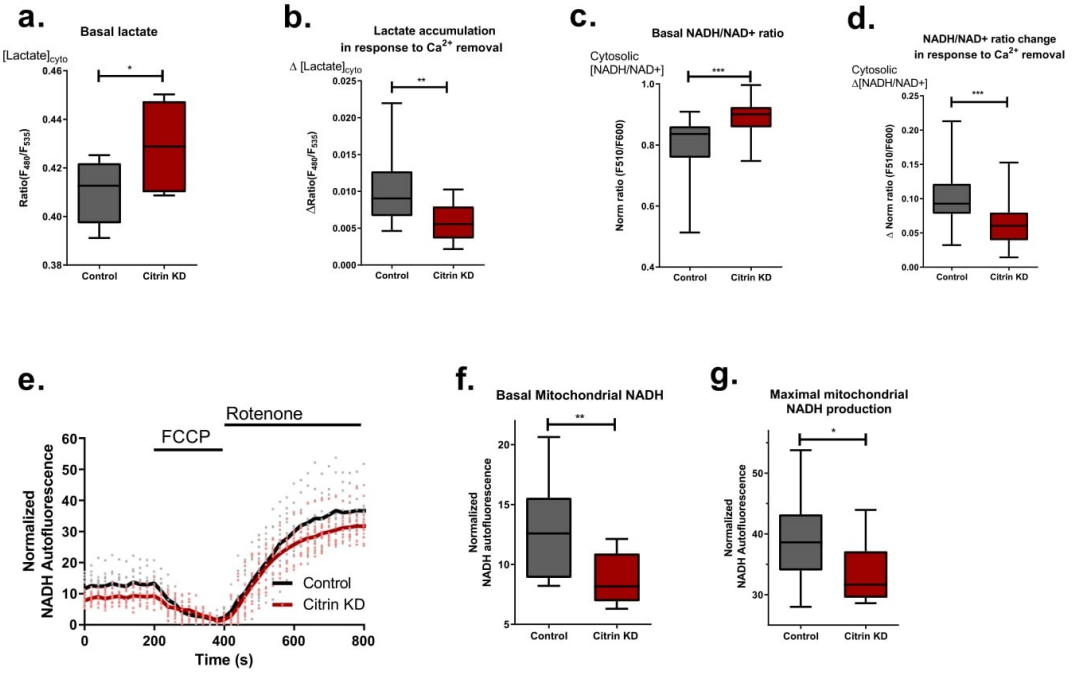

Fig. 5 Citrin KD mimics the metabolic alterations happening during basal Ca^{2+} drop condition. a Basal cytosolic lactate levels of control vs Citrin KD in 2 Ca^{2+} (unpaired *t*-test, $n = 7$; $^{*}p = 0.0411$). **b** Lactate accumulation after extracellular Ca^{2+} removal (as in Fig. 4 a) in control vs Citrin KD (unpaired *t*-test, $n = 15$ for control, $n = 13$ for citrin KD; $^{**}p = 0.0064$). **c** Basal cytosolic NADH/NAD^+ ratio of control vs Citrin KD in 2 Ca^{2+} (unpaired *t*-test, $n = 30$ for control, $n = 18$ for citrin KD; $^{***}p = 0.0005$). **d** NADH/NAD^+ ratio change after extracellular Ca^{2+} removal (as in Fig. 4 e) in control vs Citrin KD (unpaired *t*-test, $n = 29$ for control, $n = 18$ for citrin KD; $^{**}p = 0.0002$). **e** Average traces (solid lines) and single data points of mitochondrial NADH autofluorescence measurements in control and Citrin KD cells. **f** Statistical comparison of basal mitochondrial NADH in control vs Citrin KD shown in panel **e** (unpaired *t*-test, $n = 11$; $^{**}p = 0.0064$). **g** Maximal NADH production in control vs Citrin KD cells shown in panel **e** (unpaired *t* = test, $n = 11$; $^{*}p = 0.0333$).

performed with the removal of extracellular Ca^{2+} (Fig. 4a–c). The absence of a more pronounced difference in basal and maximal OCR for citrin KD compared to controls is likely stemming from low transfection efficiency in EA.hy926 cells (Supplementary Fig. 5a–d), which is especially problematic for the kind of experiments that lack positive transfection marker as we have recently shown[21].

Furthermore, we tested whether MCU over expression (OE) or MICU1 KD, which can increase mitochondrial Ca^{2+} uptake[13] or basal matrix Ca^{2+} level[42], respectively, will rescue the metabolic defects of citrin KD. Neither MCU OE nor MICU1 KD could rescue reduced basal mitochondrial ATP level or ATP production of citrin KD cells (Fig. 6c, d), emphasizing once more the importance of citrin and IMS Ca^{2+} for regulation of basal mitochondrial bioenergetics. Despite the dominating role of citrin over MCU for mitochondrial bioenergetics under resting conditions, both proteins share the fundamental importance on histamine-stimulated mitochondrial ATP production (Fig. 6e, f), even though citrin KD doesn't affect basal mitochondrial Ca^{2+} or mitochondrial Ca^{2+} uptake upon stimulation (Supplementary Fig. 9a, b).

Citrin controls pyruvate availability for mitochondria. Because the cytosolic NADH recycling function of MAS is involved in regulation of pyruvate production by providing NAD^+ for glycolysis, we further analyzed the impact of citrin knockdown and IMS Ca^{2+} imbalance on mitochondrial pyruvate supply by measuring cytosolic pyruvate. Since the sensitivity of the genetically encoded pyruvate sensor Pyronic[43] used in this study did not allow measurements of small pyruvate fluctuations[43] (Fig. 7a), we used inhibitors of the monocarboxylate transporters (MCT) and lactate dehydrogenase (LDH), AR-C155858 and GSK 2837808 A, respectively, to facilitate cytosolic pyruvate accumulation (Fig. 7b). The amount of cytosolic pyruvate accumulation after inhibition of MCT and LDH represents the flux of pyruvate to these respective proteins. While basal cytosolic pyruvate levels were similar in control cells and cells with disturbed basal subcellular Ca^{2+} homeostasis (Fig. 7a), pyruvate accumulation is increased under reduced Ca^{2+} condition and in citrin-depleted cells (Fig. 7b). Interestingly, there was no further difference in pyruvate accumulation between normal and reduced Ca^{2+} conditions in citrin-depleted cells (Fig. 7b). These findings indicate that LDH and MCT use more pyruvate during IMS Ca^{2+} imbalance or in the absence of citrin, thus diminishing pyruvate availability for mitochondria.

To further test this hypothesis we have measured mitochondrial pyruvate directly when going from glucose-free buffer to glucose containing one, thus estimating the mitochondrial pyruvate supply. We have compared control, citrin KD and MCU KD conditions in the presence (Fig. 7c) and absence of extracellular Ca^{2+} (Fig. 7d), and confirmed that citrin and IMS Ca^{2+} control pyruvate supply of mitochondria, as both citrin KD and removal of extracellular Ca^{2+} reduced mitochondrial pyruvate supply (Fig. 7c–e). Importantly, MCU doesn't seem to be involved in this process as MCU KD didn't affect

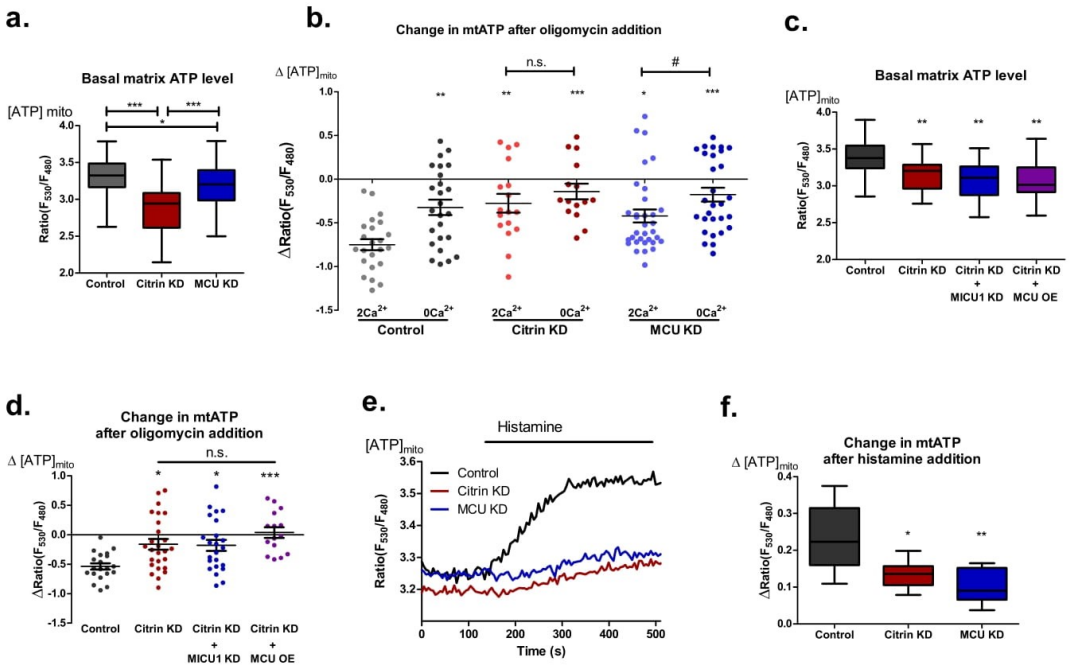

Fig. 6 Citrin/IMS Ca^{2+} are more important for basal mitochondrial bioenergetics than MCU/matrix Ca^{2+}. **a** Statistical analysis of basal mitochondrial ATP levels represented by mtAT1.03 ratio in control, MCU KD and citrin KD (One-way ANOVA with Tukey's multiple comparison test, $^{*}p < 0.05$, $^{***}p < 0.001$, $n = 57$ for control, $n = 32$ for citrin KD, $n = 62$ for MCU KD). **b** Statistical analysis of the change in mitochondrial ATP level after 2 µM oligomycin addition in control, MCU KD and citrin KD cells +/− extracellular Ca^{2+} (One-way ANOVA with Tukey's multiple comparison test, $n = 23$ (control 2 Ca^{2+}), 25 (control 0 Ca^{2+}), 17 (citrin KD 2 Ca^{2+}), 15 (citrin KD 0 Ca^{2+}), 33 (MCU KD 2 Ca^{2+}), 29 (MCU KD 0 Ca^{2+}), $^{*}p < 0.05$, $^{**}p < 0.01$, $^{***}p < 0.001$; unpaired *t*-test, citrin KD 2 Ca vs citrin KD 0 Ca, n.s. $p = 0.3519$; unpaired *t*-test, MCU KD 2 Ca vs MCU KD 0 Ca, # $p = 0.0286$). **c** Statistical analysis of basal mitochondrial ATP levels represented by mtAT1.03 ratio in control, citrin KD, citrin and MICU1 double KD, and citrin KD MCU OE cells (One-way ANOVA with Tukey's multiple comparison test, $^{**}p < 0.01$, $n = 20$ for control, $n = 26$ for citrin KD, $n = 23$ for citrin and MICU1 double KD, $n = 15$ for citrin KD MCU OE). **d** Statistical analysis of the change in mitochondrial ATP level after 2 µM oligomycin addition in control, citrin KD, citrin and MICU1 double KD, and citrin KD MCU OE cells (One-way ANOVA with Tukey's multiple comparison test, $^{*}p < 0.05$, $^{***}p < 0.001$, n.s. $p > 0.05$, $n = 20$ for control, $n = 26$ for citrin KD, $n = 23$ for citrin and MICU1 double KD, $n = 15$ for citrin KD MCU OE). **e** Representative traces of mitochondrial ATP measurements upon histamine stimulation in control, citrin KD and MCU KD cells. **f** Statistical analysis of histamine induced mitochondrial ATP production as shown in **e** (One-way ANOVA with Tukey's multiple comparison test, $^{*}p < 0.05$, $^{**}p < 0.01$, $n = 6$ for control, $n = 8$ for citrin KD, $n = 7$ for MCU KD).

mitochondrial pyruvate supply in the presence of extracellular Ca^{2+}, while perturbing basal subcellular homeostasis in MCU KD cells did (Fig. 7c–e). Additionally, MCU OE didn't rescue the reduced mitochondrial pyruvate supply of citrin KD cells (Supplementary Fig. 10).

Less pyruvate availability for mitochondria would explain worsened mitochondrial bioenergetics under these conditions. To test this assumption, we measured mitochondrial ATP production under normal and 0 Ca^{2+} conditions, but this time, we supplemented experimental buffers with 1 mM pyruvate. Pyruvate supplementation rescued the effect of IMS Ca^{2+} imbalance on mitochondrial ATP production (Fig. 7f), supporting the hypothesis that reduced pyruvate availability for mitochondria is one of the reasons for worsened mitochondrial bioenergetics when subcellular/IMS Ca^{2+} homeostasis is disturbed.

MAM, but not cytosolic, Ca^{2+} flux determines basal mitochondrial bioenergetics. Since the ER represents the main source for mitochondrial Ca^{2+} that is transferred predominantly via the MAMs, we wanted to understand how exactly the removal of extracellular Ca^{2+} affects mitochondrial bioenergetics. Cytosol and the MAMs are the two routes through which Ca^{2+} might be engaged in the regulation of basal mitochondrial energetics. Theoretically, Ca^{2+} from both these sources could influence IMS Ca^{2+} homeostasis as there is no apparent threshold at the OMM for Ca^{2+} exchange. To address this question, we deployed the intracellular Ca^{2+} chelating agents BAPTA-AM and EGTA-AM. Notably, BAPTA has faster Ca^{2+} binding and is known to be able to buffer spatial Ca^{2+} in e.g. the MAM region[44], whereas EGTA is a rather slow Ca^{2+} chelator and, thus, its effectiveness is limited to buffering global cytosolic Ca^{2+} fluctuations[44]. Basal mitochondrial ATP, as well as mitochondrial ATP production, were greatly reduced when the cells were treated with BAPTA-AM but not EGTA-AM, pointing to the importance of basal MAM-IMS Ca^{2+} homeostasis for regulation of citrin and, subsequently, mitochondrial bioenergetics (Fig. 8a, b). To further elaborate which proteins of the Ca^{2+} toolkit[5] are actually involved in the basal Ca^{2+} homeostasis within the MAM/IMS, we assessed the effect of the IP_3R inhibitor Xestospongin C[45], store-operated Ca^{2+} entry (SOCE) inhibitor Pyrozole 6 (Pyr6)[46] and short transient receptor potential channel 3 (TRPC3) inhibitor Pyrozole 10 (Pyr10)[46]. Xestospongin C, but not Pyr6 or Pyr10, reduced mitochondrial ATP production and reversed the ATP synthase

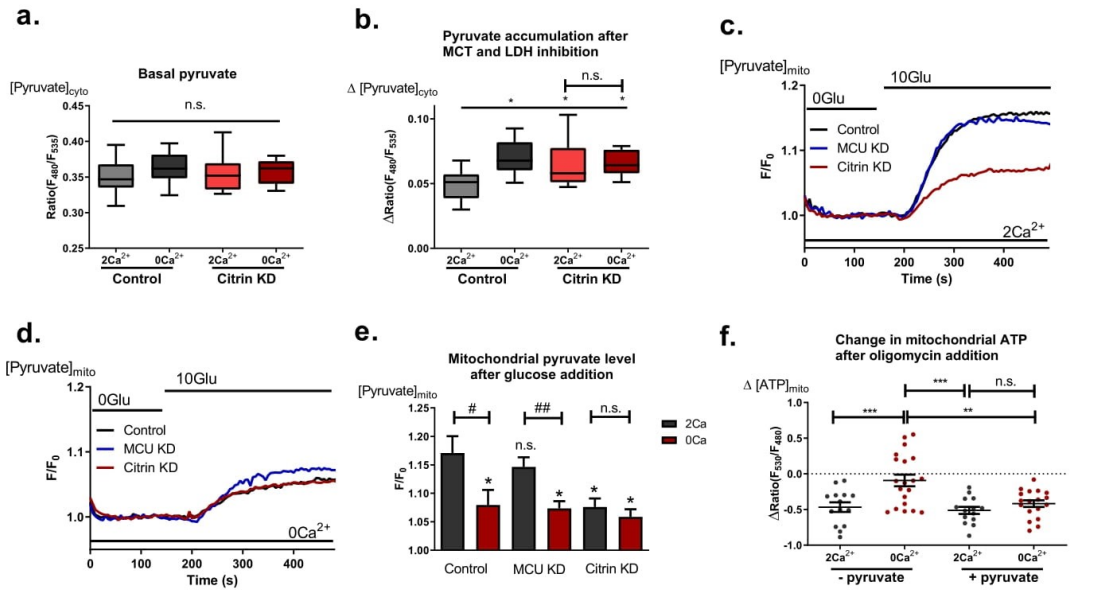

Fig. 7 Citrin activity regulates pyruvate's fate. a Basal cytosolic pyruvate levels measured with Pyronic in control vs. knockdown of citrin in the presence and absence of extracellular Ca^{2+} (One-Way ANOVA with Tukey's multiple comparison test, $n = 9$ for control 2 Ca^{2+} and 0 Ca^{2+}, $n = 10$ for citrin KD 2 Ca^{2+} and 0 Ca^{2+}; **b** Cytosolic pyruvate accumulation in response to LDH and MCT inhibition with GSK 2837808 A and AR-C155858, respectively (One-Way ANOVA with Tukey's multiple comparison test, $^{*}p < 0.05$, $n = 9$ for control 2 Ca^{2+} and 0 Ca^{2+}, $n = 10$ for citrin KD 2 Ca^{2+} and 0 Ca^{2+}). **c** Representative traces of mitochondrial pyruvate measurements with mito-PyronicSF in the presence of extracellular Ca^{2+} under control, citrin KD and MCU KD conditions. **d** Representative traces of mitochondrial pyruvate measurements with mito-PyronicSF in the absence of extracellular Ca^{2+} under control, citrin KD and MCU KD conditions. **e** Statistical analysis of mitochondrial pyruvate measurements as shown in **c** and **d** (One-Way ANOVA with Tukey's multiple comparison test, $n = 11$ for control 2 Ca^{2+}, $n = 10$ for control 0 Ca^{2+}, $n = 12$ for MCU KD 2 Ca^{2+}, $n = 8$ for MCU KD 0 Ca^{2+}, $n = 14$ for citrin KD 2 Ca^{2+}, $n = 7$ for citrin KD 0 Ca^{2+}, $^{*}p < 0.05$, n.s. $p > 0.05$; unpaired *t*-test, $^{\#}p < 0.034$, $^{\#\#}p = 0.006$, n.s., $p = 0.463$). **f** Comparison of mitochondrial ATP dynamics after 2 µM oligomycin addition in the presence and absence of extracellular Ca^{2+} ±1 mM pyruvate supplementation (One-Way ANOVA with Tukey's multiple comparison test, $^{**}p < 0.01$, $^{***}p < 0.001$, $n = 14$ for 2 Ca^{2+} no pyruvate), 20 for 0 Ca^{2+} no pyruvate, 14 for 2 Ca^{2+} pyruvate, 18 for 0 Ca^{2+} pyruvate).

direction (Fig. 8c), supporting the importance of IP_3Rs in MAM/IMS Ca^{2+} flux even under basal conditions. Interestingly, the impact of combined application of Pyr6 and Pyr10 was similar to that of Xestospongin C (Fig. 8c) and 0 Ca^{2+} (Fig. 2c), likely due to the need of basal plasma membrane Ca^{2+} flux for continuous ER refilling and maintenance of MAM-IMS Ca^{2+} homeostasis.

To validate the results obtained with pharmacological inhibition, we have performed similar experiments with knockdown of IP_3R2 and Orai1 as the main proteins responsible for MAM[47] and SOCE[48] pathways of Ca^{2+} delivery to IMS, respectively (Fig. 8d, e). KD of both genes showed a reduction of basal mitochondrial ATP level and ATP production, with IP_3R2 KD having a much stronger effect on mitochondrial bioenergetics than Orai1 KD (Fig. 8d, e). These results support the observations made with the pharmacological tools and emphasize the importance of MAM-IMS Ca^{2+} flux as the regulating mechanism of basal mitochondrial bioenergetic wiring.

Discussion

This work was designed to investigate principal regulating mechanisms of basal mitochondrial bioenergetics as fundamental processes for conditioning cellular metabolic wiring. To achieve this goal, we have deployed a common protocol of extracellular Ca^{2+} removal that allowed us to distinguish differential regulation of mitochondrial metabolism by basal subcellular Ca^{2+} homeostasis. Short-term removal of extracellular Ca^{2+} yields slight and reversible drops in basal Ca^{2+} levels of multiple organelles and sub-organellar compartments (Fig. 1a, Supplementary Fig. 1). Initially, our prediction was that mitochondrial bioenergetics will worsen as the result of basal drop in matrix Ca^{2+} due to diminished activity of mitochondrial Ca^{2+}-sensitive dehydrogenases (Fig. 2e, f). However, the diminished NADH production by mitochondria under reduced basal Ca^{2+} condition was rescued by 1 mM pyruvate supplementation (Fig. 3a, c). This observation cast a doubt on our prediction that this slight drop in basal Ca^{2+} in mitochondrial matrix was the reason for the worsened mitochondrial bioenergetics under this condition. Since the reported K_Ds of matrix dehydrogenases for Ca^{2+} ions in live cells are in the high nM–µM range[16], possibly the observed acute reduction of 20–40 nM in the matrix was not affecting them. Subsequent direct measurements of mitochondrial pyruvate uptake capability and pyruvate dehydrogenase activity revealed that both are not affected in the given timeframe by the resulting 15% drop of basal Ca^{2+} level (Fig. 3d–g). In line with these functional experiments, the PDH phosphorylation was only slightly increased by short-term removal of extracellular Ca^{2+} (Fig. 3h, i). Collectively, these results indicate that disrupted basal intracellular Ca^{2+} homeostasis achieved by short-term removal of extracellular Ca^{2+} can affect something other than or in addition to mitochondrial dehydrogenases.

The increased ECAR in Seahorse® experiments in the absence of extracellular Ca^{2+} pointed to an increase in glycolytic activity under this condition (Fig. 4a). In line with this finding, lactate

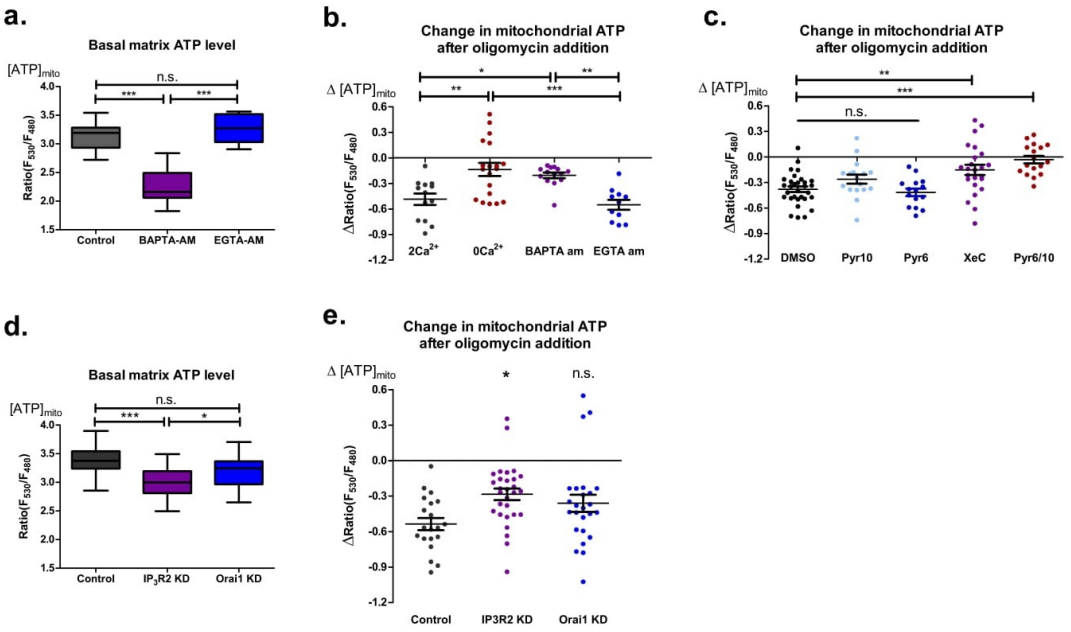

Fig. 8 Mitochondrial bioenergetics are influenced by basal MAM Ca^{2+} flux. a Basal matrix ATP levels in control cells and cells incubated with 50 µM BAPTA-AM or 50 µM EGTA-AM for 30 min (One-Way ANOVA with Tukey's multiple comparison test, $^{***}p < 0.001$, $n = 32$ for control, $n = 14$ for BAPTA-AM, $n = 11$ for EGTA-AM). **b** Analysis of mitochondrial ATP change after 2 µM oligomycin addition to cells perfused with 2 Ca^{2+} or 0 Ca^{2+}, and pre-incubated with 50 µM BAPTA-AM or 50 µM EGTA-AM (One-Way ANOVA with Tukey's multiple comparison test, $^{*}p < 0.05$, $^{**}p < 0.01$, $^{***}p < 0.001$, $n = 13$ for 2 Ca^{2+}, $n = 19$ for 0 Ca^{2+}, $n = 14$ for BAPTA-AM, $n = 11$ for EGTA-AM). **c** Analysis of mitochondrial ATP change after 2 µM oligomycin addition to cells incubated with DMSO control ($n = 31$), 3 µM Pyr6 ($n = 17$), 3 µM Pyr10 ($n = 15$), 10 µM XeC ($n = 24$), and 3 µM Pyr6/3 µM Pyr10 ($n = 17$), One-Way ANOVA with Tukey's multiple comparison test, $^{**}p < 0.01$, $^{***}p < 0.001$. **d** Basal matrix ATP levels in control, IP_3R2 KD and Orai1 KD cells (One-Way ANOVA with Tukey's multiple comparison test, $^{***}p < 0.001$, $^{*}p < 0.05$, $n = 20$ for control, $n = 29$ for IP_3R2 KD, $n = 25$ for Orai1 KD). **e** Analysis of mitochondrial ATP change after 2 µM oligomycin addition to control, IP_3R2 KD and Orai1 KD cells (One-Way ANOVA with Tukey's multiple comparison test, $^{*}p < 0.05$ versus control, $n = 20$ for control, $n = 29$ for IP_3R2 KD, $n = 25$ for Orai1 KD).

accumulates in cells with disturbed subcellular Ca^{2+} homeostasis (Fig. 4b, c). Notably, as the lactate accumulation does not occur in the absence of glucose (Fig. 4d) and neither glucose utilization nor glucose import are affected by the removal of extracellular Ca^{2+} (Fig. 4e), this lactate accumulation under disturbed subcellular Ca^{2+} homeostasis appears to be physiological. The increase in the cytosolic NADH/NAD^+ ratio (Fig. 4f–h) upon perturbation in basal subcellular Ca^{2+} homeostasis led us to speculate that lactate accumulates as a result of increased LDH activity that is enhanced in order to support glycolysis under the condition of increased cytosolic NADH/NAD^+ ratio[39].

In line with the assumptions above, we suspected that a Ca^{2+}-sensitive process, which is responsible for cytosolic NADH/NAD^+ ratio misbalance, affects mitochondrial bioenergetics, and is involved in the metabolic rewiring of mitochondria under the condition of disturbed subcellular Ca^{2+} homeostasis achieved in our Ca^{2+} removal protocol. Accordingly, we propose the Ca^{2+}-sensitive mitochondrial solute carrier citrin (SLC25A13)[40,41,49–54] as a potential candidate responsible for Ca^{2+}-dependent metabolic rewiring of mitochondria in our model. Notably, citrin knockdown mimicked the Ca^{2+} removal phenotype in all of the measured parameters, including increased cytosolic lactate, NADH/NAD^+ ratio, reduced mitochondrial NADH and ATP production (Figs. 5, 6a, b), as well as increased pyruvate consumption by LDH (Fig. 7b) and reduced mitochondrial pyruvate supply (Fig. 7c–e). These data support the role of MAS in regulation of basal mitochondrial bioenergetics and in linking cytosolic and mitochondrial metabolism via mitochondrial surface/IMS Ca^{2+} (Fig. 9). Hence, any disruption of the IMS Ca^{2+} homeostasis results in the rewiring of metabolism, as IMS Ca^{2+} regulated citrin activity fuels the matrix with NADH equivalents and pyruvate (Fig. 7a–e) for the TCA cycle that generates electron donors (Fig. 2e, f) for ETC, making even a slight reduction in IMS Ca^{2+} (Fig. 1a) a big impact for mitochondrial bioenergetics.

Additionally, the comparison of the knockdown of citrin with that of MCU on mitochondrial ATP production (Fig. 6) and pyruvate supply (Fig. 7c–e) supports the concept of the importance of MAM-IMS Ca^{2+} modulation of mitochondrial bioenergetics via citrin but not MCU under resting conditions. In addition to its importance under resting conditions, our data indicate that citrin is as important as MCU for boosting mitochondrial bioenergetics upon stimulation (Fig. 6e, f). The importance of IMS Ca^{2+} for regulation of mitochondrial bioenergetics and basal metabolic wiring is further supported by our findings that neither MCU OE nor MICU1 KD can rescue defective mitochondrial bioenergetics resulting from citrin KD (Fig. 6c, d, Supplementary Fig. 10a, b). These findings highlight the importance of MAS and its regulation by MAM-IMS Ca^{2+} flux under resting and stimulated conditions and, thus, Ca^{2+}-activated citrin (and MAS) essentially need to be considered besides Ca^{2+}-sensitive matrix dehydrogenases when evaluating Ca^{2+}-activated processes that control mitochondrial bioenergetics.

In a recent study it has been shown that pyruvate utilization by mitochondria is Ca^{2+} dependent[55]. Notably, mitochondrial

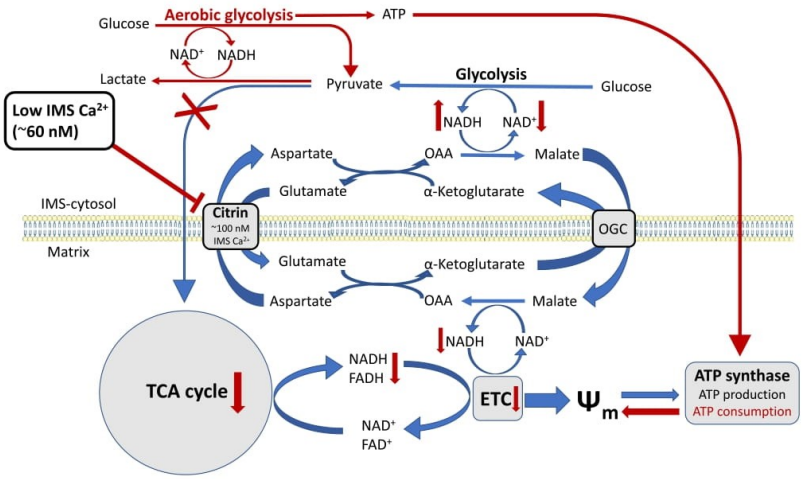

Fig. 9 Schematic representation of IMS Ca^{2+} homeostasis as fundamental regulator of resting cytosolic and mitochondrial metabolism. IMS Ca^{2+} modulates citrin/malate-aspartate shuttle activity with basal IMS Ca^{2+} level being set at around 100 nM by ER-mitochondrial Ca^{2+} flux. Main processes that are regulated by basal IMS Ca^{2+} driven MAS activity are shown with blue arrows, and consist of MAS recycling NAD^+ for glycolysis and glycolytic products going through TCA cycle and ETC. Disruption of this Ca^{2+} homeostasis leads to metabolic rewiring, shown here with red arrows and text. As a result, cells switch to aerobic glycolysis, rely on LDH for NADH recycling, and have reduced OxPhos. OAA, oxaloacetate; OGC, oxoglutarate/malate carrier protein.

pyruvate metabolism has two Ca^{2+} regulation phases. First, direct, Ca^{2+}-dependent regulation of pyruvate utilization by mitochondrial matrix dehydrogenases, and second, indirect, Ca^{2+}-dependent regulation of pyruvate availability for mitochondria by citrin/MAS activity. Since in addition to direct substrate supply to mitochondria, citrin, in a Ca^{2+}-sensitive manner, recycles cytosolic NADH and makes NAD^+ available for glycolysis, it controls production and fate of pyruvate as shown here and by others[52,56], while not affecting the mitochondrial pyruvate transport itself (Fig. 3f, g). When the cytosolic NADH/NAD^+ ratio is increased as a result of basal MAM/IMS Ca^{2+} disruption and reduced citrin activity, pyruvate gets converted to lactate by LDH with a concurrent conversion of NADH to NAD^+, thus reestablishing the balanced redox ratio of NAD to sustain glycolysis. In support of this view, a recent study pointed to the need for NAD^+ in driving aerobic glycolysis[57]. But as a consequence of this metabolic rewiring, mitochondria get less pyruvate and produces less ATP, and in some cases deploy ATP synthase to sustain the proton gradient at the expense of ATP to avoid a total collapse of membrane potential leading to apoptosis.

Relevance and importance of current work on the fundamental issue of the differential involvement of citrin and MCU-dependent matrix dehydrogenases in regulating basal metabolic setting of a cell is further supported by a recent preprint showing the involvement of aralar1 in boosting glycolysis and OxPhos upon stimulation in neurons[58]. Additionally, it was shown that cancer cells need a higher expression of citrin for proliferation and invasiveness, which can be counteracted by citrin down regulation[52]. In contrast to increased metabolism under citrin OE condition in these tumors, patients with citrin deficiency in form of type 2 citrullinemia struggle with various age-dependent metabolic pathologies that can be managed with proper diet[59]. Our present findings that point to the crucial role of MAS, as the main NADH shuttle in endothelial cells, in the regulation of mitochondrial bioenergetics are in line with previous reports in various tumor cells[52,60,61]. Under the basal condition, MAS continuously delivers NADH equivalents to the mitochondrial matrix, while maintaining glycolysis and pyruvate supply by delivering NAD^+ into the cytosol[61]. Mitochondrial dehydrogenases oxidize TCA cycle substrates and fuel ETC by producing electron donors (NADH). The activity of both systems under resting conditions are controlled and synchronized by IMS and matrix Ca^{2+} that are both supported by a basal Ca^{2+} cycling in the MAMs (Fig. 8a–e, Fig. 9). Our data presented herein indicate that as soon as this basal subcellular Ca^{2+} homeostasis/cycling is disturbed, the activity of the Ca^{2+}-regulated citrin is reduced, thus, delaying TCA cycle substrate supply and thus electron donor supply for the respiratory chain, while rerouting pyruvate to LDH. Our present data further indicate that under resting conditions, Ca^{2+} influx into the mitochondrial matrix via the MCU is less important for regulation of basal mitochondrial bioenergetics than IMS Ca^{2+} regulated citrin activity. This could serve as a preemptive mechanism under conditions of disturbed subcellular Ca^{2+} homeostasis because the lack of citrin/MAS activity protects mitochondria against substrate overflow in light of reduced activity of Ca^{2+} sensitive matrix dehydrogenases. One could argue that citrin is one order of magnitude more sensitive to Ca^{2+}[62] than matrix dehydrogenases and even small Ca^{2+} fluctuations could then unnecessarily disturb mitochondrial function. However, our data indicate that matrix dehydrogenases do not sense small and short-term disturbances in basal subcellular Ca^{2+} homeostasis and keep basal activity, thus putting citrin in charge of responding to slight and brief variations in basal Ca^{2+} homeostasis. However, in order to achieve maximal mitochondrial ATP production, citrin and matrix dehydrogenases are synchronized upon stimulation by an IP_3-generating agonist (e.g., histamine) by the huge Ca^{2+} transfer from the MAMs towards the IMS and mitochondrial matrix. In light of this cooperative action of citrin and the dehydrogenases, it appears beneficial for some cells to up-regulate citrin in addition to increasing MAMs and mitochondrial Ca^{2+} uptake machinery in order to take full benefit of increased Ca^{2+} supply by providing more fuel for the Ca^{2+} sensitive dehydrogenases[52,63].

Our data point to a continuous PM-ER-MAM-IMS Ca^{2+} flux to maintain mitochondrial surface/IMS Ca^{2+} as a safeguard for the metabolic wiring of basal mitochondrial bioenergetics via

Ca^{2+}-controlled citrin. Disturbance of this subcellular Ca^{2+} homeostasis instantly rewires mitochondrial bioenergetics into a pseudo-hypoxic state of enhanced glycolysis due to the lack of citrin activity while mitochondria struggle to preserve their Ψ_{mito}.

Methods

Cell culture and transfection. EA.hy926 (provided by Dr. C.J.S. Edgell, University of North Carolina, Chapel Hill, NC, USA) and HeLa S3 (ATCC CCL-2.2) cells were grown in Dulbecco's Modified Eagle's Medium (DMEM) (Sigma-Aldrich; Vienna, Austria) containing 10% FCS, penicillin (100 U/ml), streptomycin (100 µg/ml), amphotericin (1.25 µg/ml), 1 g/L glucose and 4 mM glutamine in a humidified incubator (37 ºC, 5% CO_2, 95% air). Origin of cells was confirmed by STR-profiling by the cell culture facility of ZMF (Graz). Cells were regularly tested for mycoplasma contamination and were negative. For all microscopy experiments with genetically encoded sensors or knockdown experiments using siRNA, cells were plated on 30 mm glass coverslips and transfected at 60-80% confluence (EA.hy926) or 40% confluence (HeLa) with 1 µg plasmid DNA encoding an appropriate sensor alone or together with siRNA using 2.5 µl (EA.hy926) or 3 µl (HeLa) of TransFast transfection reagent (Promega, Madison, WI, USA) in 1 ml of antibiotic-free medium (EA.hy926) or 1 ml serum- and antibiotic-free medium (HeLa) for 16–20 h. Afterward, the transfection media was replaced by full culture medium. All experiments were performed 40–48 h after transfection. Prior to experiments, cells were adjusted to room temperature and shortly kept in experimental storage buffer (2 mM Ca^{2+}, 138 mM NaCl, 1 mM $MgCl_2$, 5 mM KCl, 10 mM HEPES, 2.6 mM $NaHCO_3$, 0.44 mM KH_2PO_4, amino acid, and vitamin mix, 10 mM glucose, 2 mM L-glutamine, 1% Penicillin/Streptomycin, 1% Fungizone, pH adjusted to 7.4). Citrin siRNA (UAAAUAUGCACCUAGUUUCCUtt), MCU siRNA (GCC AGAGACAGACAAUACUtt), IP_3R2 siRNA (GAGAAGGCUCGAUGCUGAG ACUUGAtt)[64], Orai1 siRNA (CGUGCACAAUCUCAACUCGtt), and scrambled siRNA control (UUCUCCGAACGUGUCACGU) were custom synthesized by Microsynth (Balgach, Switzerland).

Quantitative PCR. Total mRNA was isolated using PeqGOLD Total RNA Kit (VWR Peqlab, Leuven, Belgium), and reverse transcription was done using Applied Biosystems High Capacity cDNA Reverse Transcription kit (Thermo Fisher Scientific Baltics UAB, Vilnus, LT). qPCR was performed using Promega GOTaq® qPCR Master Mix (Madison, USA) on BIO-RAD CFX96™Real-Time System. Knockdown efficiency was determined using specific primers for citrin (forward: GCCCTTTAACTTGGCTGAGG; reverse: CCCAGACCAAACCTGTAGGC) and MCU (forward: CACTCGGGGCGCTACTG; reverse: TGTACTACCGTCTCCC CTGG) and normalized to GAPDH.

Western blot. For KD validation, cells were seeded on 10 cm dishes, transfected with respective siRNAs and harvested 48 h post transfection. Rabbit polyclonal citrin antibody (Abcam, ab96303) at 1:1000 dilution and rabbit monoclonal MCU antibody (Cell Signaling Technology, D2Z3B, #14997) at 1:1000 dilution were used for immunoblotting. A 1:5000 dilution of goat anti-rabbit secondary antibody was used (Santa Cruz Biotechnology, sc-2054). For phosphorylated PDH assessment, cells on 10 cm dishes were incubated in experimental storage buffer for 20 min to adjust to room temperature, followed by 5 min incubation in 2 Ca^{2+} buffer. After, cells were either incubated in 2 Ca^{2+} buffer for 5 min, in 0 Ca^{2+} for 5 min, or in 0 Ca^{2+} buffer for 1 h. Following the incubation times, cells were washed with ice cold nominally Ca^{2+} free buffer and harvested on ice. Phosphorylated PDH was blotted with 1:1000 dilution of rabbit mAb P-PDH S293 (Cell Signaling Technology, E4V9L, #37115), and total PDH with 1:1000 dilution of rabbit mAb PDH (Cell Signaling Technology, C54G1, #3205). A 1:5000 dilution of goat anti-rabbit secondary antibody was used (Santa Cruz Biotechnology, sc-2054). Broad Range (10-250 kDa) Color Prestained Protein Standard ladder (NEB, P7719S) was used in all blots.

Live cell imaging. All live-cell microscopy experiments were performed on an Olympus IX73 inverted microscope if not mentioned otherwise. The microscope is equipped with an UApoN340 40× oil immersion objective (Olympus, Japan) and a CCD Retiga R1 camera (Q-imaging, Canada). For illumination, a LedHUB® (Omnicron, Germany) equipped with 340, 385, 455, 470, and 550 nm LEDs in combination with CFP/YFP/RFP (CFP/YFP/mCherry-3X, Semrock, USA) or GFP (GFP-3035D, Semrock, USA) filter set was used. During the measurements cells were continuously perfused by a gravity-based perfusion system (NGFI, Graz, Austria). Data acquisition and control of the fluorescence microscope was performed using Visiview 4.2.01 (Visitron, Germany).

Ca^{2+} measurements. EA.hy926 cells were perfused with calcium containing physiological buffer (2 mM Ca^{2+}, 135 mM NaCl, 1 mM $MgCl_2$, 5 mM KCl, 10 mM HEPES, 10 mM glucose, pH adjusted to 7.4) and the basal calcium level were recorded for 2–3 min. Then, the buffer was changed to Ca^{2+} free buffer (138 mM NaCl, 1 mM $MgCl_2$, 5 mM KCl, 10 mM HEPES, 0.1 mM EGTA, 10 mM glucose, pH adjusted to 7.4) in perfusion and the corresponding changes were recorded in cytosol, ER, IMS and mitochondria using FURA2-AM, D1ER[65], IMS-GEM-GECO1[66,67], and 4mtD3cpv[68] Ca^{2+} indicators respectively. For FURA2-AM loading, cells were incubated in storage buffer with 3 µM FURA2-AM for 30 min at room temperature and washed with fresh storage buffer. FURA2-AM was sequentially excited with 340 nm and 385 nm LEDs and emission collected with GFP emission filter set. 4mtD3cpv was excited with 455 nm LED and emission simultaneously collected with CFP/YFP/RFP filter set and 505dcxr beam-splitter (Semrock, USA). The same set up as for 4mtD3cpv was used for imaging cells expressing D1ER. IMS-GEM-GECO1 was excited with 385 nm LED and emission collected at 480 nm and 530 nm using a CFP/YFP/RFP filter set and 505dcxr beam-splitter.

Basal cytosolic Ca^{2+} level, as well as the corresponding drop due to extracellular Ca^{2+} removal, were normalized using the minimal Ca^{2+} level achieved by Ca^{2+} free buffer with 1 mM EGTA and 4 µM Ionomycin, a Ca^{2+} specific ionophore. Basal ER Ca^{2+} level, as well as the corresponding drop due to extracellular Ca^{2+} removal, were normalized using maximal releasable ER Ca^{2+} achieved with 100 µM histamine, an IP_3 generating agonist, and 15 µM BHQ, a SERCA inhibitor, in Ca^{2+} free buffer. IMS and mitochondrial Ca^{2+} concentrations were determined via achieving minimum and maximum Ca^{2+} signals by varying buffer solutions in the presence of ionomycin as previously described[68]. Shortly, after recording basal Ca^{2+} level for 2 min, cells were perfused with 0 Ca^{2+} buffer containing 4 µM ionomycin for 15 min to achieve a minimal Ca^{2+} concentration. After, cells were perfused with 2 Ca^{2+} in the presence of ionomycin to achieve the maximal. For some experiments, the initial ionomycin addition resulted in higher peak, in these cases, the highest ratio was taken as maximum. For the mitochondrial Ca^{2+} uptake experiment, cells were perfused with 2 Ca^{2+} buffer for 1.5 min and stimulated with 100 µM histamine for 2 min. The maximum ratio change achieved was quantified.

ER-plasma membrane and ER-mitochondria contact sites. ER-plasma membrane contact cites were imaged using SIM setup composed of a 405-, 488-, 515-, 532- and a 561-nm excitation laser introduced at the back focal plane inside the SIM box with a multimodal optical fiber. For super-resolution, a CFI SR Apochromat TIRF ×100-oil (NA 1.49) objective was mounted on a Nikon-Structured Illumination Microscopy (N-SIM) System with standard widefield and SIM filter sets and equipped with two Andor iXon3 EMCCD cameras mounted to a two camera imaging adapter (Nikon Austria, Vienna, Austria). For calibration and reconstruction of SIM images the Nikon software Nis-Elements (Nikon Austria, Vienna, version 4.51.00 64 bit) was used. Prior to each measurement, laser adjustment was checked by projecting the laser beam through the objective at the top cover of the bright field arm of the microscope.

Total internal reflection microscopy was done using the N-SIM TIRF grating for 488 nm laser wavelength. Cells expressing an inactive version of ERAT4.01[69] and grown on 1.5H high-precision glass coverslips were incubated in 0 Ca^{2+} or 2 Ca^{2+} buffer for 5 min, placed with the respective buffer into the live-cell chamber, and imaged. Reconstruction of SIM images was done using the NIS-Elements software. For further analysis, the images were background subtracted using the Mosaic suite background subtractor, median filtered with a radius of 3 pixel, and auto thresholded using an Otsu threshold for segmentation. The segmented images were analyzed using Fiji with the included particle analyzer to measure size and count of ER patches. The total area of the cells was analyzed manually by measuring the cell size with an ROI.

For ER-mitochondria contacts, EA.hy926 cells were transfected with mitochondrial matrix targeted DsRed fluorescent protein and on the next day infected with a virus carrying an ER targeted inactive version of CFP-YFP FRET based ATP sensor ERAT4.01. Cells were imaged on a confocal spinning disk microscope (Axio Observer.Z1 from Zeiss, Gottingen, Germany) equipped with a 100x objective lens (Plan-Fluor x100/1.45 Oil, Zeiss), a motorized filter wheel (CSUX1FW, Yokogawa Electric Corporation, Tokyo, Japan) on the emission side, AOTF-based laser merge module for laser line 405, 445, 473, 488, 561, and 561 nm (Visitron Systems) and a Nipkow-based confocal scanning unit (CSU-X1, Yokogawa Electric Corporation). The ERAT1.03 and mitochondrial DsRed were alternately excited with 488 and 561 nm laser lines, respectively, and emissions were acquired at 530 and 600 nm using a charged CCD camera (CoolSNAP-HQ, Photometrics, Tucson, AZ, USA). Z-stacks of both channels in 0.2 µm increments were recorded. VisiView acquisition software (Universal Imaging, Visitron Systems) was used to acquire the imaging data. Images were blind deconvoluted with NIS-elements v5.20.02 (Nikon, Austria). The colocalization was determined on a single-cell level using ImageJ and the plugin coloc2. The Pearson coefficient and the Costes tresholded Manders 1 or 2 coefficients were calculated.

Mitochondrial ATP and membrane potential measurements. Mitochondrial ATP in EA.hy926 and HeLa cells was measured using mitochondrial matrix targeted AT1.03[30] (gift from Hiromi Imamura, Kyoto University, Kyodai Graduate School of Biostudies, Japan), a genetically encoded ATP sensor. The sensor was excited with 455 nm LED and emission collected at 480 nm and 530 nm using a CFP/YFP/RFP filter set and 505dcxr beam-splitter. Cells were perfused with Ca^{2+} buffer alone or Ca^{2+} buffer followed by 0 Ca^{2+} buffer. Mitochondrial ATP production or consumption was assessed by the addition of 2 µM oligomycin (Sigma-Aldrich, Vienna, Austria) in perfusion. Decrease of the ATP below basal level after oligomycin addition was considered to be ATP production, whereas increase of the ATP above the basal level was considered to be ATP consumption by the ATP

synthase. For the rescue of ATP production experiments, cell were sequentially perfused with Ca^{2+} buffer (2 min), 0 Ca^{2+} buffer (6 min), nutrient supplemented Ca^{2+} buffer (experimental storage buffer, 10 min), and Ca^{2+} buffer (3 min) before perfusing with 2 µM oligomycin. For simultaneous membrane potential measurements, cells transfected with mtAT1.03 sensor were incubated with 20 nM TMRM for at least 30 min in experimental storage buffer at room temperature right before measurements. All of the buffers used afterward in perfusion contained the same concentration of TMRM. TMRM data was used qualitatively to determine the direction of ATP synthase after oligomycin addition and to correlate with ATP measurements. For mitochondrial ATP production after histamine addition—cells were perfused in Ca^{2+} buffer for 2 min, after which cells were perfused with 10 µM histamine for 6–7 min. Change in mitochondrial ATP 6 min after histamine addition was quantified.

For mitochondrial ATP measurements with BAPTA-AM and EGTA-AM, EA.hy926 cells were incubated with 50 µM solution of respective chelators in experimental storage buffer for 30 min, washed with fresh buffer, and measured afterward on Olympus IX73 inverted microscope while perfused with $Ca2^{+}$ containing buffer.

For mitochondrial ATP measurements with Xestospongin C (10 µM)[45], Pyrozole 6 (3 µM), Pyrozole 10 (3 µM)[46] and combination of Pyrozole 6 and 10 (3 µM each), EA.hy926 cells were incubated with respective inhibitors or DMSO in 2 Ca^{2+} buffer for 15 min, washed and imaged on an iMic inverted and advanced fluorescent microscope using a x20 magnification objective (Fluar x20/0.75, Zeiss, Göttingen, Germany) with a motorized sample stage (TILL Photonics, Graefling, Germany) without perfusion. Concentrations used should represent 75% inhibition or higher and were taken from respective publications[45,46]. After baseline recording, 2X oligomycin was added for a final concentration of 2 µM. For control and acquisition, Live Acquisition 2 (TILL Photonics) software was used. The sensor was excited at wavelength of 430 nm; emission was collected simultaneously at 535 and 480 nm using an optical beam-splitter (Dichroic 69008ET-ECFP/EYFP/mCherry). Data processing was performed with the Offline Analysis application (TILL Photonics). The inhibitor concentrations were corresponding to 60–70% inhibition from respective source publications.

Mitochondrial NADH autofluorescence measurements. Mitochondrial NADH autofluorescence was monitored using 340 nm LED as previously described[70]. Shortly, EA.hy926 cells were perfused with 2 Ca^{2+} buffer, followed by perfusion with 1 µM FCCP until the signal flattens, and then perfused with 2 µM rotenone until a plateau is reached. Mitochondrial NADH production was quantified as maximum NADH autofluorescence achieved by Complex I inhibition with 2 µM rotenone, normalized to the basal autofluorescence after subtracting the minimal autofluorescence reached by 1 µM FCCP. For Ca^{2+} free experiments, cells were perfused with 0 Ca^{2+} buffer after 2 min in 2 Ca^{2+} buffer, with subsequent additions of FCCP and rotenone in 0 Ca^{2+} buffer. For the rescue experiments, cells were switched back to 2 Ca^{2+} buffer for 10 min after 0 Ca^{2+} buffer.

Measurement of mitochondrial respiration. 35,000 cells were plated on XF96 polystyrene cell culture microplates (Seahorse®, Agilent, CA, USA) 24 h before the experiment. For the KD experiments, cells were transfected in 10 cm dishes overnight and seeded on XF96 polystyrene cell culture microplates 24 h before the experiment. Thirty minutes before the measurement, cell medium was changed to XF assay medium supplemented with 1 mM sodium pyruvate, 2 mM glutamine and 5.5 mM D-glucose and incubated in non-CO_2 37 °C incubator. Prior to loading the plate, XF assay media was refreshed and Ca^{2+} free assay media was added to respective wells. XF96 extracellular flux analyzer was used to measure oxygen consumption rate (OCR) and extracellular acidification rate (ECAR). OCR (pmol O2/min) and ECAR (mpH/min) values were normalized to protein content. For the rescue, ECAR was assessed following injection of 25 µl 7x Ca^{2+} buffer after basal ECAR in 0 Ca^{2+} was measured. Protein concentration of each well was determined with the Pierce™ BCA Protein Assay Kit (Thermo Scientific, Rockford, IL, USA).

Live cell metabolite measurements. All live cell metabolite measurements were done in EA.hy926 cells. Mitochondrial citrate and pyruvate were measured using genetically-encoded sensors mito-Citron1[35] (gift from Robert Campbell, Addgene plasmid # 134305) and mito-PyronicSF[36] (gift from Luis Felipe Barros, Addgene plasmid # 124813) respectively. Both sensors were excited with 470 nm LED and emission collected with a GFP filter set. After acquiring baseline readout in 2 Ca^{2+} or 0 Ca^{2+} buffers, cells were switched to 1 mM pyruvate in 2 Ca^{2+} or 0 Ca^{2+} buffer in perfusion. For experiments in 0 Ca^{2+} condition, cells were kept 3 min in 0 Ca^{2+} buffer prior to the start of the measurement to bring total time in 0 Ca^{2+} to 5 min. For mitochondrial pyruvate supply experiments, cells were perfused in 0 glucose + /− Ca^{2+} buffer for 5 min before the start of the measurement. After, 2 min baseline was taken in 0 glucose buffer with subsequent switch to ten glucose-containing buffer. The plateau phase in the respective ten glucose buffer was quantified.

Cytosolic lactate was measured with Laconic[71] (gift from Luis Felipe Barros, Addgene plasmid # 44238). Cells expressing Laconic were excited with 455 nm LED and emission collected at 480 nm and 530 nm using a CFP/YFP/RFP filter set and 505dcxr beam-splitter. After acquiring basal readout in 2 Ca^{2+}, the buffer was changed to 0 Ca^{2+} in perfusion and measured for 5–6 min. The increase in lactate after 5 min was quantified. For the rescue experiment, after 0 Ca^{2+} buffer, cells were perfused with 2 Ca^{2+} buffer for 10 min.

Cytosolic glucose was measured using FLII12Pglu-700µδ6[72] (gift from Wolf Frommer, Addgene plasmid # 17866). Cells expressing FLII12Pglu-700µδ6 were excited with 455 nm LED and emission collected at 480 nm and 530 nm using a CFP/YFP/RFP filter set and 505dcxr beam-splitter. Cells were perfused with either 2 Ca^{2+} or 0 Ca^{2+} buffers, after baseline recording, the perfusion buffer was changed to respective glucose-free buffer, after the signal reached a new flat baseline, glucose was re-added in perfusion.

Cytosolic pyruvate was measured with Pyronic[43] (gift from Luis Felipe Barros, Addgene plasmid # 51308). Cells expressing Pyronic were excited with 455 nm LED and emission collected at 480 nm and 530 nm using a CFP/YFP/RFP filter set and 505dcxr beam-splitter. After acquiring a baseline readout in 2 Ca^{2+} or 0 Ca^{2+} buffers, Lactate dehydrogenase (LDH) inhibitor GSK 2837808A[73] and Monocarboxylate transporter (MCT) inhibitor AR-C155858[74] were added in perfusion. Pyruvate accumulation was quantified after 5 min application.

Cytosolic NADH/NAD$^+$ ratio. Cytosolic NADH/NAD ratio was measured using Peredox[38] (gift from Gary Yellen, Addgene plasmid # 32383). EA.hy926 cells expressing Peredox were excited with 385 nm and 550 nm LEDs and emission collected using a CFP/YFP/RFP filter set and 565 LPXR beam-splitter (Semrock, USA). Basal readout in 2 Ca^{2+} buffer, as well as the change after perfusion with 0 Ca^{2+} buffer, was recorded. For rescue experiments, cells were further perfused for 10 min with 2 Ca^{2+} buffer. After every measurement, the green to red emission ratio, representing NADH/NAD$^+$ ratio, was normalized to maximum (1.0) and minimum (0) using 10 mM lactate and 10 mM pyruvate, respectively.

Cell viability and apoptosis assays. Cells were seeded on 96-well plates and left in an incubator under standard conditions for 24 h to settle. Afterward, cell viability was assessed with the CellTiter-Blue® Cell Viability Assay (Promega, Madison, USA) and the activity of caspase 3/7 was investigated as an indicator for apoptosis with the Caspase-Glo® 3/7 Assay (Promega, Madison, USA). Both assays were performed as per company instructions. Staurosporine was applied in a concentration of 1 µM for 16 h as a positive control for reduced cell viability and increased apoptosis. Finally, cells were washed and the protein concentration of each well was determined with the Pierce™ BCA Protein Assay Kit (Thermo Scientific, Rockford, IL, USA) in order to normalize the results.

Statistical analysis and reproducibility. Number of independent experiments is indicated in each figure legend along with the used statistical test and *p*-value. Statistical analyses, including student's *t*-test and analysis of variance (ANOVA) with Tukey post hoc test, were performed on GraphPad Prism software version 5.04 (GraphPad Software, San Diego, CA, USA) or Microsoft Excel (Microsoft Office 2013). All box and whisker plots show minimum to maximum values with the central line showing the median and boxes extending from 25–75% of the data set. All scatter plots show single cells. Differences with $p < 0.05$ were considered to be statistically significant.

Reporting summary. Further information on research design is available in the Nature Research Reporting Summary linked to this article.

Data availability

The source data used to generate the graphs and charts in the main manuscript and in the Supplementary Figures are available in Supplementary Data 1. Any additional data and resources used in the current manuscript are available from the corresponding author on reasonable request. Genetically encoded sensors used in the current manuscript that are available from Addgene: mito-Citron1[35] (gift from Robert Campbell, Addgene plasmid # 134305), mito-PyronicSF[36] (gift from Luis Felipe Barros, Addgene plasmid # 124813), Laconic[71] (gift from Luis Felipe Barros, Addgene plasmid # 44238), FLII12Pglu-700µδ6[72] (gift from Wolf Frommer, Addgene plasmid # 17866), Pyronic[43] (gift from Luis Felipe Barros, Addgene plasmid # 51308), Peredox[38] (gift from Gary Yellen, Addgene plasmid # 32383), 4mtD3cpv[68] (gift from Amy Palmer and Roger Tsien, Addgene plasmid #36324). Constructs not listed above are available upon reasonable request from the corresponding author.

Received: 3 June 2021; Accepted: 28 December 2021;
Published online: 20 January 2022

References

1. Medbo, J. I. & Tabata, I. Anaerobic energy release in working muscle during 30 s to 3 min of exhausting bicycling. *J. Appl. Physiol.* **75**, 1654–1660 (1993).

2. Molenaar, D., Van Berlo, R., De Ridder, D. & Teusink, B. Shifts in growth strategies reflect tradeoffs in cellular economics. *Mol. Syst. Biol.* **5**, 323 (2009).
3. DeBerardinis, R. J. et al. Beyond aerobic glycolysis: transformed cells can engage in glutamine metabolism that exceeds the requirement for protein and nucleotide synthesis. *Proc. Natl. Acad. Sci. USA* **104**, 19345–19350 (2007).
4. Fernandez-De-Cossio-Diaz, J. & Vazquez, A. Limits of aerobic metabolism in cancer cells. *Sci. Rep.* **7**, 1–8 (2017).
5. Berridge, M. J., Lipp, P. & Bootman, M. D. The versatility and universality of calcium signalling. *Nat. Rev. Mol. Cell Biol.* **1**, 11–21 (2000).
6. Brini, M., Ottolini, D., Calì, T. & Carafoli, E. Calcium in health and disease. *Met. Ions Life Sci.* **13**, 81–137 (2013).
7. Groschner, L. N., Waldeck-Weiermair, M., Malli, R. & Graier, W. F. Endothelial mitochondria-less respiration, more integration. *Pflügers Arch.* **464**, 63–76 (2012).
8. Rossi, A., Pizzo, P. & Filadi, R. Calcium, mitochondria and cell metabolism: a functional triangle in bioenergetics. *Biochim. Biophys. Acta Mol. Cell Res.* **1866**, 1068–1078 (2019).
9. Madreiter-Sokolowski, C. T. et al. Tracking intra- and inter-organelle signaling of mitochondria. *FEBS J.* **286**, 4378–4401 (2019).
10. Giacomello, M. et al. Ca^{2+} hot spots on the mitochondrial surface are generated by Ca^{2+} mobilization from stores, but not by activation of store-operated Ca^{2+} channels. *Mol. Cell* **38**, 280–290 (2010).
11. Marchi, S. et al. Mitochondrial and endoplasmic reticulum calcium homeostasis and cell death. *Cell Calcium* **69**, 62–72 (2018).
12. Baughman, J. M. et al. Integrative genomics identifies MCU as an essential component of the mitochondrial calcium uniporter. *Nature* **476**, 341–345 (2011).
13. Stefani, D., De, Raffaello, A., Teardo, E., Szabò, I. & Rizzuto, R. A forty-kilodalton protein of the inner membrane is the mitochondrial calcium uniporter. *Nature* **476**, 336–340 (2011).
14. Kamer, K. J. & Mootha, V. K. The molecular era of the mitochondrial calcium uniporter. *Nat. Rev. Mol. Cell Biol.* **16**, 545–553 (2015).
15. Waldeck-Weiermair, M. et al. Rearrangement of MICU1 multimers for activation of MCU is solely controlled by cytosolic Ca(2.). *Sci. Rep.* **5**, 15602 (2015).
16. Denton, R. M. Regulation of mitochondrial dehydrogenases by calcium ions. *Biochim. Biophys. Acta Bioenerg.* **1787**, 1309–1316 (2009).
17. Bravo, R. et al. Increased ER-mitochondrial coupling promotes mitochondrial respiration and bioenergetics during early phases of ER stress. *J. Cell Sci.* **124**, 2143–2152 (2011).
18. Peruzzo, R., Costa, R., Bachmann, M., Leanza, L. & Szabò, I. Mitochondrial metabolism, contact sites and cellular calcium signaling: implications for tumorigenesis. *Cancers* **12**, 2574 (2020).
19. Müller, M. et al. Mitochondria and calcium regulation as basis of neurodegeneration associated with aging. *Front. Neurosci.* **12**, 470 (2018).
20. Sharma, N., Arora, S., Saurav, S. & Motiani, R. K. Pathophysiological significance of calcium signaling at mitochondria-associated endoplasmic reticulum membranes (MAMs). *Curr. Opin. Physiol.* **17**, 234–242 (2020).
21. Koshenov, Z. et al. Sigma-1 receptor promotes mitochondrial bioenergetics by orchestrating ER Ca^{2+} leak during early ER stress. *Metab. 2021* **11**, 422 (2021).
22. Csordás, G. et al. Structural and functional features and significance of the physical linkage between ER and mitochondria. *J. Cell Biol.* **174**, 915–921 (2006).
23. Madreiter-Sokolowski, C. T. et al. Enhanced inter-compartmental Ca^{2+} flux modulates mitochondrial metabolism and apoptotic threshold during aging. *Redox Biol.* **20**, 458–466 (2019).
24. Madreiter-Sokolowski, C. T., Malli, R. M. & Graier, W. F. Mitochondrial-endoplasmic reticulum interplay: a lifelong on-off relationship? *Contact (Thousand Oaks)* **2**, 2515256419861227 (2019).
25. Chami, M. et al. Role of SERCA1 truncated isoform in the proapoptotic calcium transfer from ER to mitochondria during ER stress. *Mol. Cell* **32**, 641–651 (2008).
26. Madreiter-Sokolowski, C. T. et al. PRMT1-mediated methylation of MICU1 determines the UCP2/3 dependency of mitochondrial Ca^{2+} uptake in immortalized cells. *Nat. Commun.* **7**, 12897 (2016).
27. Koshenov, Z. et al. The contribution of uncoupling protein 2 to mitochondrial Ca^{2+} homeostasis in health and disease—a short revisit. *Mitochondrion* **55**, 164–173 (2020).
28. Chakraborty, P. K. et al. MICU1 drives glycolysis and chemoresistance in ovarian cancer. *Nat. Commun.* **8**, 14634 (2017).
29. Peruzzo, R. & Szabo, I. Contribution of mitochondrial ion channels to chemo-resistance in cancer cells. *Cancers* **11**, 761 (2019).
30. Imamura, H. et al. Visualization of ATP levels inside single living cells with fluorescence resonance energy transfer-based genetically encoded indicators. *Proc. Natl. Acad. Sci. USA* **106**, 15651–15656 (2009).
31. Denton, R. M., McCormack, J. G. & Edgell, N. J. Role of calcium ions in the regulation of intramitochondrial metabolism. Effects of Na^{+}, Mg^{2+} and ruthenium red on the Ca^{2+}-stimulated oxidation of oxoglutarate and on pyruvate dehydrogenase activity in intact rat heart mitochondria. *Biochem. J* **190**, 107–117 (1980).
32. Denton, R. M. Regulation of mitochondrial dehydrogenases by calcium ions. *Biochim. Biophys. Acta Bioenerg.* **1787**, 1309–1316 (2009).
33. Denton, R. M., Randle, P. J. & Martin, B. R. Stimulation by calcium ions of pyruvate dehydrogenase phosphate phosphatase. *Biochem. J* **128**, 161–163 (1972).
34. Pettit, F. H., Roche, T. E. & Reed, L. J. Function of calcium ions in pyruvate dehydrogenase phosphatase activity. *Biochem. Biophys. Res. Commun.* **49**, 563–571 (1972).
35. Zhao, Y., Shen, Y., Wen, Y. & Campbell, R. E. High-performance intensiometric direct- and inverse-response genetically encoded biosensors for citrate. *ACS Cent. Sci.* **6**(8), 1441–1450 (2020).
36. Arce-Molina, R. et al. A highly responsive pyruvate sensor reveals pathway-regulatory role of the mitochondrial pyruvate carrier MPC. *Elife* **9**, e53917 (2020).
37. Denton, R. M. et al. The hormonal regulation of pyruvate dehydrogenase complex. *Adv. Enzyme Regul.* **36**, 183–198 (1996).
38. Hung, Y. P., Albeck, J. G., Tantama, M. & Yellen, G. Imaging cytosolic NADH-NAD^{+} redox state with a genetically encoded fluorescent biosensor. *Cell Metab.* **14**(4), 545–554 (2011).
39. Fan, J. et al. Tyrosine phosphorylation of lactate dehydrogenase A is important for NADH/NAD^{+} redox homeostasis in cancer cells. *Mol. Cell. Biol.* **31**(24), 4938–4950 (2011).
40. Arco, A. D. E. L., Agudo, M. & Satrústegui, J. Characterization of a second member of the subfamily of calcium-binding mitochondrial carriers expressed in human non-excitable tissues. *Biochem. J* **345**, 725–732 (2000).
41. Palmieri, L. et al. Citrin and aralar1 are Ca^{2+}-stimulated aspartate/glutamate transporters in mitochondria. *EMBO J.* **20**, 5060–5069 (2001).
42. Gottschalk, B. et al. MICU1 controls cristae junction and spatially anchors mitochondrial Ca^{2+} uniporter complex. *Nat. Commun.* **10**, 3732 (2019).
43. San Martín, A. et al. Imaging mitochondrial flux in single cells with a FRET sensor for pyruvate. *PLoS One* **9**(1), e85780 (2014).
44. Madreiter-Sokolowski, C. T., Gottschalk, B., Sokolowski, A. A., Malli, R. & Graier, W. F. Dynamic control of mitochondrial Ca^{2+} levels as a survival strategy of cancer cells. *Front. Cell Dev. Biol.* **9**, 1–14 (2021).
45. Gafni, J. et al. Xestospongins: potent membrane permeable blockers of the inositol 1,4,5–trisphosphate receptor. *Neuron* **19**(3), 723–733 (1997).
46. Schleifer, H. et al. Novel pyrazole compounds for pharmacological discrimination between receptor-operated and store-operated Ca^{2+} entry pathways. *Br. J. Pharmacol.* **167**(8), 1712–1722 (2012).
47. Bartok, A. et al. IP3 receptor isoforms differently regulate ER-mitochondrial contacts and local calcium transfer. *Nat. Commun.* **10**, 3726 (2019).
48. Prakriya, M. et al. Orai1 is an essential pore subunit of the CRAC channel. *Nature* **443**, 230–233 (2006).
49. Lasorsa, F. M. et al. Recombinant expression of the Ca^{2+} -sensitive aspartate/glutamate carrier increases mitochondrial ATP production in agonist-stimulated Chinese hamster ovary cells. *J. Biol. Chem.* **278**, 38686–38692 (2003).
50. Rubi, B., Arco, A., del, Bartley, C., Satrustegui, J. & Maechler, P. The malate-aspartate NADH shuttle member Aralar1 determines glucose metabolic fate, mitochondrial activity, and insulin secretion in beta cells. *J. Biol. Chem.* **279**, 55659–55666 (2004).
51. Contreras, L. et al. Ca^{2+} activation kinetics of the two aspartate-glutamate mitochondrial carriers, Aralar and Citrin. *J. Biol. Chem.* **282**, 7098–7106 (2007).
52. Rabinovich, S. et al. The mitochondrial carrier citrin plays a role in regulating cellular energy during carcinogenesis. *Oncogene* **39**, 164–175 (2020).
53. Mármol, P. et al. Requirement for aralar and its Ca^{2+} -binding sites in Ca^{2+} signal transduction in mitochondria from INS-1 Clonal β-cells. *J. Biol. Chem.* **284**, 515–524 (2008).
54. Borst, P. The malate–aspartate shuttle (Borst cycle): how it started and developed into a major metabolic pathway. in. *IUBMB Life* **72**, 2241–2259 (2020).
55. Wescott, A. P., Kao, J. P. Y., Lederer, W. J. & Boyman, L. Voltage-energized calcium-sensitive ATP production by mitochondria. *Nat. Metab.* **1**, 975–984 (2019).
56. Szibor, M. et al. Cytosolic, but not matrix, calcium is essential for adjustment of mitochondrial pyruvate supply. *J. Biol. Chem.* **295**, 4383–4397 (2020).
57. Luengo, A. et al. Increased demand for NAD^{+} relative to ATP drives aerobic glycolysis. *Mol. Cell* **81**, 691–707 e6 (2021).
58. Pérez-Liébana, I. et al. A feed-forward Ca^{2+} -dependent mechanism boosting glycolysis and OXPHOS by activating aralar-malate-aspartate shuttle, upon neuronal stimulation. *bioRxiv* 429391, https://www.biorxiv.org/content/10.1101/2021.02.02.429391v1 (2021).
59. Hayasaka, K. Metabolic basis and treatment of citrin deficiency. *J. Inherit. Metab. Dis.* **44**, 110–117 (2021).

60. Greenhouse, W. V. & Lehninger, A. L. Occurrence of the malate-aspartate shuttle in various tumor types. *Cancer Res.* **36**, 1392–1396 (1976).
61. Greenhouse, W. V. & Lehninger, A. L. Magnitude of malate-aspartate reduced nicotinamide adenine dinucleotide shuttle activity in intact respiring tumor cells. *Cancer Res.* **37**, 4173–4181 (1977).
62. Thangaratnarajah, C., Ruprecht, J. J. & Kunji, E. R. S. Calcium-induced conformational changes of the regulatory domain of human mitochondrial aspartate/glutamate carriers. *Nat. Commun.* **5**, 5491 (2014).
63. Madreiter-Sokolowski, C. T. et al. Resveratrol specifically kills cancer cells by a devastating increase in the Ca^{2+} coupling between the greatly tethered endoplasmic reticulum and mitochondria. *Cell. Physiol. Biochem.* **39**, 1404–1420 (2016).
64. Huang, X. et al. ERP44 inhibits human lung cancer cell migration mainly via IP3R2. *Aging (Albany NY)* **8**, 1276 (2016).
65. Palmer, A. E., Jin, C., Reed, J. C. & Tsien, R. Y. Bcl-2-mediated alterations in endoplasmic reticulum Ca^{2+} analyzed with an improved genetically encoded fluorescent sensor. *Proc. Natl. Acad. Sci. USA* **101**, 17404–17409 (2004).
66. Zhao, Y. et al. An expanded palette of genetically encoded Ca^{2+} indicators. *Science* **333**, 1888–1891 (2011).
67. Waldeck-Weiermair, M. et al. Development and application of sub-mitochondrial targeted Ca^{2+} biosensors. *Front. Cell. Neurosci.* **13**, 449 (2019).
68. Palmer, A. E. et al. Ca^{2+} indicators based on computationally redesigned calmodulin-peptide pairs. *Chem. Biol.* **13**, 521–530 (2006).
69. Vishnu, N. et al. ATP increases within the lumen of the endoplasmic reticulum upon intracellular Ca^{2+} release. *Mol. Biol. Cell* **25**, 368–379 (2014).
70. Bartolomé, F. & Abramov, A. Y. Measurement of mitochondrial nadh and fad auto fluorescence in live cells. *Methods Mol. Biol.* **1264**, 263–270 (2015).
71. San Martín, A. et al. A genetically encoded FRET Lactate sensor and its use to detect the Warburg effect in single cancer cells. *PLoS One* **8**, e57712 (2013).
72. Takanaga, H., Chaudhuri, B. & Frommer, W. B. GLUT1 and GLUT9 as major contributors to glucose influx in HepG2 cells identified by a high sensitivity intramolecular FRET glucose sensor. *Biochim. Biophys. Acta Biomembr* **1778**, 1091–1099 (2008).
73. Billiard, J. et al. Quinoline 3-sulfonamides inhibit lactate dehydrogenase A and reverse aerobic glycolysis in cancer cells. *Cancer Metab.* **1**, 19 (2013).
74. Ovens, M. J., Davies, A. J., Wilson, M. C., Murray, C. M. & Halestrap, A. P. AR-C155858 is a potent inhibitor of monocarboxylate transporters MCT1 and MCT2 that binds to an intracellular site involving transmembrane helices 7–10. *Biochem. J* **425**, 523–530 (2010).

Acknowledgements

The authors wish to thank Mrs. Anna Schreilechner, BSc, for her great work in maintaining cell culture. We are greatly indebted to Dr. Edgell (University of North Carolina, Chapel Hill, NC, U.S.A.) for providing us with the human endothelial cell line EA.hy926.

This work was supported/funded by the Austrian Science Fund (FWF) (DK-MCD W1226), MEFO Graz, BioTechMed Graz, Nikon Austria, and the Medical University of Graz. Z.K. and F.E.O. are supported by the FWF (DK-MCD W1226), and M.H. by MEFO Graz in course of the doctoral college DK-MCD.

Author contributions

Conceptualization and design of the work, Z.K. and W.F.G.; acquisition of data, Z.K., F.E.O., M.H., B.G., R.R.; analysis of data, Z.K., B.G.; interpretation of data, Z.K., W.F.G.; writing—original draft preparation, Z.K.; writing–review and editing, B.G., R.M., W.F.G.; All authors have read and agreed to the published version of the manuscript.

Competing interests

The authors declare no competing interests.

Additional information

Supplementary information The online version contains supplementary material available at https://doi.org/10.1038/s42003-022-03019-2.

Correspondence and requests for materials should be addressed to Wolfgang F. Graier.

Peer review information *Communications Biology* thanks Rajender K Motiani, Simone Patergnani and the other, anonymous, reviewers for their contribution to the peer review of this work. Primary Handling Editors: Eve Rogers. Peer reviewer reports are available.

Reprints and permission information is available at http://www.nature.com/reprints

Publisher's note Springer Nature remains neutral with regard to jurisdictional claims in published maps and institutional affiliations.

metabolites

MDPI

Article

Sigma-1 Receptor Promotes Mitochondrial Bioenergetics by Orchestrating ER Ca^{2+} Leak during Early ER Stress

Zhanat Koshenov [1], Furkan E. Oflaz [1], Martin Hirtl [1], Johannes Pilic [1], Olaf A. Bachkoenig [1], Benjamin Gottschalk [1], Corina T. Madreiter-Sokolowski [1], Rene Rost [1], Roland Malli [1,2] and Wolfgang F. Graier [1,2,*]

[1] Molecular Biology and Biochemistry, Gottfried Schatz Research Center, Medical University of Graz, Neue Stiftingtalstraße 6/6, 8010 Graz, Austria; zhanat.koshenov@medunigraz.at (Z.K.); furkan.oflaz@medunigraz.at (F.E.O.); martin.hirtl@medunigraz.at (M.H.); johannes.pilic@medunigraz.at (J.P.); olaf.bachkoenig@medunigraz.at (O.A.B.); benjamin.gottschalk@medunigraz.at (B.G.); corina.madreiter@medunigraz.at (C.T.M.-S.); rene.rost@medunigraz.at (R.R.); roland.malli@medunigraz.at (R.M.)

[2] BioTechMed Graz, Mozartgasse 12/II, 8010 Graz, Austria

* Correspondence: wolfgang.graier@medunigraz.at

Abstract: The endoplasmic reticulum (ER) is a complex, multifunctional organelle of eukaryotic cells and responsible for the trafficking and processing of nearly 30% of all human proteins. Any disturbance to these processes can cause ER stress, which initiates an adaptive mechanism called unfolded protein response (UPR) to restore ER functions and homeostasis. Mitochondrial ATP production is necessary to meet the high energy demand of the UPR, while the molecular mechanisms of ER to mitochondria crosstalk under such stress conditions remain mainly enigmatic. Thus, better understanding the regulation of mitochondrial bioenergetics during ER stress is essential to combat many pathologies involving ER stress, the UPR, and mitochondria. This article investigates the role of Sigma-1 Receptor (S1R), an ER chaperone, has in enhancing mitochondrial bioenergetics during early ER stress using human neuroblastoma cell lines. Our results show that inducing ER stress with tunicamycin, a known ER stressor, greatly enhances mitochondrial bioenergetics in a time- and S1R-dependent manner. This is achieved by enhanced ER Ca^{2+} leak directed towards mitochondria by S1R during the early phase of ER stress. Our data point to the importance of S1R in promoting mitochondrial bioenergetics and maintaining balanced H_2O_2 metabolism during early ER stress.

Keywords: sigma-1 receptor; mitochondrial bioenergetics; ER stress; UPR; ER Ca^{2+} leak; mitochondrial Ca^{2+}; mitochondrial metabolism

Citation: Koshenov, Z.; Oflaz, F.E.; Hirtl, M.; Pilic, J.; Bachkoenig, O.A.; Gottschalk, B.; Madreiter-Sokolowski, C.T.; Rost, R.; Malli, R.; Graier, W.F. Sigma-1 Receptor Promotes Mitochondrial Bioenergetics by Orchestrating ER Ca^{2+} Leak during Early ER Stress. *Metabolites* **2021**, *11*, 422. https://doi.org/10.3390/metabo11070422

Academic Editor: Ajit Divakaruni

Received: 17 May 2021
Accepted: 24 June 2021
Published: 26 June 2021

1. Introduction

Among a wide array of functions attributed to the endoplasmic reticulum (ER), its protein folding and Ca^{2+} signaling capabilities are perhaps the most studied ones. These functions require meticulous control and regulation, where disturbance of either can result in ER stress with serious pathological outcomes [1]. ER stress represents an inability of ER to properly fold and process proteins in its lumen, resulting in their accumulation and disruption of regular ER functions. There are three main proteins that sense and act upon ER stress, namely, double-stranded RNA-dependent protein kinase (PRK)-like ER kinase (PERK), activating transcription factor 6 (ATF6), and inositol requiring enzyme 1 (IRE1), which form the core of ER unfolded protein response (UPR) [2]. The primary function of UPR is to restore ER homeostasis following ER stress and involves halt of new protein synthesis, while increasing ER chaperone gene expression. These processes are accompanied by the removal of unfolded proteins (ERAD) from the ER lumen [3]. Importantly, since UPR is energetically demanding, the ER requires more ATP, mainly supplied by mitochondria [4]. Hence, it has been reported that ER-mitochondria tethering

is increased during the early stages of ER stress to exchange Ca^{2+} more efficiently and to promote mitochondrial ATP production [5]. Nevertheless, prolonged ER stress and UPR were shown to lead to apoptosis, due to mitochondrial Ca^{2+} overload [6].

Sigma-1 receptor (S1R), an ER chaperone mainly residing in mitochondria-associated ER membranes (MAMs), was implicated in both Ca^{2+} signaling and cell survival during ER stress [7]. Under ER stress, S1R was shown to interact with several prominent ER proteins, including inositol 1,4,5-trisphosphate receptor 3 (IP_3R3) and IRE1. Association of S1R with IP_3R3 was shown to stabilize the latter at the MAMs and increase ER-mitochondrial Ca^{2+} signaling [7], whereas interaction of S1R with IRE1 was shown to sustain prolonged UPR by IRE1 [8]. Numerous reports demonstrated the involvement of ER stress and S1R deficiency in various neurodegenerative diseases [9,10] and cancer [11], emphasizing the importance of elucidating the exact role of S1R in ER stress. In this work, we scrutinize the involvement of S1R in promoting mitochondrial bioenergetics during the early phases of ER stress by imaging mitochondrial and ER activities in single cells with high-resolution fluorescence microscopy. Using SH-SY5Y neuroblastoma cells, we have been able to demonstrate that S1R is indispensable for increased mitochondrial bioenergetics during early ER stress. We could show that this is achieved by an ER Ca^{2+} leak that is directed towards mitochondria by S1R.

2. Results

2.1. XBP1 Splicing Increases during Early ER Stress and Is Not Affected by Sigma-1 Receptor Knock-Down

To induce ER stress, SH-SY5Y neuroblastoma cells were treated with 0.6 µM tunicamycin for 2 h and 8 h. The X-box binding protein 1 (XBP1) splicing by IRE1, a well-established marker of ER stress [12,13], was not changed by S1R knock-down (S1R KD), while it was increased in cells treated with tunicamycin for 2 h that dramatically increased upon 8 h treatment (Figure 1a–c).

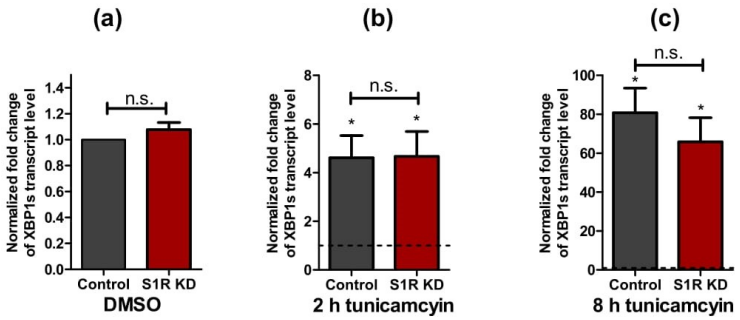

Figure 1. Impact of tunicamycin treatment on XBP1 splicing levels. Bar graphs represent mean ± SEM of spliced XBP1 transcript levels in control and S1R KD SH-SY5Y neuroblastoma cells under control conditions (**a**) or after tunicamycin treatment for 2 h (**b**) and 8 h (**c**). Dashed lines represent the transcript level of spliced XBP1 in the respective DMSO treated cells. Paired t-test, n = 3, * $p < 0.05$ against corresponding DMSO treated cells; unpaired t-test between control and S1R KD, n = 3, n.s.—not significant.

Since the majority of the experiments in this work were performed using single cells co-transfected with a genetically encoded sensor and siRNA, we quantified the knock-down efficiency in co-transfected GFP-positive sorted cells, which showed much higher knock-down efficiency compared to unsorted cells (Figure S1a,b).

2.2. Sigma-1 Receptor Is Essential for Increased Mitochondrial ATP Level during Early ER Stress

To assess the impact of S1R on mitochondrial bioenergetics during the early phases of ER stress, we measured mitochondrial ATP levels of SH-SY5Y cells using a genetically encoded mitochondria-targeted ATP probe, mtAT1.03 [14] after 2 h and 8 h of tunicamycin treatment. Mitochondrial ATP was maximally increased after 2 h and slightly after 8 h of tunicamycin treatment of control cells (Figure 2a). Basal mitochondrial ATP levels remained unaffected in cells treated with siRNA against S1R (Figure 2a,b). The mitochondrial ATP increases in response to tunicamycin at both time points were, however, abolished by S1R knock-down (Figure 2b), indicating the involvement of S1R in raising mitochondrial ATP during tunicamycin-induced ER stress. To further validate these results, we have used a selective S1R antagonist, BD1047 [15]. Similar to the knock-down of S1R, BD1047 did not affect basal ATP levels within mitochondria, but greatly attenuated the mitochondrial ATP elevations in response to 2 h and 8 h tunicamycin treatment (Figure 2c), thus supporting the need for S1R to increase mitochondrial ATP during early ER stress. Interestingly, neither knock-down nor BD1047 affected mitochondrial ATP levels without tunicamycin treatment (Figure 2d), implying the importance of S1R for mitochondrial ATP production primarily during ER stress.

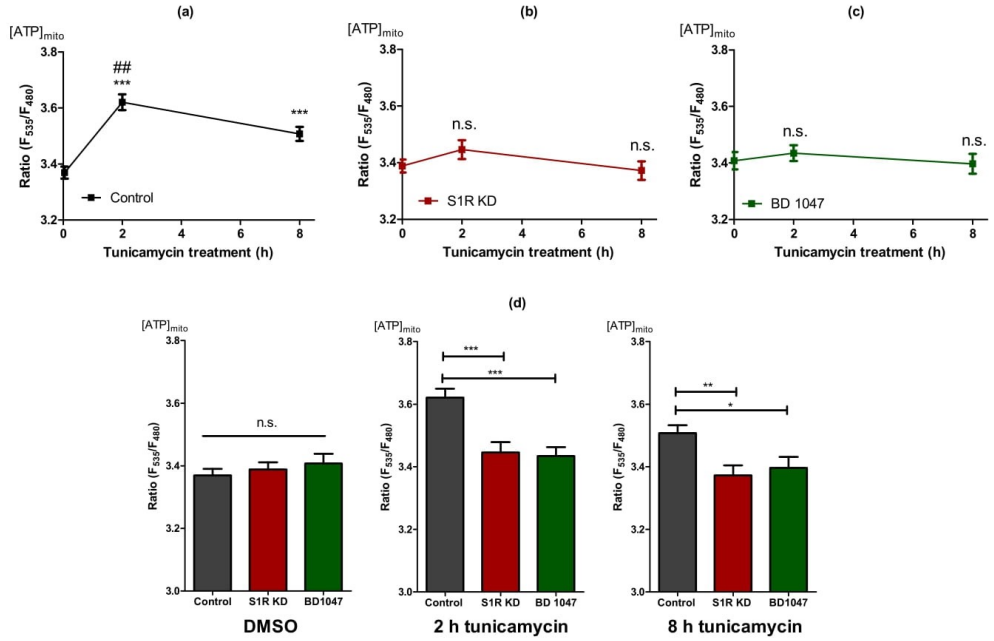

Figure 2. The increase in mitochondrial ATP levels during early ER stress is dependent on S1R. Time course of mitochondrial ATP levels after tunicamycin treatment, presented as mean ± SEM and assessed by the mitochondrial-targeted ATP biosensor AT1.03 in control SH-SY5Y cells (**a**), in cells with S1R KD (**b**) or after treatment with BD 1047 (**c**). (**d**) Bar graphs represent MEAN ± SEM of mitochondrial ATP levels in control (black), S1R KD (red), and BD1047 treated (green) cells before tunicamycin treatment (left), after 2 h (middle), or 8 h (right) tunicamycin treatment. One-way ANOVA with Tukey's multiple comparison test, * $p < 0.05$, ** $p < 0.01$, *** $p < 0.001$, ## $p < 0.001$ (comparison between control cells after 2 h and 8 h tunicamycin treatment), n.s.—not significant; Control DMSO (174 cells/18 experiments), Control 2 h tunicamycin (97 cells/10 experiments), Control 8 h tunicamycin (120 cells/11 experiments), S1R KD DMSO (141 cells/15 experiments), S1R KD 2 h tunicamycin (67 cells/7 experiments), S1R KD 8 h tunicamycin (74 cells/8 experiments), BD1047 DMSO (93 cells/9 experiments), BD1047 2 h tunicamycin (80 cells/7 experiments), BD1047 8 h tunicamycin (100 cells, 9 experiments).

2.3. Sigma-1 Receptor Is Promoting Mitochondrial Hyperpolarisation and NADH Consumption during Early ER Stress

Next, we investigated mitochondrial membrane potential (Ψ_m) using tetramethylrhodamine methyl ester (TMRM), a cationic fluorescent dye that accumulates in mitochondria in a membrane potential-dependent manner (Figure S2a). Ψ_m serves as a marker for mitochondrial bioenergetic status and was increased after 2 h of tunicamycin treatment, and restored to control levels after 8 h of treatment (Figure 3a). The increase in Ψ_m after 2 h was significantly lower in S1R KD cells in comparison to control cells (Figure 3b,c). The effect of S1R antagonist BD1047 was comparable to that of the siRNA-mediated KD (Figure S2b,c). Similar to mitochondrial ATP data, Ψ_m emphasizes the importance of S1R for mitochondrial bioenergetics during the initial steps of ER stress.

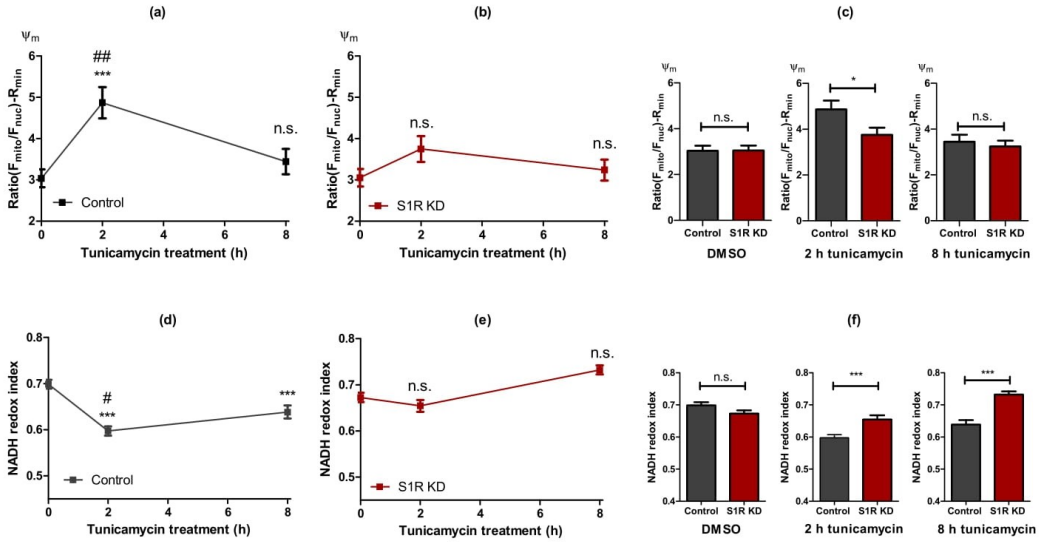

Figure 3. Alterations in the mitochondrial bioenergetic status are largely dependent on S1R during early ER stress. Time course of Ψ_m after tunicamycin treatment, presented as mean ± SEM and assessed by the mitochondrial to nucleus TMRM fluorescence ratio in control SH-SY5Y cells (**a**) and in cells with S1R KD (**b**). Bar graphs represent MEAN ± SEM of Ψ_m in control (black) and S1R KD (red) cells before tunicamycin treatment (left), after 2 h (middle), or 8 h (right) tunicamycin treatment (**c**). Time course of NADH redox index after tunicamycin treatment, presented as MEAN ± SEM and assessed NADH autofluorescence in control SH-SY5Y cells (**d**) and in cells with S1R KD (**e**). Bar graphs represent MEAN ± SEM of NADH redox index in control (black) and S1R KD (red) cells before tunicamycin treatment (left), after 2 h (middle), or 8 h (right) tunicamycin treatment (**f**). One-way ANOVA with Tukey's multiple comparison test (**a**,**b**,**d**,**e**), *** $p < 0.001$, ## $p < 0.01$ and # $p < 0.05$ (control 2 h tunicamycin against control 8hr tunicamycin), n.s.—not significant; unpaired t-test (**c**,**f**), *** $p < 0.001$, * $p < 0.05$, n.s.—not significant; Ψ_m: Control DMSO (57 cells/10 experiments), Control 2hr tunicamycin (31 cell/5 experiments), Control 8hr tunicamycin (42 cells/7 experiments), S1R KD DMSO (54 cells/10 experiments), S1R KD 2 h tunicamycin (29 cells/5 experiments), S1R KD 8 h tunicamycin (40 cells/7 experiments); NADH redox index: Control DMSO (208 cells/9 experiments), Control 2 h tunicamycin (203 cell/6 experiments), Control 8 h tunicamycin (143 cells/6 experiments), S1R KD DMSO (243 cells/9 experiments), S1R KD 2hr tunicamycin (111 cells/5 experiments), S1R KD 8hr tunicamycin (129 cells/6 experiments).

We next evaluated mitochondrial NADH redox index [16] as an additional readout for mitochondrial bioenergetics, measured as mitochondrial NADH autofluorescence normalized to the minimum and maximum values achieved by uncoupling and blocking of NADH dehydrogenase complex, respectively. NADH redox index was decreased by 2 h of tunicamycin treatment and less so by 8 h of treatment (Figure 3d), which indicates more

energized mitochondria. Since the NADH redox index represents NADH/NAD^+ ratio, the decline of this ratio, combined with increased mitochondrial membrane potential and ATP, means more flux of electron donors (NADH) to the electron transport chain (ETC). S1R KD abolished this reduction of the NADH redox index at both time points (Figure 3e). The difference between the control group and the S1R knock-down was only apparent during ER stress induction by tunicamycin treatment (Figure 3f).

Since tunicamycin-induced alterations in mitochondrial ATP, Ψ_m, and NADH redox index were abolished by S1R KD and/or the usage of an S1R antagonist, we assume S1R to serve as a key player in controlling mitochondrial bioenergetics during ER stress. Hence, because the 2 h treatment with tunicamycin resulted in a pronounced boost in mitochondrial bioenergetics, and this increase is approaching baseline status after 8 h of ER stress, S1R seems to be crucial, particularly during the early phase of ER stress.

2.4. Early ER Stress Gives Rise to an Increased ER Ca^{2+} Flux That Is Directed towards Mitochondria by Sigma-1 Receptor

To clarify the mechanism of how S1R is facilitating the increase of mitochondrial bioenergetics during early ER stress, we investigated mitochondria-associated ER membranes (MAMs). Although increased MAMs were reported for HeLa cells after 4 h of ER stress [5], we observed no change in the MAMs of tunicamycin treated control cells or the respective S1R knock-down cells (Figure S3a,b).

Further on, we investigated whether ER stress is associated with an ER Ca^{2+} leak by using genetically-encoded ER Ca^{2+} probe D1ER [17]. Thereby, the ER Ca^{2+} leak was estimated by the change in ER Ca^{2+} level in response to the removal of extracellular Ca^{2+}, which excludes the possibility of ER Ca^{2+} refilling. ER Ca^{2+} leak was increased by tunicamycin treatment for 2 and 8 h in control cells (Figure 4a). Interestingly, ER Ca^{2+} leak remained unaffected by tunicamycin treatment in S1R KD (Figure 4b), and BD1047 treated (Figure 4c) cells, but was found to be elevated in untreated S1R KD and BD1047 cells compared to controls (Figure 4d, left panel). In addition to the ER Ca^{2+} leak, we observed an unexpected increase in basal ER Ca^{2+} load with 2 and 8 h of tunicamycin treatment (Figure S4a). Similar to the leak, basal ER Ca^{2+} of S1R KD cells did not change with tunicamycin treatment (Figure S4b) and was higher in non-treated S1R KD cells compared to controls (Figure S4d, left panel), whereas the basal ER Ca^{2+} of BD1047 treated cells did not differ from controls (Figure S4c,d).

The increase in ER Ca^{2+} leak in response to tunicamycin could explain increased mitochondrial bioenergetics in control cells, since the increased leak would supply mitochondria with more Ca^{2+} under these conditions. However, since a similarly strong ER Ca^{2+} leak was also established by S1R knock-down and BD1047 treatment, but without changes in mitochondrial bioenergetics, further experiments were necessary to clarify these differences.

Thus, we also quantified basal mitochondrial Ca^{2+} level using the genetically encoded mitochondria-targeted Ca^{2+} biosensor, 4mtD3cpv [18]. We observed increased mitochondrial Ca^{2+} levels in control cells in response to tunicamycin treatment (Figure 4e). Interestingly, mitochondrial Ca^{2+} levels were not significantly affected by S1R knock-down cells with or without tunicamycin treatment (Figure 4f,g) despite the increased ER Ca^{2+} leak (Figure 4b,d). These results point to a possible function of S1R during early ER stress, which is directing the enhanced ER Ca^{2+} leak towards sites of mitochondrial Ca^{2+} uptake, while the knock-down of S1R yields an undirected ER Ca^{2+} leak, which is less sensed by mitochondria. The fact that ER Ca^{2+} leak was not changed between 2 h and 8 h of tunicamycin treatment (Figure 4a), but mitochondrial Ca^{2+} level is diminished from 2 h to 8 h of ER stress (Figure 4e), points to a possibility that S1R's "directing" activity of ER Ca^{2+} leak is a time-dependent phenomenon. The diminishing of the mitochondrial Ca^{2+} increase after 8 h of ER stress also explains the return of mitochondria to the basal bioenergetic state observed in control cells (Figures 2a and 3a,d).

To test whether the observed differences in mitochondrial Ca^{2+} were due to the direction of the ER Ca^{2+} leak and not associated with Ca^{2+} "permeability" of the mitochondrial inner membrane, we measured Ca^{2+} levels in the mitochondrial inter-membrane space (IMS) using a recently developed IMS-targeted genetically encoded ratiometric Ca^{2+} sensor, IMS-GEM-GECO [19,20]. IMS Ca^{2+} closely followed the same trends as the mitochondrial Ca^{2+}, with an increase after 2 h of tunicamycin treatment, which was normalized after 8 h of treatment (Figure 4h and Figure S5a). In S1R depleted and BD1047 treated cells, tunicamycin treatment did not elevate IMS Ca^{2+} after 2 h and 8 h (Figure 4i,j and Figure S5b,c), thus supporting our assumption of a specific role of S1R as an orchestrator of the enhanced ER Ca^{2+} leak during early ER stress, directing the Ca^{2+} leak towards mitochondrial Ca^{2+} uptake sites.

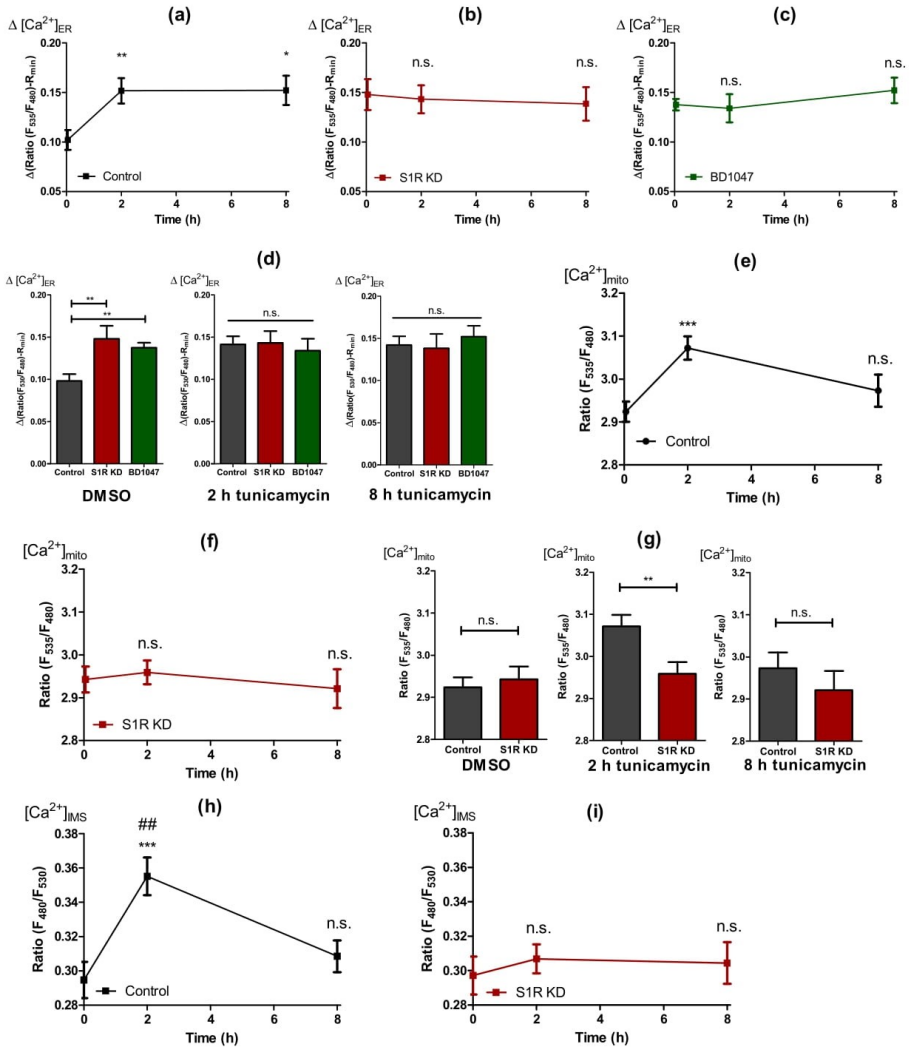

Figure 4. *Cont.*

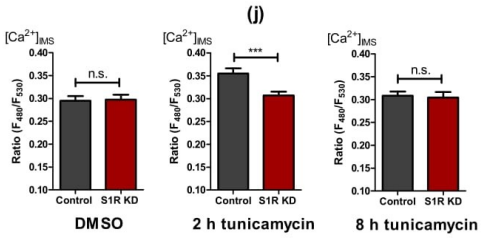

Figure 4. Cells develop an enhanced ER Ca^{2+} leak that is directed towards mitochondria by S1R during early ER stress. Time course of ER Ca^{2+} leak after tunicamycin treatment, presented as mean ± SEM and assessed by change in normalized D1ER ratio in control (**a**), S1R KD (**b**) and BD1047 treated (**c**) SH-SY5Y cells. Bar graphs represent MEAN ± SEM of ER Ca^{2+} leak in control (black), S1R KD (red) and BD1047 treated (green) cells before tunicamycin treatment (left), after 2 h (middle), or 8 h (right) tunicamycin treatment (**d**). Time course of mitochondrial Ca^{2+} level after tunicamycin treatment, presented as MEAN ± SEM and assessed by 4mtD3cpv ratio in control SH-SY5Y cells (**e**) and in cells with S1R KD (**f**). Bar graphs represent MEAN ± SEM of mitochondrial Ca^{2+} levels in control (black) and S1R KD (red) cells before tunicamycin treatment (left), after 2 h (middle), or 8 h (right) tunicamycin treatment (**g**). Time course of IMS Ca^{2+} level after tunicamycin treatment, presented as MEAN ± SEM and assessed by IMS-GEM-GECO ratio in control SH-SY5Y cells (**h**) and in cells with S1R KD (**i**). Bar graphs represent MEAN ± SEM of IMS Ca^{2+} levels in control (black) and S1R KD (red) cells before tunicamycin treatment (left), after 2 h (middle), or 8 h (right) tunicamycin treatment (**j**). One-way ANOVA with Tukey's multiple comparison test (**a**–**c**,**e**,**f**,**h**,**i**), *** $p < 0.001$, ** $p < 0.01$, * $p < 0.05$, ## $p < 0.01$ (for h, control 2 h tunicamycin against control 8 h tunicamycin), n.s.—not significant; unpaired t-test (**d**,**g**,**j**), *** $p < 0.001$, ** $p < 0.01$, * $p < 0.05$, n.s.—not significant; ER Ca^{2+} leak: Control DMSO (43 cells/15 experiments), Control 2 h tunicamycin (44 cell/16 experiments), Control 8 h tunicamycin (38 cells/12 experiments), S1R KD DMSO (19 cells/9 experiments), S1R KD 2 h tunicamycin (27 cells/10 experiments), S1R KD 8 h tunicamycin (19 cells/6 experiments), BD1047 DMSO (23 cells/11 experiments), BD1047 2 h tunicamycin (9 cells/6 experiments), BD1047 8 h tunicamycin (18 cells/6 experiments); Mitochondrial Ca^{2+}: Control DMSO (38 cells/14 experiments), Control 2 h tunicamycin (40 cell/13 experiments), Control 8 h tunicamycin (29 cells/8 experiments), S1R KD DMSO (35 cells/14 experiments), S1R KD 2 h tunicamycin (38 cells/12 experiments), S1R KD 8 h tunicamycin (25 cells/8 experiments); IMS Ca^{2+}: Control DMSO (37 cells/4 experiments), Control 2 h tunicamycin (35 cell/4 experiments), Control 8 h tunicamycin (28 cells/3 experiments), S1R KD DMSO (38 cells/4 experiments), S1R KD 2 h tunicamycin (39 cells/4 experiments), S1R KD 8 h tunicamycin (36 cells/4 experiments).

2.5. Sigma-1 Receptor Protects against Increased Mitochondrial ROS Production during ER Stress

Along with Ca^{2+} signaling and energy metabolism, mitochondrial reactive oxygen species (ROS) production plays a significant part in mitochondrial and cellular fitness under ER stress [21,22]. As it has been reported that S1R has an important role in mitochondrial ROS metabolism [8,23], we investigated the contribution of S1R to mitochondrial ROS production in our model of early ER stress in SH-SY5Y neuroblastoma cells. We monitored mitochondrial ROS using the genetically encoded mitochondrial ROS sensor, mitoHyper7 [24]. Induction of ER stress in control cells with tunicamycin for 2 h did not yield a change in mitochondrial ROS, whereas after 8 h of treatment, mitochondrial ROS levels significantly increased (Figure 5a). On the other hand, tunicamycin treatment resulted in a reasonably linear increase in mitochondrial ROS in S1R knock-down cells, with drastically increased ROS levels after 8 h of treatment (Figure 5b). Basal mitochondrial ROS, as well as ROS levels after 2 h and 8 h of tunicamycin treatment, were increased by S1R knock-down (Figure 5c). These results indicate that S1R prevents mitochondrial ROS production during early ER stress.

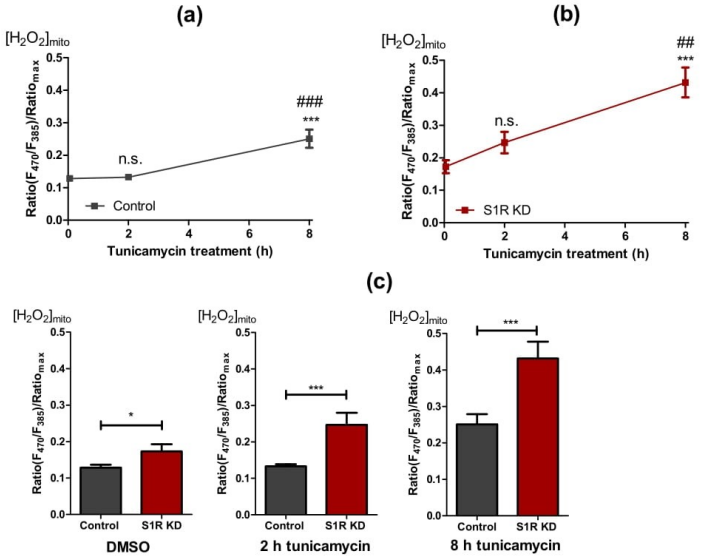

Figure 5. S1R KD is accompanied by increased ROS levels. Time course of mitochondrial H_2O_2 levels after tunicamycin treatment, presented as mean ± SEM and assessed by the mitoHyPer7 in control SH-SY5Y cells (**a**) and in cells with S1R KD (**b**). Bar graphs represent mean ± SEM of mitochondrial H_2O_2 levels in control (black) and S1R KD (red) cells before tunicamycin treatment (left), after 2 h (middle), or 8 h (right) tunicamycin treatment (**c**). Comparison of the mitochondrial ROS level in control and S1R KD cells at corresponding treatment durations (error bars are SEM); One-way ANOVA with Tukey's multiple comparison test (**a**,**b**), *** $p < 0.001$, ## $p < 0.01$ (for b, S1R KD 8 h against S1R KD 2 h), ### p < 0.001 (for a, control 8 h against control 2 h), n.s.—not significant; unpaired t-test (**c**), * $p < 0.05$, *** $p < 0.001$; Control DMSO (22 cells/7 experiments), Control 2 h tunicamycin (32 cell/10 experiments), Control 8 h tunicamycin (22 cells/6 experiments), S1R KD DMSO (19 cells/9 experiments), S1R KD 2 h tunicamycin (27 cells/10 experiments), S1R KD 8 h tunicamycin (19 cells/6 experiments).

3. Discussion

Since ER stress and UPR are hallmarks of many human pathologies, including neurodegeneration and cancer [9,11], we have attempted to clarify the involvement of S1R in mitochondrial bioenergetics during the early phases of ER stress. We have induced ER stress in SH-SY5Y neuroblastoma cells with tunicamycin treatment for 2 and 8 h and validated it by quantifying XBP1 splicing (Figure 1a,b). Our data did not support previously reported findings that S1R affects XBP1 splicing [8], which is likely explained by the low knock-down efficiency of S1R in our model system (Figure S1a). Low knock-down efficiency is stemming out of a low transfection rate (10%) and the absence of a marker for transfected cells in the qPCR analysis used to quantify XBP1 splicing. When the knock-down efficiency was assessed in co-transfected GFP-positive sorted cells, S1R mRNA level was reduced by 75% (Figure S1b). Consequently, the absence of a significant difference in XBP1 splicing between control and S1R knock-down cells is not definitive. A slight reduction of XBP1 splicing in S1R KD cells was observed after 8 h of tunicamycin treatment and might indicate the reduced IRE1 activity because of S1R knock-down. For all the remaining experiments, we have inclined towards single-cell measurements.

Having established ER stress induction over time in vitro, we could demonstrate that mitochondrial bioenergetics are getting substantially augmented after 2 h of ER stress (Figures 2a and 3a,d). S1R seems to play a major role in this adaptation, since knock-down and a pharmacological antagonist of S1R almost eliminated respective responses

(Figures 2b,c and 3b,e and Figure S2c). In search for a possible mechanism of action of S1R, we measured the amount of MAMs, as it has been reported that MAMs are increasing during early or later stages of ER stress [5,25]. Our results in SH-SY5Y cells showed no detectable changes in MAMs after 2 h and 8 h of tunicamycin treatment in control or S1R knock-down cells (Figure S3a,b). The possible reasons for discrepancies with published data could be specificities of cell lines used, as most of the reported studies were performed in HeLa cells [5,25].

Next, we looked directly into ER Ca^{2+} leak, since it can influence mitochondrial energetics during ER stress and was previously reported to be increased during ER stress [26,27]. In line with these reports, we have observed increased ER Ca^{2+} leak after 2 h and 8 h of tunicamycin treatment in control cells (Figure 4a). Still, surprisingly, a similar leak was present in untreated S1R knock-down and BD1047 treated cells, which did not change with tunicamycin treatment (Figure 4b–d). This was a puzzling finding, since the increased leak in S1R KD and BD1047 treatment did not fit together with mitochondrial energetics data, unless the Ca^{2+} leak was not directed towards mitochondria in knock-down BD1047 treated cells.

We could elaborate supportive data for the latter as mitochondrial, and IMS Ca^{2+} levels were increased after 2 h of tunicamycin treatment in control and not in S1R KD and antagonist treated cells (Figure 4e–j and Figure S5a–c), despite the presence of comparable ER Ca^{2+} leak after 2 h and 8 h of ER stress in all conditions. The prevalence of the increased Ca^{2+} level in the IMS during early ER stress in control and not in S1R KD and BD1047 treated cells validates the driving role of S1R directed ER Ca^{2+} leak as a promoter of mitochondrial bioenergetics and removes the possibility of hampered permeability of mitochondrial inner membrane as a result of reduced level or activity of S1R. Additionally, since the reduction of S1R expression by siRNA or the activity by the antagonist on its own was enough to trigger ER Ca^{2+} leak (Figure 4d, left panel) that was not directed to mitochondria, it is easy to speculate that S1R is essential for ER homeostasis under unstressed conditions as well.

In support of our findings, a recent study elegantly showed a UPR-independent function of IRE1, where it serves as a scaffold for IP_3R at the MAMs [28], and another study showed that S1R stabilizes IRE1 during ER stress at the MAM region [8]. Together with these interesting reports, our current work points towards the function of S1R as a director of ER Ca^{2+} towards mitochondria during early ER stress as a mechanism to increase mitochondrial bioenergetics to eventually supply more ATP for UPR. Diminishing mitochondrial ATP and bioenergetics after 8 h of ER stress (Figures 2a and 3a,d) despite the same enhanced ER Ca^{2+} leak (4a) in control cells adds an extra argument in support of time dependency of S1R orchestrated ER Ca^{2+} leak directed at mitochondria. In support of this claim, it was previously shown that S1R redistributes from the MAM region towards the remaining parts of the ER after prolonged ER stress [7], hence its ER leak directing function would be decreasing as ER stress progresses further. As a result, the ER Ca^{2+} leak would no longer be pointed towards mitochondria, as evidenced by a drop of the mitochondrial and IMS Ca^{2+} levels back to basal levels after 8 h of ER stress (Figure 4e,h).

Although the matter of ER Ca^{2+} leak directed towards sites of mitochondrial Ca^{2+} uptake by S1R to enhance mitochondrial bioenergetics to supply ATP for ER UPR seems fitting to the overall picture, the molecular identity of protein(s) responsible for the S1R controlled mitochondria-directed ER Ca^{2+} leak is not clear. We are tempted to speculate that IP_3R3 is the likely candidate, but this claim needs further investigation. Our findings of increased basal ER Ca^{2+} levels that we observed in S1R knock-down cells and control cells treated with tunicamycin are not clear and need further attention. One possible explanation might be that S1R antagonizes store-operated Ca^{2+} entry (SOCE) [29]; hence the knock-down of S1R might result in increased ER Ca^{2+} level as a result of increased SOCE. Additionally, increased mitochondrial ATP production during early ER stress (Figure 2a) could enhance ER Ca^{2+} sequestration through sarco(endo)plasmic reticulum Ca^{2+}-ATPase (SERCA) activity.

By increasing mitochondrial bioenergetics during early ER stress, S1R maintains a supply of ATP to fuel UPR to restore ER homeostasis, but in the meanwhile, it is known that enhanced oxidative phosphorylation can generate ROS. To compensate for this, S1R shows the ability to moderate excessive ROS production, as we have demonstrated S1R's importance in maintaining a balanced ROS metabolism under resting and ER stress conditions (Figure 5). These findings are supported by published data emphasizing the involvement of S1R in protection against oxidative stress and provide a possible mechanism for enhanced cell death of S1R deficient cells undergoing ER stress [7,8,23]. Taken together, by simultaneously enhancing mitochondrial bioenergetics and reducing ROS generation, S1R acts as a pro-survival agent for a cell facing ER stress.

In conclusion, we have demonstrated that S1R plays a crucial role during the early stages of ER stress, whereby it promotes mitochondrial bioenergetics by directed Ca^{2+} mobilization and protects against mitochondrial ROS elevation. We provide novel mechanistic insights into the complex ER-to-mitochondria communication during the onset of ER stress which might have multiple implications in different human pathologies, and highlight the need for further studies involving pre-clinical disease models involving ER stress, such as Alzheimer's disease and other neurodegenerative disorders.

4. Materials and Methods

List of abbreviations and sensors used in the study.

Abbreviation	Expanded Version
ER	Endoplasmic reticulum
UPR	Unfolded protein response
S1R	Sigma-1 Receptor
PERK	Double-stranded RNA-dependent protein kinase (PRK)-like ER kinase
ATF6	Activating transcription factor 6
IRE1	Inositol requiring enzyme 1
ERAD	Endoplasmic-reticulum-associated protein degradation
MAMs	Mitochondria-associated ER membranes
IP_3R3	Inositol 1,4,5-trisphosphate receptor
XBP1	X-box binding protein 1
KD	Knock-down
siRNA	Small interfering RNA
GFP	Green fluorescent protein
DMSO	Dimethyl sulfoxide
ATP	Adenosine triphosphate
FRET	Förster resonance energy transfer
Ψ_m	Mitochondrial membrane potential
NADH	Nicotinamide adenine dinucleotide
IMS	Mitochondrial inter-membrane space
ROS	Reactive oxygen species
SERCA	Sarco(endo)plasmic reticulum Ca^{2+}-ATPase

Sensor	Definition	Reference
mtAT1.03	Genetically encoded mitochondrial matrix targeted FRET-based ATP biosensor	[14]
TMRM	Tetramethylrhodamine methyl ester	
D1ER	Genetically encoded ER targeted FRET-based Ca^{2+} biosensor	[17]
4mtD3cpv	Genetically encoded mitochondrial matrix targeted FRET-based Ca^{2+} biosensor	[18]
IMS-GEM-GECO	Genetically encoded mitochondrial IMS targeted ratiometric Ca^{2+} biosensor	[19,20]
mitoHyper7	Genetically encoded mitochondrial matrix targeted ratiometric ROS biosensor	[24]

4.1. Cell Culture and Transfection

Human neuroblastoma SH-SY5Y cells (Sigma-Aldrich, catalogue number 94030304, lot number 18I031, passage number 11) were grown in Dulbecco's Modified Eagle's Medium (DMEM) (Sigma-Aldrich; Vienna, Austria) containing 10% FCS, penicillin (100 U/mL), streptomycin (100 µg/mL), amphotericin (1.25 µg/mL), 1 g/L glucose and 4 mM glutamine

in a humidified incubator (37 °C, 5% CO_2, 95% air). Cells were used until passage 20. Cells were tested for mycoplasma contamination and were negative. For all microscopy experiments with S1R knock-down (siRNA sequence: 5′-GCU CAC CAC CUA CCU CUU UdTdT-3′) with or without genetically encoded sensors, cells were plated on 30 mm glass coverslips and transfected at 60–80% confluence with siRNA using 3 µL of TransFast transfection reagent (Promega, Madison, WI, USA) in 1 mL serum- and antibiotic-free medium with or without 1 µg plasmid DNA encoding an appropriate sensor for 10–16 h. Afterward, the transfection media was replaced by a full culture medium. All experiments were performed 40–48 h after transfection. Prior to experiments, cells were adjusted to room temperature and shortly kept in experimental storage buffer (2 mM Ca^{2+}, 138 mM NaCl, 1 mM $MgCl_2$, 5 mM KCl, 10 mM HEPES, 2.6 mM $NaHCO_3$, 0.44 mM KH_2PO_4, amino acid, and vitamin mix, 10 mM glucose, 2 mM L-glutamine, 1% Penicillin/Streptomycin, 1% Fungizone, pH adjusted to 7.4).

Tunicamycin (0.6 µM, 1/10.000 dilution from DMSO stock) or DMSO (1/10.000 dilution) were added to the culture medium for indicated times, and treated cells were incubated in the humidified incubator. BD1047 (Cat. No. 0956, Tocris, Abingdon, UK) was dissolved in water and used at a final concentration of 10 µM and added along with tunicamycin or DMSO, and was also present in the experimental storage buffer.

4.2. Quantitative PCR and XBP1 Splicing

Total mRNA was isolated using RNeasy® Mini Kit (Qiagen, Hilden, Germany), and reverse transcription was done using Applied Biosystems High-Capacity cDNA Reverse Transcription kit (Thermo Fisher Scientific Baltics UAB, Vilnus, Lithuania). qPCR was performed using Promega GOTaq® qPCR Master Mix (Madison, WI, USA). Knock-down efficiency was determined using specific primers for S1R (Forward: CACTCGGGGCGCTACTG; reverse: TGTACTACCGTCTCCCCTGG) and normalized to HPRT1 and GAPDH (for sorted cells). Spliced XBP1 was analyzed with specific primers (forward: GCTGAGTCCGCAGCAGGT; reverse: CTGGGTCCAAGTTGTCCAGAAT). Spliced XBP1s were normalized to HPRT1.

4.3. Live Cell Imaging

All live-cell microscopy experiments were performed on an Olympus IX73 inverted microscope if not mentioned otherwise. The microscope is equipped with an UApoN340 40× oil immersion objective (Olympus, Tokyo, Japan) and a CCD Retiga R1 camera (Q-imaging, Tucson, AZ, Canada). For illumination, a LedHUB® (Omicron, Vienna, Germany) equipped with 340, 385, 455, 470, and 550 nm LEDs in combination with CFP/YFP/RFP (CFP/YFP/mCherry-3X, Semrock, Rochester, NY, USA) or GFP (GFP-3035D, Semrock, Rochester, NY, USA) filter set was used. Alternatively, an AnglerFish F-G/O (NGFI, Grraz, Austria) has been used. Data acquisition and control of the fluorescence microscope were performed using Visiview 4.2.01 (Visitron, Puchheim, Germany).

4.4. Mitochondrial ATP, Membrane Potential and NADH Redox Index Measurements

Mitochondrial ATP was measured using genetically encoded mitochondrial matrix targeted ATP sensor AT1.03 [14] (gift from Hiromi Imamura, Kyoto University, Kyodai Graduate School of Biostudies, Japan). The sensor was excited with 455 nm LED and emission collected at 480 nm and 530 nm using a CFP/YFP/RFP filter set and 505dcxr beam-splitter. Background-subtracted emission ratio of 530/480 was analyzed.

Mitochondrial membrane potential was measured using tetramethylrhodamine methyl ester (TMRM). TMRM was excited with 550 nm LED and emission collected at 600 nm using CFP/YFP/RFP filter set. Cells were incubated with 20 nM TMRM in an experimental storage buffer for 20 min at room temperature. During the measurement, cells were perfused with physiological buffer (2 mM Ca^{2+}, 135 mM NaCl, 1 mM $MgCl_2$, 5 mM KCl, 10 mM HEPES, 10 mM glucose, pH adjusted to 7.4) using a gravity-based perfusion system (NGFI, Graz, Austria). After the baseline recording, cells were perfused with physiological

buffer containing 1 µm FCCP to fully depolarize mitochondria to obtain the minimum values. Background-subtracted TMRM fluorescence ratio of mitochondrial to nucleus region was used as readout.

Mitochondrial NADH autofluorescence was monitored using 340 nm LED as previously described [16]. Shortly, SH-SY5Y cells were perfused with physiological buffer to record baseline reading, followed by perfusion with 0.5 µM FCCP until the signal reached the minimum and flatted, and then perfused with 2 µM rotenone until a plateau is reached. Mitochondrial NADH redox index was quantified as background-subtracted baseline autofluorescence normalized by subtracting the minimum value reached by FCCP and divided by the maximum value reached by rotenone.

4.5. ER Ca^{2+} Measurements

ER Ca^{2+} was measured with genetically encoded ER Ca^{2+} sensor D1ER [17] on an inverted wide field microscope (Observer.A1, Carl Zeiss GmbH, Vienna, Austria) equipped with a 40x objective (Plan Apochromat 1,3 NA Oil DIC (UV) VIS-IR, Carl Zeiss GmbH, Vienna, Austria) and a standard CFP/YFP filter cube. D1ER was excited with 425 nm and emission collected with 505dcxr beam-splitter on two sides of the camera (CCD camera, Coolsnap Dyno, Photometrics, Tucson, AZ, USA). Data acquisition and control of the fluorescence microscope setup were performed using the NIS-Elements AR software (Nikon, Vienna, Austria). Basal D1ER emission ratio (emission 530 nm/480 nm) was recorded for 2 min, while the cells were perfused with physiological buffer followed by 8 min perfusion with physiological buffer without Ca^{2+} (138 mM NaCl, 1 mM $MgCl_2$, 5 mM KCl, 10 mM HEPES, 0.1 mM EGTA, 10 mM glucose, pH adjusted to 7.4). After this, the ER Ca^{2+} was emptied by perfusing the cells with 4 µM ionomycin in Ca^{2+} free buffer. Background-subtracted emission ratio of D1ER was normalized to the minimum ratio reached by ionomycin. ER Ca^{2+} leak was quantified as the D1ER ratio drop after 8 min of perfusion with Ca^{2+} free buffer.

4.6. ER-Mitochondria Co-Localization

ER was labeled with D1ER and mitochondria stained with TMRM (50 nM). Cells were imaged on a confocal spinning disk microscope (Axio Observer.Z1 from Zeiss, Gottingen, Germany) equipped with 100× objective lens (Plan-Fluor x100/1.45 Oil, Zeiss), a motorized filter wheel (CSUX1FW, Yokogawa Electric Corporation, Tokyo, Japan) on the emission side, AOTF-based laser merge module for laser line 405, 445, 473, 488, 561, and 561 nm (Visitron Systems) and a Nipkow-based confocal scanning unit (CSU-X1, Yokogawa Electric corporation). The D1ER and TMRM were alternately excited with 488 and 561 nm laser lines, respectively, and emissions were acquired at 530 and 600 nm using a charged CCD camera (CoolSNAP-HQ, Photometrics, Tucson, AZ, USA). Z-stacks of both channels in 0.2 µm increments were recorded. VisiView acquisition software (Universal Imaging, Visitron Systems) was used to acquire the imaging data. Images were blindly deconvoluted with NIS-elements v5.1 (Nikon, Vienna, Austria). The colocalization was determined on a single-cell level using ImageJ and the plugin coloc2. The Pearson coefficient was calculated.

4.7. Mitochondrial and IMS Ca^{2+} Measurements

Mitochondrial Ca^{2+} was measured using genetically encoded matrix targeted Ca^{2+} sensor 4mtD3cpv [18]. The sensor was excited with 455 nm LED and emission collected at 480 nm and 530 nm using a CFP/YFP/RFP filter set and 505dcxr beam-splitter. Background-subtracted emission ratio of 530 nm/480 nm was analyzed.

IMS Ca^{2+} was measured using genetically encoded IMS targeted Ca^{2+} sensor IMS-GEM-GECO [19,20]. The sensor was excited with 385 nm LED and emission collected at 480 nm and 530 nm using a CFP/YFP/RFP filter set and 505dcxr beam-splitter. Background-subtracted emission ratio of 480 nm/530 nm was analyzed.

4.8. Mitochondrial ROS Measurements

Mitochondrial ROS was measured using genetically encoded matrix targeted ROS sensor mitoHyper7 [24]. The sensor was excited with 385 nm and 470 nm LEDs and emission collected with GFP filter set. After recording the baseline, the cells were perfused with 200 µM H_2O_2 to get the maximum readout. The background-subtracted and normalized ratio of 470 nm/385 nm was analyzed.

4.9. Data Analysis

The number of independent experiments is indicated in each figure legend along with the used statistical test and *p* value. For single-cell experiments, cells were used for analysis. Statistical analyses, including Student's t-test and Analysis of variance (ANOVA) with Tukey post hoc test, were performed on GraphPad Prism software version 5.04 (GraphPad Software, San Diego, CA, USA) and Microsoft Excel (Microsoft Office 2013).

Supplementary Materials: The following are available online at https://www.mdpi.com/article/10.3390/metabo11070422/s1, Figure S1: Knock-down efficiency of S1R siRNA in unsorted (a) and sorted (b) cells determined by qRT-PCR and normalized to housekeeping gene, Figure S2: Protocol for Ψm measurements and the impact of BD1047 on Ψm, Figure S3: Tunicamycin treatment and S1R KD do not affect ER-mitochondria co-localization in SH-SY5Y neuroblastoma cells, Figure S4: Tunicamycin treatment and S1R KD increase the basal ER Ca2+ level, Figure S5: Time course of IMS Ca2+ level after tunicamycin treatment.

Author Contributions: Conceptualization, Z.K. and W.F.G.; methodology, Z.K., R.R., W.F.G.; software, B.G.; validation, Z.K., F.E.O., M.H., J.P., O.A.B., R.R.; formal analysis, Z.K., B.G.; investigation, Z.K., F.E.O., M.H., J.P., O.A.B., R.R.; resources, W.F.G.; data curation, Z.K., B.G.; writing—original draft preparation, Z.K.; writing—review and editing, C.T.M.-S., R.M., W.F.G.; visualization, Z.K.; supervision, W.F.G.; project administration, W.F.G.; funding acquisition, W.F.G. All authors have read and agreed to the published version of the manuscript.

Funding: This work was supported by the Austrian Science Fund (FWF) (J4205-B27 to C.M.-S., DK-MCD W1226 to W.F.G, P28529, and I3716 to R.M.), the MEFO Graz (to W.F.G.), Nikon Austria (to W.F.G.).

Institutional Review Board Statement: Not applicable.

Informed Consent Statement: Not applicable.

Data Availability Statement: The data presented in this study are available on request from the corresponding author and also contained within the main article and supplements.

Acknowledgments: The authors thank Anna Schreilechner, BSc, for her great work in preparing the cells.

Conflicts of Interest: The authors declare no conflict of interest. The funders had no role in the design of the study; in the collection, analyses, or interpretation of data; in the writing of the manuscript, or in the decision to publish the results.

References

1. Almanza, A.; Carlesso, A.; Chintha, C.; Creedican, S.; Doultsinos, D.; Leuzzi, B.; Luís, A.; McCarthy, N.; Montibeller, L.; More, S.; et al. Endoplasmic reticulum stress signalling—From basic mechanisms to clinical applications. *FEBS J.* **2019**, *286*, 241–278. [CrossRef]
2. Schröder, M.; Kaufman, R.J. The mammalian unfolded protein response. *Annu. Rev. Biochem.* **2005**, *74*, 739–789. [CrossRef] [PubMed]
3. Travers, K.J.; Patil, C.K.; Wodicka, L.; Lockhart, D.J.; Weissman, J.S.; Walter, P. Functional and genomic analyses reveal an essential coordination between the unfolded protein response and ER-associated degradation. *Cell* **2000**, *101*, 249–258. [CrossRef]
4. Yong, J.; Bischof, H.; Burgstaller, S.; Siirin, M.; Murphy, A.; Malli, R.; Kaufman, R.J. Mitochondria supply ATP to the ER through a mechanism antagonized by cytosolic Ca^{2+}. *eLife* **2019**, *8*. [CrossRef] [PubMed]
5. Bravo, R.; Vicencio, J.M.; Parra, V.; Troncoso, R.; Muñoz, J.P.; Bui, M.; Quiroga, C.; Rodriguez, A.E.; Verdejo, H.E.; Ferreira, J.; et al. Increased ER–mitochondrial coupling promotes mitochondrial respiration and bioenergetics during early phases of ER stress. *J. Cell Sci.* **2011**, *124*, 2143–2152. [CrossRef]

6. Deniaud, A.; El Dein, O.S.; Maillier, E.; Poncet, D.; Kroemer, G.; Lemaire, C.; A Brenner, C. Endoplasmic reticulum stress induces calcium-dependent permeability transition, mitochondrial outer membrane permeabilization and apoptosis. *Oncogene* **2007**, *27*, 285–299. [CrossRef] [PubMed]
7. Hayashi, T.; Su, T.-P. Sigma-1 Receptor Chaperones at the ER- Mitochondrion Interface Regulate Ca^{2+} Signaling and Cell Survival. *Cell* **2007**, *131*, 596–610. [CrossRef] [PubMed]
8. Mori, T.; Hayashi, T.; Hayashi, E.; Su, T.-P. Sigma-1 Receptor Chaperone at the ER-Mitochondrion Interface Mediates the Mitochondrion-ER-Nucleus Signaling for Cellular Survival. *PLoS ONE* **2013**, *8*, e76941. [CrossRef]
9. Hetz, C.; Saxena, S. ER stress and the unfolded protein response in neurodegeneration. *Nat. Rev. Neurol.* **2017**, *13*, 477–491. [CrossRef]
10. Ryskamp, D.A.; Korban, S.; Zhemkov, V.; Kraskovskaya, N.; Bezprozvanny, I. Neuronal Sigma-1 Receptors: Signaling Functions and Protective Roles in Neurodegenerative Diseases. *Front. Neurosci.* **2019**, *13*, 862. [CrossRef]
11. Chen, X.; Cubillos-Ruiz, J.R. Endoplasmic reticulum stress signals in the tumour and its microenvironment. *Nat. Rev. Cancer* **2021**, *21*, 71–88. [CrossRef]
12. Calfon, M.; Zeng, H.; Urano, F.; Till, J.H.; Hubbard, S.R.; Harding, H.P.; Clark, S.G.; Ron, D. IRE1 couples endoplasmic reticulum load to secretory capacity by processing the XBP-1 mRNA. *Nat. Cell Biol.* **2002**, *415*, 92–96. [CrossRef]
13. Yoon, S.-B.; Park, Y.-H.; Choi, S.-A.; Yang, H.-J.; Jeong, P.-S.; Cha, J.-J.; Lee, S.; Lee, S.H.; Lee, J.-H.; Sim, B.-W.; et al. Real-time PCR quantification of spliced X-box binding protein 1 (XBP1) using a universal primer method. *PLoS ONE* **2019**, *14*, e0219978. [CrossRef]
14. Imamura, H.; Nhat, K.P.H.; Togawa, H.; Saito, K.; Iino, R.; Kato-Yamada, Y.; Nagai, T.; Noji, H. Visualization of ATP levels inside single living cells with fluorescence resonance energy transfer-based genetically encoded indicators. *Proc. Natl. Acad. Sci. USA* **2009**, *106*, 15651–15656. [CrossRef]
15. Matsumoto, R.R.; Bowen, W.D.; Tom, M.A.; Vo, V.N.; Truong, D.D.; De Costa, B.R. Characterization of two novel σ receptor ligands: Antidystonic effects in rats suggest σ receptor antagonism. *Eur. J. Pharmacol.* **1995**, *280*, 301–310. [CrossRef]
16. Bartolomé, F.; Abramov, A.Y. Measurement of Mitochondrial NADH and FAD Autofluorescence in Live Cells. *Methods Mol. Biol.* **2015**, *1264*, 263–270. [CrossRef] [PubMed]
17. Palmer, A.E.; Jin, C.; Reed, J.C.; Tsien, R.Y. Bcl-2-mediated alterations in endoplasmic reticulum Ca^{2+} analyzed with an improved genetically encoded fluorescent sensor. *Proc. Natl. Acad. Sci. USA* **2004**, *101*, 17404–17409. [CrossRef] [PubMed]
18. Palmer, A.E.; Giacomello, M.; Kortemme, T.; Hires, S.A.; Lev-Ram, V.; Baker, D.; Tsien, R.Y. Ca^{2+} Indicators Based on Computationally Redesigned Calmodulin-Peptide Pairs. *Chem. Biol.* **2006**, *13*, 521–530. [CrossRef] [PubMed]
19. Waldeck-Weiermair, M.; Gottschalk, B.; Madreiter-Sokolowski, C.T.; Ramadani-Muja, J.; Ziomek, G.; Klec, C.; Burgstaller, S.; Bischof, H.; Depaoli, M.R.; Eroglu, E.; et al. Development and Application of Sub-Mitochondrial Targeted Ca^{2+} Biosensors. *Front. Cell. Neurosci.* **2019**, *13*, 449. [CrossRef] [PubMed]
20. Zhao, Y.; Araki, S.; Wu, J.; Teramoto, T.; Chang, Y.-F.; Nakano, M.; Abdelfattah, A.S.; Fujiwara, M.; Ishihara, T.; Nagai, T.; et al. An expanded palette of genetically encoded Ca^{2+} indicators. *Science* **2011**, *333*, 1888–1891. [CrossRef] [PubMed]
21. Bhandary, B.; Marahatta, A.; Kim, H.-R.; Chae, H.-J. An involvement of oxidative stress in endoplasmic reticulum stress and its associated diseases. *Int. J. Mol. Sci.* **2012**, *14*, 434–456. [CrossRef]
22. Bjorkman, S.H.; Pereira, R.O. The Interplay Between Mitochondrial Reactive Oxygen Species, Endoplasmic Reticulum Stress, and Nrf2 Signaling in Cardiometabolic Health. *Antioxid. Redox Signal.* **2021**, *2020*, 8220. [CrossRef]
23. Pal, A.; Fontanilla, D.; Gopalakrishnan, A.; Chae, Y.-K.; Markley, J.L.; Ruoho, A.E. The sigma-1 receptor protects against cellular oxidative stress and activates antioxidant response elements. *Eur. J. Pharmacol.* **2012**, *682*, 12–20. [CrossRef]
24. Pak, V.V.; Ezerina, D.; Lyublinskaya, O.; Pedre, B.; Tyurin-Kuzmin, P.A.; Mishina, N.M.; Thauvin, M.; Young, D.; Wahni, K.; Gache, S.A.M.; et al. Ultrasensitive Genetically Encoded Indicator for Hydrogen Peroxide Identifies Roles for the Oxidant in Cell Migration and Mitochondrial Function. *Cell Metab.* **2020**, *31*, 642–653.e6. [CrossRef]
25. Madreiter-Sokolowski, C.T.; Gottschalk, B.; Sokolowski, A.A.; Malli, R.; Graier, W.F. Dynamic Control of Mitochondrial Ca2+ Levels as a Survival Strategy of Cancer Cells. *Front. Cell Dev. Biol.* **2021**, *9*, 1–14. [CrossRef] [PubMed]
26. Flourakis, M.; Van Coppenolle, F.; Lehen'Kyi, V.; Beck, B.; Skryma, R.; Prevarskaya, N. Passive calcium leak via translocon is a first step for iPLA 2 -pathway regulated store operated channels activation. *FASEB J.* **2006**, *20*, 1215–1217. [CrossRef] [PubMed]
27. Chami, M.; Oules, B.; Szabadkai, G.; Tacine, R.; Rizzuto, R.; Brechot, P.P. Role of SERCA1 Truncated Isoform in the Proapoptotic Calcium Transfer from ER to Mitochondria during ER Stress. *Mol. Cell* **2008**, *32*, 641–651. [CrossRef]
28. Carreras-Sureda, A.; Jaña, F.; Urra, H.; Durand, S.; Mortenson, D.E.; Sagredo, A.; Bustos, G.; Hazari, Y.; Ramos-Fernández, E.; Sassano, M.L.; et al. Non-canonical function of IRE1α determines mitochondria-associated endoplasmic reticulum composition to control calcium transfer and bioenergetics. *Nat. Cell Biol.* **2019**, *21*, 755–767. [CrossRef]
29. Srivats, S.; Balasuriya, D.; Pasche, M.; Vistal, G.; Edwardson, J.M.; Taylor, C.; Murrell-Lagnado, R.D. Sigma1 receptors inhibit store-operated Ca^{2+} entry by attenuating coupling of STIM1 to Orai1. *J. Cell Biol.* **2016**, *213*, 65–79. [CrossRef]

3 Discussion

During the course of my studies, I have investigated cellular and mitochondrial Ca^{2+} homeostasis and regulation of mitochondrial bioenergetics by Ca^{2+} ions. In the review article titled "The contribution of uncoupling protein 2 to mitochondrial Ca^{2+} homeostasis in health and disease - a short revisit", we give historical perspective to the research in the field of uncoupling proteins, with focus on uncoupling protein 2[46]. We then discuss new findings on UCP2 and its relevance in aging, cancer and neurodegenerative diseases, and compare mechanism of action of UCP2 in regards to its proposed function as a proton uncoupler versus its involvement in mitochondrial Ca^{2+} uptake[46]. Since UCP2 is described to be involved in so many pathologies, understanding its correct mode of action is paramount. Although different in theory, both uncoupling and Ca^{2+} uptake functions can be achieved by the same mechanism. A recent study by our group has demonstrated that MICU1 is keeping mitochondrial cristae junction structure and enables maintaining two separate membrane potentials, one for the cristae membrane and other for mitochondrial inner boundary membrane[24]. It has been shown that UCP2 can modulate MICU1 function upon MICU1 methylation by PRMT1[45], thus involving UCP2 in the spatial regulation of mitochondrial membrane potential, and by extent mitochondrial proton gradient. These findings provide a possible hint at dual function of UCP2 in regulation mitochondrial Ca^{2+} uptake and membrane potential without directly uncoupling IMM proton gradient.

Although direct uncoupling of the proton gradient by UCP2 has not been extensively proven, an uncoupling by means of fatty acid shuttling or MICU1 regulations appears to be more likely[115]. As it has been reported that MICU1 methylation by PRMT1 involves UCP2 in mitochondrial Ca^{2+} uptake and that PRMT1 expression is increased during aging[46,54], it is safe to assume that the correlation of large body of research on UCP2 involvement in age associated diseases is likely to be stemming from its involvement in regulation of mitochondrial Ca^{2+} uptake. Additionally, our group has proposed an uncoupling mechanism that combines mitochondrial Ca^{2+} uptake machinery and dissipation of proton gradient by UPC2. According to this model, by binding to methylated MICU1, UCP2 can lower the opening threshold of MICU1 oligomers, leading to opening of cristae junction. Opening of cristae junction leads to proton leakage from the cristae lumen into the IMS, resulting in loss of the proton gradient between matrix and cristae lumen[24]. Possible proton gradient uncoupling mechanisms of UCP2 are shown in Figure 6. Further validation of proposed mechanisms of action for UPC2 are needed given the importance of UCP2 in health and disease.

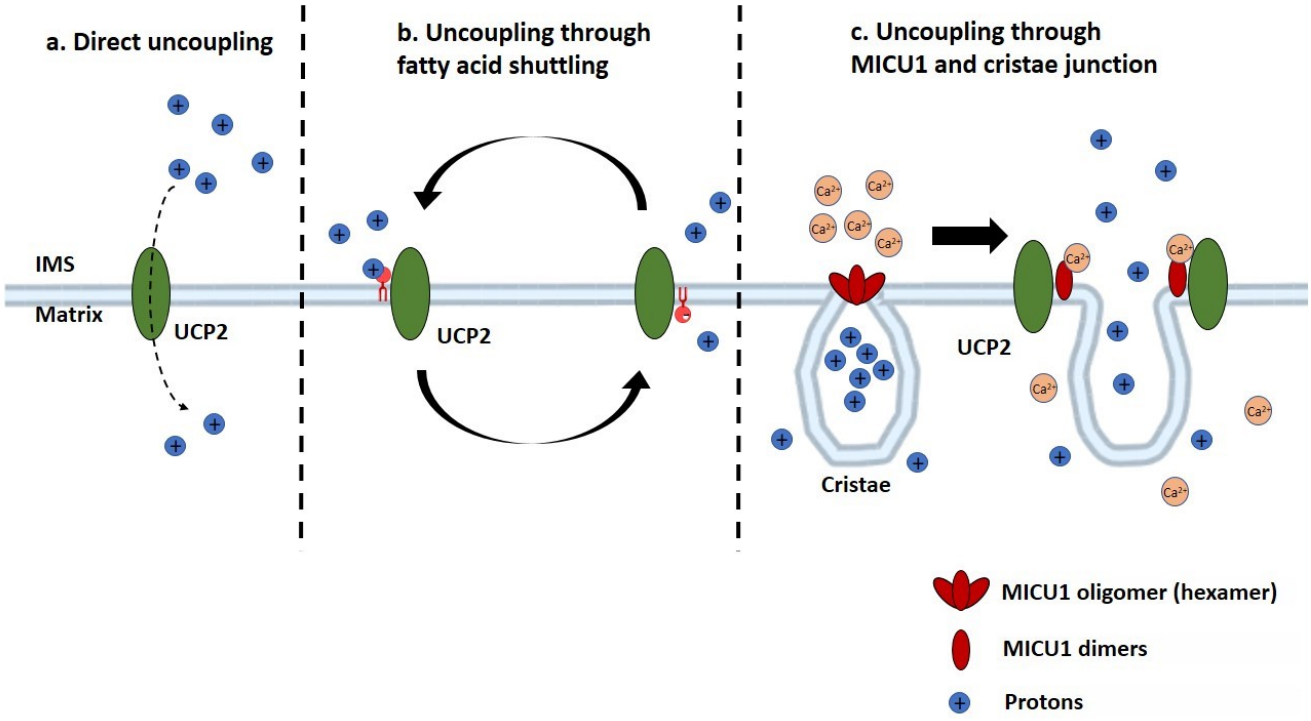

Figure 6. *Three possible ways of proton gradient uncoupling by UCP2.* ***a.*** *Direct uncoupling was proposed based on 60% protein homology of UCP2 to UCP1; according to this model, UCP2 shuttles protons down their electrochemical gradient.* ***b.*** *The second model proposes UCP2 uncoupling of the proton gradient by fatty acid shuttling; upon transfer of anionic fatty acids from matrix to IMS or cristae lumen facing side of the IMM, fatty acids get protonated in low pH environment, allowing them to slip back into the matrix, thus carrying a net positive charge into the matrix and uncoupling the proton gradient from ATP synthesis.* ***c.*** *Uncoupling through disassembly of MICU1 oligomers and opening of cristae junction; in case of MICU1 methylation by PRMT1, UCP2 can directly bind to MICU1 and facilitate the lowering of MICU1 opening threshold, thus opening the cristae junction in response to IMS Ca^{2+} elevations and dissipating the proton gradient of the cristae membrane by letting protons escape into IMS.*

Even though mitochondrial Ca^{2+} uptake has a tremendous role in regulation of mitochondrial bioenergetics, we have demonstrated that IMS Ca^{2+} is as important as matrix Ca^{2+} in this regard[3]. Our data suggest that upon stimulation of mitochondrial bioenergetics by means of ER Ca^{2+} release to achieve the maximal mitochondrial ATP production, IMS and matrix Ca^{2+} has similar contribution, as citrin knock down yielded the same reduction in ATP production as MCU knock down[3]. This finding suggests that both mechanisms complement each other when it comes to maximum productivity of

mitochondria under stimulation, whereby MAS sustains increased substrate supply and matrix dehydrogenases assure electron donor generation. But the situation under basal conditions looks different. In unstimulated, basal state, mitochondrial bioenergetics are more dependent on IMS Ca^{2+} as it controls steady substrate supply to mitochondria and maintains glycolytic flux from glucose to pyruvate[3]. Thus, it is important to consider the differences between the two mitochondrial sub-compartments when studying Ca^{2+} regulation of mitochondrial bioenergetics.

As we have demonstrated, cells readily respond to even small changes in Ca^{2+} homeostasis and react to it within minutes. That is achieved due to low Ca^{2+} activation concentration of MAS, which is around 100 nM for citrin and 300 nM for aralar, in contrast to micromolar activation concentrations for matrix dehydrogenases[62,63,68,75]. This allows cells to respond to reduced IMS Ca^{2+} levels which can result from reduced extracellular Ca^{2+}, increased cytosolic Ca^{2+} buffering, or reduced ER-mitochondrial communication. As we have observed, cells can respond to such changes within minutes by rewiring their metabolism ahead of long term expression level reprogramming. Thus, Ca^{2+} signalling and Ca^{2+} regulation of vital processes allows for such fast processing of environmental changes and responding to them with metabolic alterations.

One of the mitochondrial response mechanisms to altered sub-cellular Ca^{2+} homeostasis is the switch of mitochondrial F_0F_1 ATP synthase to reverse mode, in which it pumps protons out of the matrix to maintain negative membrane potential in face of reduced MAS activity[3] (Figure 7). This switch is crucial, since hampered NADH shuttle activity leads to disruption of TCA cycle substrate supply, which lowers matrix NADH production and ETC activity, leading to the collapse of mitochondrial membrane potential. Thus, reversal of the ATP synthase rescues cells from apoptosis at the cost of mitochondrial ATP production[3].

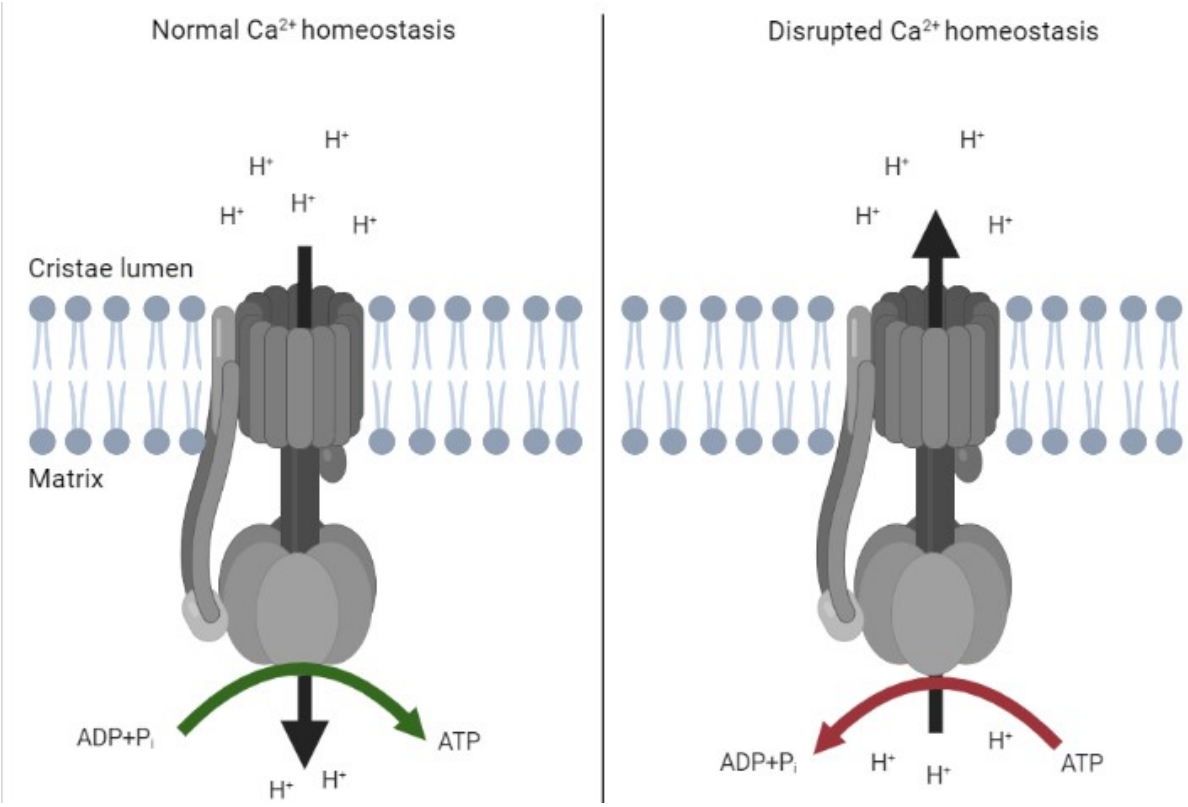

Figure 7. *Reversal of mitochondrial F_0F_1 ATP synthase direction from ATP production under normal Ca^{2+} homeostasis (left) to ATP consumption under disrupted Ca^{2+} homeostasis (right). Upon reversal, ATP synthase pumps protons out of the matrix into cristae lumen, thus maintaining negative membrane potential at cost of ATP production.*

Additionally, our findings provide a new perspective for metabolic and genetic disorders involving malate-aspartate shuttle, glucose metabolism and Ca^{2+} misbalance. Type II citrullinemia is a genetic disorder caused by citrin deficiency and is characterized by hampered glucose metabolism, especially in liver[116,117]. Thus, main pathogenesis of citrin deficiency is considered to be hepatic energy deficit. Low carbohydrate diet supplemented with medium-chain triglyceride are recommended to treat the symptoms by bypassing the malate-aspartate shuttle[116,117]. Our study on citrin mediated metabolic rewiring provides additional insight into type II citrullinemia and supports the approach for metabolic treatment of the disease, based on careful dietary supplementation, as we were able to rescue the effects of reduced MAS activity by pyruvate supplementation[3].The schematic representation in Figure 8 summarizes the metabolic alterations happening during citrin/MAS inactivity, due to either calcium insufficiency or genetic defects in MAS components. It is worth noting that cancer cells express high levels of lactate dehydrogenase (LDH) and are able to partially rescue the defective

activity of citrin/MAS under reduced basal Ca^{2+} level, thus providing an additional therapeutic approach based on introducing alternative means for NADH recycling[118]. A recent study has provided a new tool to manipulate cellular and systemic NAD/NADH levels via enzymatic NADH recycling[119]. The tool is based on Lactobacillus brevis (Lb) NOX1, which oxidizes NADH to NAD^+, consuming oxygen and forming a water molecule in the process[119]. The same group developed another tool using bacterial lactate oxidase and catalase that converts lactate and oxygen to pyruvate and water[120]. Both of these tools were demonstrated to rescue mitochondrial disorders resulting in reductive stress and NAD/NADH imbalance. As a consequence, fitting metabolic treatment approaches can be developed for various metabolic disorders, given we understand the fundamental science behind the disease.

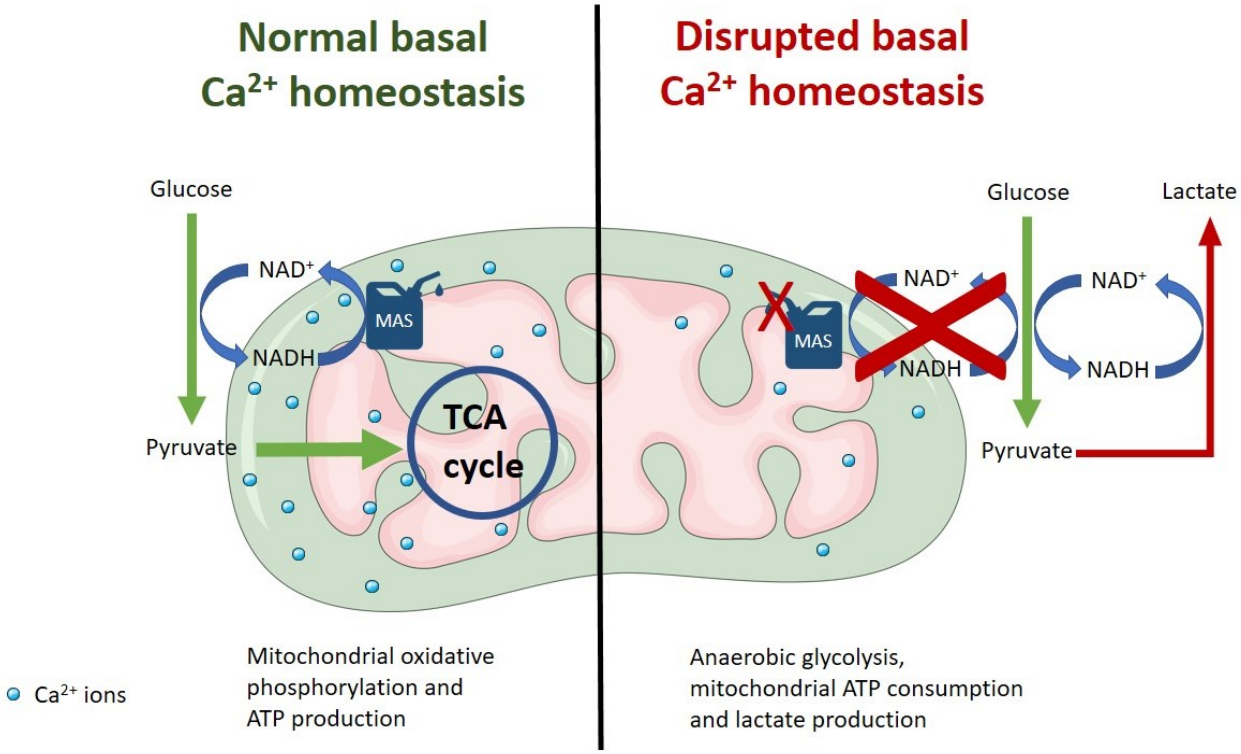

Figure 8. *Schematic representation of MAS function under normal (left) and pathological (right) conditions. Under normal Ca^{2+} homeostasis, MAS recycles cytosolic NADH and mains substrate supply to matrix. Upon intracellular Ca^{2+} drop, especially at the mitochondrial IMS, MAS activity is hampered, resulting in reduced NADH recycling, which can lead to reduced glycolysis. Cancer cells and other cell types with elevated lactate dehydrogenase, can rescue this by producing lactate and recycling NADH in this way. But as a consequence, pyruvate does not enter TCA cycle and only two molecules of ATP are produced from one molecule of glucose.*

In addition to cancer cells and non-excitable cells, MAS was shown to be fundamental for neurons [70,121] and pancreatic beta cells[122]. Malate-aspartate shuttle is described as a "gas pedal" of mitochondria, and was shown to be indispensable for boosting mitochondrial activity in highly energy demanding neurons[123,124]. Importance of MAS for insulin secretion is self-explanatory, as pancreatic beta cells are the main glucose sensors in a body and need to have a smooth glucose metabolism. It was shown that MAS impaired beta cells have defective glucose stimulated insulin release (GSIS)[122,125]. We have conducted preliminary studies in pancreatic beta cells as well, and saw the effects of reduced basal IMS Ca^{2+} on glucose metabolism. In contrast to cancer cells that are easily reprogrammed, pancreatic beta cells do not expression high levels of LDH, thus they can't rescue the hampered glucose metabolism by rerouting glycolysis towards LDH[126,127]. Even if such way was possible, for example by overexpressing LDH, it would be counterproductive for beta cells, as they need to fully metabolise the glucose in mitochondria to extract ATP, which then is used to block ATP sensitive K^+ channels on the plasma membrane. The latter yields membrane depolarization that triggers cytosolic Ca^{2+} oscillations, which induce fusion of insulin containing vesicles with the plasma membrane and secretion of insulin[127,128].

Another aspect that needs careful consideration, is the Ca^{2+} source and Ca^{2+} route to IMS and matrix. Since there is no apparent threshold for cytosolic Ca^{2+} to reach IMS, we expected at first that cytosolic Ca^{2+} can modulate the activity of IMS residing NADH shuttles. But as our experiments have shown, Ca^{2+} coming from the ER through ER-mitochondria contact sites regulates the activity of the shuttles[3]. This finding is in contrast to several studies that have shown that global cytosolic Ca^{2+} can influence the activity of MAS, but these studies were performed in isolated mitochondria, thus lack the real setting of an intact cell[77]. Although it is worthy to mention that we studied only the regulation under basal state, and we think that the studies performed by others hold true under stimulated conditions, when rise in global cytosolic Ca^{2+}, for example coming from store operated Ca^{2+} entry, can easily reach IMS and activate MAS.

In sharp contrast to IMS, matrix is more restrictive in allowing Ca^{2+} ions. The threshold set my MICU1-2 on MCUC is high, so that it doesn't allow global, sub-threshold Ca^{2+} elevations to enter mitochondrial matrix[26,129]. Hence, the main route for matrix Ca^{2+} uptake is through specialized Ca^{2+} hotspots at ER-mitochondria contact sites, MAMs. MAMs are enriched in Ca^{2+} channels, such as IP3Rs, which are reported to be directly coupled to outer mitochondrial membrane residing VDAC channels by glucose-regulated protein 75 (GRP75)[130,131]. Upon release of Ca^{2+} from ER through IP3Rs, Ca^{2+} concentration at the microdomains reaches several µM and is translated into matrix[26]. Such

large Ca^{2+} signalling events synchronize both NADH shuttles and matrix dehydrogenases. Interestingly, this sort of high threshold for mitochondrial Ca^{2+} uptake is characteristic of non-excitable cells, whereas excitable cells, such as pancreatic beta cells or neurons, have much lower Ca^{2+} uptake threshold. It can be a manifestation of their high energy demand for secretion and information processing, respectively, and this mode of Ca^{2+} uptake is more suitable given the basal cytosolic Ca^{2+} oscillations of these cells. Lower mitochondrial Ca^{2+} uptake threshold can be achieved by altering the ratio of MCU:MICU1:MICU2, as was reported for liver, heart, and skeletal muscle cells[22] (Figure 9).

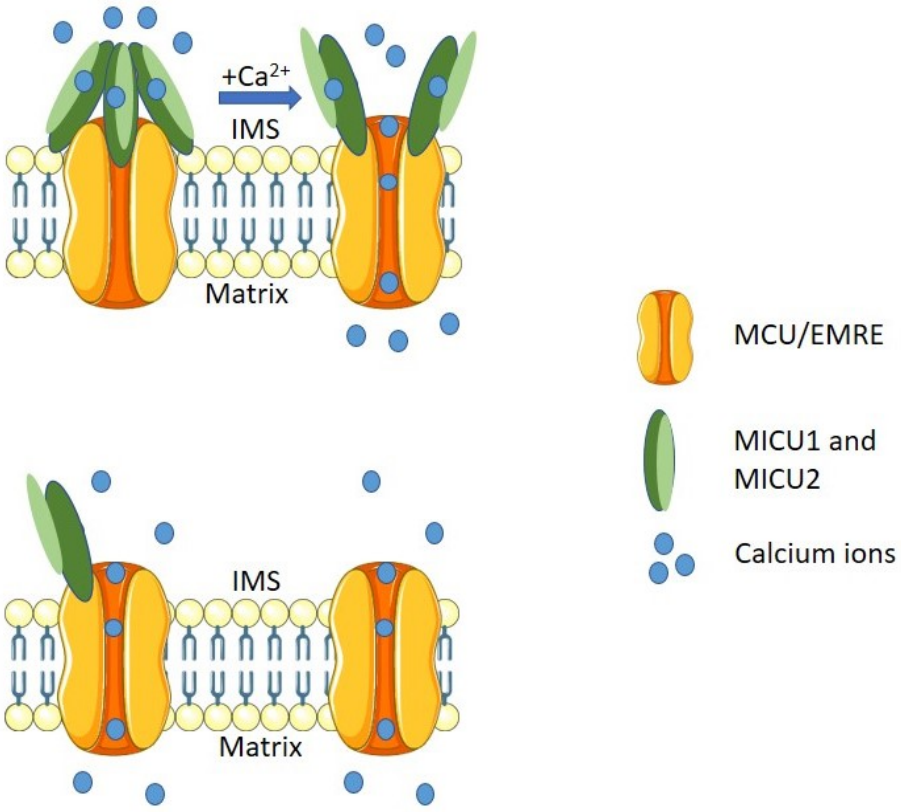

Figure 9. *MCUC of non-excitable cells (above) versus MCUC of excitable cells (below). Excitable cells have higher ratio of MCU to MICU1/2, thus have lower mitochondrial Ca^{2+} uptake threshold.*

Irrespective of cell type, ER stress is reported to affect Ca^{2+} signalling between ER and mitochondria and to boost mitochondrial bioenergetics. Large body of research is dedicated in deciphering events happening at different stages of ER stress. We have dwelled into the events happening during early

stages of ER stress induced by known ER stressor – tunicamycin[93]. Tunicamycin blocks the first step of glycoprotein synthesis and thus triggers ER stress and UPR[93]. Additionally, we wanted to study the involvement of Sigma-1 receptor (S1R) in the early ER stress, since S1R is frequently implicated in ER-mitochondrial communication. The induction of ER stress with tunicamycin boosted mitochondrial bioenergetics parameters, such as mitochondrial ATP level, membrane potential, and NADH redox index, after 2 hours of treatment. These parameters went back to basal levels after 8 hours of treatment, suggesting time dependent phenomenon. Interestingly, S1R knock-down eliminated the increased mitochondrial bioenergetics after 2 hours of ER stress, suggesting that it is S1R dependent[93].

In order to gather more information on the mechanism of time and S1R dependent enhancement of mitochondrial bioenergetics, we evaluated ER-mitochondrial tethering. As others have reported increased tethering between ER and mitochondrial after couple hours of ER stress[92], we measured ER-mitochondria co-localization after 2 and 8 hours of ER stress. In contrast to previous reports, we did not detect increased tethering in SH-SY5Y human neuroblastoma cells line[93]. The difference with published reports can be stemming from difference in cell line used, since previous reports were not done in SH-SY5Y cells. Additionally, the method we deployed for ER-mitochondria co-localization analysis does not have the highest resolution, thus a better alternative method might be necessary in the future work. On the other hand, we detected enhanced ER Ca^{2+} leak after both 2 and 8 hours of ER stress. Enhanced ER Ca^{2+} leak can be considered as an alternative to tethering, since it is the functional consequence of increased tethering between the organelles. We then tested the involvement of Sigma-1 receptor in enhanced ER Ca^{2+} leak. Knock-down of S1R increased ER Ca^{2+} leak without ER stress induction, while combination of S1R knock-down and tunicamycin treatment did not have an additive effect[93]. These findings suggest that S1R knock-down may mimic ER stress and induce the Ca^{2+} leak, or that S1R is needed for the control of the ER Ca^{2+} leak and the S1R knock-down results in uncontrolled leak. On the other hand, persistence of the same ER Ca^{2+} leak after 2 and 8 hours of stress and return of the mitochondrial bioenergetics back to basal after 8 hours may be an indication of mitochondrial Ca^{2+} overload, or it can also mean that the ER Ca^{2+} leak is no longer directed at mitochondria after 8 hours of stress. Although, only the latter provides more likely explanation to the fact that despite the presence of enhanced ER Ca^{2+} leak in S1R knock-down cells, mitochondrial bioenergetics do not seem to be affected by it.

To test these assumptions, we measured mitochondrial matrix Ca^{2+} levels. ER stress induction by tunicamycin treatment for 2 hours increased matrix Ca^{2+} levels in control cells, but not in S1R knock-

down cells. Matrix Ca^{2+} levels of control cells after 8 hours of ER stress returned to basal levels, while in S1R knock-down cells it remained unchanged from both basal and 2 hour tunicamycin treated levels[93]. These data clarifies the time dependency of the mitochondrial bioenergetics boost: the increased matrix Ca^{2+} level after 2 hours of ER stress can be the reason for increased mitochondrial bioenergetics at that time point. Since the matrix Ca^{2+} level goes back down after 8 hours, so does the mitochondrial bioenergetics. S1R knock-down cells, however, don't have the increased Ca^{2+} levels and don't have boosted bioenergetics. What still remains interesting, is that S1R knock-down cells have enhanced ER Ca^{2+} leak, but not elevated matrix Ca^{2+} levels, which begs the question whether S1R knock-down impairs mitochondrial Ca^{2+} uptake. To test if S1R KD cells have impaired matrix Ca^{2+} uptake, we measured IMS Ca^{2+} levels under ER stress. If IMS Ca^{2+} levels would be elevated in both control and S1R knock-down cells, it would mean that S1R is required for mitochondrial Ca^{2+} uptake. IMS Ca^{2+} dynamics mimicked that of matrix Ca^{2+}, and was elevated only in control cells after 2 hours of ER stress, while S1R knock-down cells didn't have a significant change in IMS Ca^{2+} levels. Absence of elevated Ca^{2+} in IMS and matrix of S1R knock-down cells would mean that elevated ER Ca^{2+} leak observed in these cells is not directed towards mitochondria. In support of this view, it has been reported that S1R redistributes from MAMs towards rest of the ER upon prolonged ER stress and after ER Ca^{2+} depletion[95]. Additionally, S1R was shown to serve as a scaffold for ER Ca^{2+} release channels and to stabilize IP3Rs in their open state[95,99]. Taken together, these published works together with our findings suggests a time dependent mechanism of action for S1R under ER stress (Figure 10). Under resting condition, S1R is localized to the MAM region, where it serves as a scaffold and stabilizer of Ca^{2+} channels, along with other reported functions. Upon ER stress induction, ER develops a Ca^{2+} leak (we have not established if S1R is somehow directly involved in the leak or not). S1R, through its scaffolding and stabilizing role, keeps the leak directed to mitochondria at the MAMs. Upon persisting ER stress (8 hours or more), S1R is redistributed within ER, thus no longer keeps the Ca^{2+} leak channels at MAMs and directed towards mitochondria.

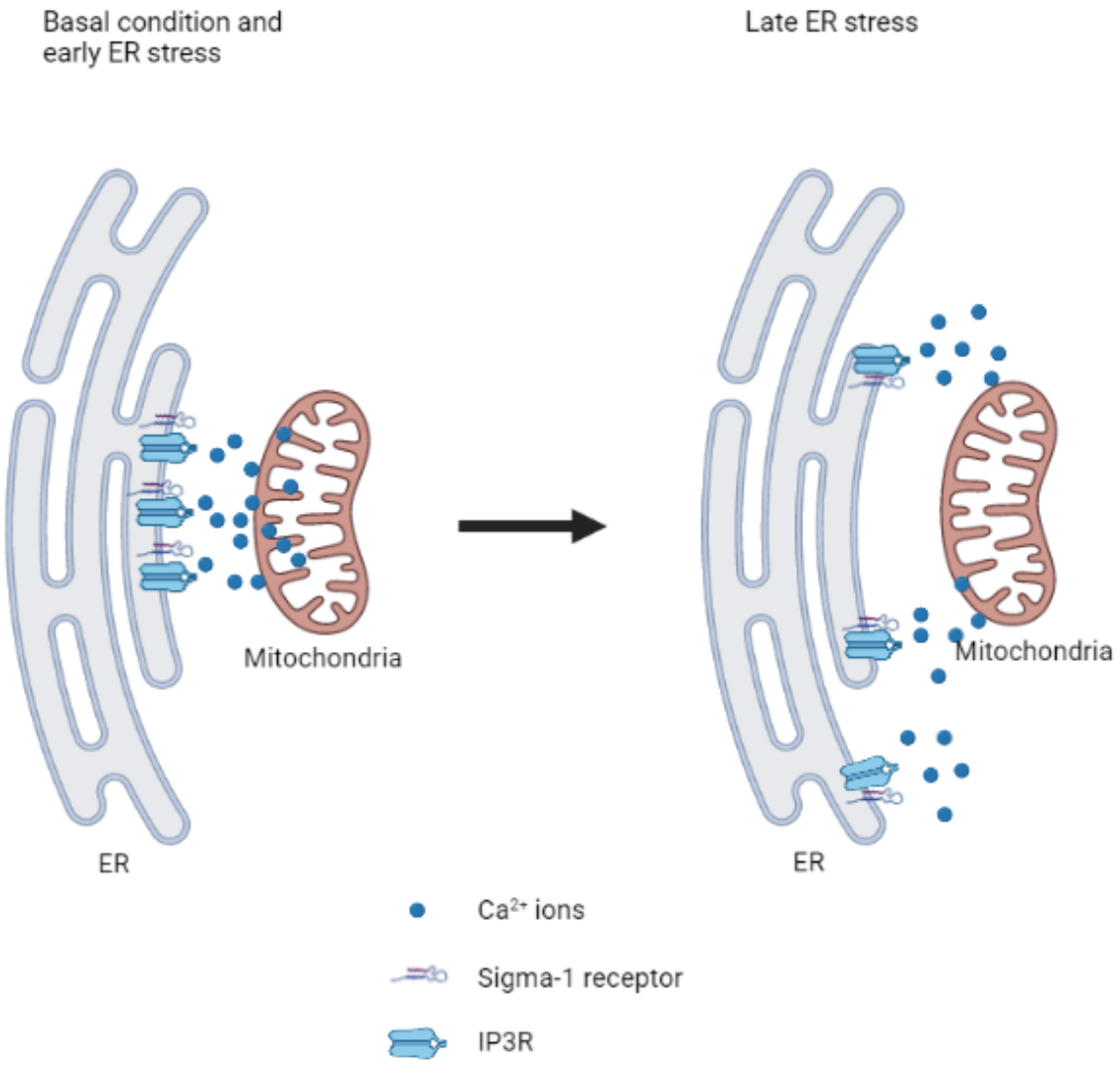

Figure 10. *S1R orchestration of mitochondria targeted ER Ca^{2+} leak during early ER stress. Under basal condition S1R is localized to the ER-mitochondria contact sites, where it anchors and stabilizes IP3Rs. That is particularly important during early ER stress, since ER develops a Ca^{2+} leak in response to ER stress. S1R maintains the leak at MAMs and ensures that mitochondria receives the Ca^{2+} leak. As a result, mitochondrial bioenergetics are boosted and mitochondria can supply ATP to ER for UPR. As the ER stress progresses, S1R redistributes towards other parts of ER and the leak is not targeted at mitochondria. This way, cells generate ATP for UPR and avoid excessive mitochondrial Ca^{2+} overload.*

In addition to ER stress, S1R receptor's activity under resting state has an impact on mitochondrial bioenergetics. We have studied the effects of pharmacological activation and inactivation of S1R by its ligands on cellular bioenergetics[103]. We have discovered that while activation of S1R boosts

mitochondrial Ca^{2+} uptake, and consequently mitochondrial ATP production, its inactivation doesn't have a major impact on either Ca^{2+} uptake or ATP production. On the other hand, S1R activation decreased cancer cell reliance on aerobic glycolysis, while inactivation increased it, suggesting a basal activity of S1R in balancing cellular reliance on glycolysis[103].

In conclusion, Ca^{2+} regulation of cellular energy metabolism is fast, highly flexible and reliable way to adapt to various external and internal signals and conditions cells may face. Despite being broad and non-specific, we and others have shown that Ca^{2+} signalling can be precise thanks to various spatial and temporal control mechanisms cells have evolved. Many age related pathologies have altered Ca^{2+} regulation of cellular bioenergetics, making fundamental research in this field our first priority to tackle associated diseases. Only by understanding intricate mechanisms involved in controlling healthy energy metabolism, can we identify therapeutic targets and deploy interventions.

References

1. Berridge MJ, Lipp P, Bootman MD. The versatility and universality of calcium signalling. *Nat Rev Mol Cell Biol*. Published online 2000. doi:10.1038/35036035

2. Usachev YM, Marchenko SM, Sage SO. Cytosolic calcium concentration in resting and stimulated endothelium of excised intact rat aorta. *J Physiol*. Published online 1995. doi:10.1113/jphysiol.1995.sp021052

3. Koshenov Z, Oflaz FE, Hirtl M, et al. Citrin mediated metabolic rewiring in response to altered basal subcellular Ca2+ homeostasis. *Commun Biol*. 2022;5(1). doi:10.1038/S42003-022-03019-2

4. Chin D, Means AR. Calmodulin: A prototypical calcium sensor. *Trends Cell Biol*. 2000;10(8):322-328. doi:10.1016/S0962-8924(00)01800-6

5. Zhivotovsky B, Orrenius S. Calcium and cell death mechanisms: A perspective from the cell death community. *Cell Calcium*. 2011;50(3):211-221. doi:10.1016/j.ceca.2011.03.003

6. Xu H, Van Remmen H. The SarcoEndoplasmic Reticulum Calcium ATPase (SERCA) pump: a potential target for intervention in aging and skeletal muscle pathologies. *Skelet Muscle*. 2021;11(1):1-9. doi:10.1186/S13395-021-00280-7/TABLES/2

7. Malli R, Frieden M, Osibow K, et al. Sustained Ca2+ Transfer across Mitochondria Is Essential for Mitochondrial Ca2+ Buffering, Store-operated Ca2+ Entry, and Ca2+ Store Refilling. *J Biol Chem*. 2003;278(45):44769-44779. doi:10.1074/jbc.M302511200

8. Gincel D, Zaid H, Shoshan-Barmatz V. Calcium binding and translocation by the voltage-dependent anion channel: a possible regulatory mechanism in mitochondrial function. *Biochem J*. 2001;358(Pt 1):147-155. doi:10.1042/0264-6021:3580147

9. Kamer KJ, Mootha VK. The molecular era of the mitochondrial calcium uniporter. *Nat Rev Mol Cell Biol*. Published online 2015. doi:10.1038/nrm4039

10. De Stefani D, Raffaello A, Teardo E, Szabó I, Rizzuto R. A forty-kilodalton protein of the inner membrane is the mitochondrial calcium uniporter. *Nature*. Published online 2011. doi:10.1038/nature10230

11. Baughman JM, Perocchi F, Girgis HS, et al. Integrative genomics identifies MCU as an essential

component of the mitochondrial calcium uniporter. *Nature*. 2011;476(7360):341-345. doi:10.1038/nature10234

12. Dhalla NS. Excitation-contraction coupling in heart. I. Comparison of calcium uptake by the sarcoplasmic reticulum and mitochondria of the rat heart. *Arch Int Physiol Biochim*. 1969;77(5):916-934. doi:10.3109/13813456909059804

13. Haworth RA, Hunter DR. The Ca2+-induced membrane transition in mitochondria: II. Nature of the Ca2+ trigger site. *Arch Biochem Biophys*. 1979;195(2):460-467. doi:10.1016/0003-9861(79)90372-2

14. Halestrap AP. What is the mitochondrial permeability transition pore? *J Mol Cell Cardiol*. 2009;46(6):821-831. doi:10.1016/J.YJMCC.2009.02.021

15. Raffaello A, Stefani D De, Sabbadin D, et al. The mitochondrial calcium uniporter is a multimer that can include a dominant-negative pore-forming subunit. *EMBO J*. 2013;32(17):2362-2376. doi:10.1038/emboj.2013.157

16. Sancak Y, Markhard AL, Kitami T, et al. EMRE is an essential component of the mitochondrial calcium uniporter complex. *Science*. 2013;342(6164):1379-1382. doi:10.1126/science.1242993

17. Perocchi F, Gohil VM, Girgis HS, et al. MICU1 encodes a mitochondrial EF hand protein required for Ca(2+) uptake. *Nature*. 2010;467(7313):291-296. doi:10.1038/nature09358

18. Plovanich M, Bogorad RL, Sancak Y, et al. MICU2, a paralog of MICU1, resides within the mitochondrial uniporter complex to regulate calcium handling. *PLoS One*. 2013;8(2):e55785. doi:10.1371/journal.pone.0055785

19. Patron M, Granatiero V, Espino J, Rizzuto R, Stefani D De. MICU3 is a tissue-specific enhancer of mitochondrial calcium uptake. *Cell Death Differ*. 2018;26(1):179-195. doi:10.1038/s41418-018-0113-8

20. Patron M, Checchetto V, Raffaello A, et al. MICU1 and MICU2 finely tune the mitochondrial Ca2+ uniporter by exerting opposite effects on MCU activity. *Mol Cell*. 2014;53(5):726-737. doi:10.1016/j.molcel.2014.01.013

21. Kamer KJ, Mootha VK. MICU1 and MICU2 play nonredundant roles in the regulation of the mitochondrial calcium uniporter. *EMBO Rep*. 2014;15(3):299-307. doi:10.1002/embr.201337946

22. Paillard M, Csordás G, Szanda G, et al. Tissue-Specific Mitochondrial Decoding of Cytoplasmic Ca2+ Signals Is Controlled by the Stoichiometry of MICU1/2 and MCU. *Cell Rep*. 2017;18(10):2291. doi:10.1016/J.CELREP.2017.02.032

23. Gottschalk B, Klec C, Leitinger G, et al. MICU1 controls cristae junction and spatially anchors mitochondrial Ca2+ uniporter complex. *Nat Commun*. 2019;10(1):3732. doi:10.1038/s41467-019-11692-x

24. Gottschalk B, Koshenov Z, Waldeck-Weiermair M, et al. MICU1 controls spatial membrane potential gradients and guides Ca2+ fluxes within mitochondrial substructures. *Commun Biol 2022 51*. 2022;5(1):1-13. doi:10.1038/s42003-022-03606-3

25. Tomar D, Dong Z, Shanmughapriya S, et al. MCUR1 Is a Scaffold Factor for the MCU Complex Function and Promotes Mitochondrial Bioenergetics. *Cell Rep*. 2016;15(8):1673-1685. doi:10.1016/j.celrep.2016.04.050

26. Giacomello M, Drago I, Bortolozzi M, et al. Ca2+ Hot Spots on the Mitochondrial Surface Are Generated by Ca2+ Mobilization from Stores, but Not by Activation of Store-Operated Ca2+ Channels. *Mol Cell*. 2010;38(2):280-290. doi:10.1016/j.molcel.2010.04.003

27. Peruzzo R, Costa R, Bachmann M, Leanza L, Szabò I. Mitochondrial metabolism, contact sites and cellular calcium signaling: Implications for tumorigenesis. *Cancers (Basel)*. Published online 2020. doi:10.3390/cancers12092574

28. Müller M, Ahumada-Castro U, Sanhueza M, Gonzalez-Billault C, Court FA, Cárdenas C. Mitochondria and calcium regulation as basis of neurodegeneration associated with aging. *Front Neurosci*. Published online 2018. doi:10.3389/fnins.2018.00470

29. Johri A, Chandra A. Connection Lost, MAM: Errors in ER–Mitochondria Connections in Neurodegenerative Diseases. *Brain Sci*. 2021;11(11). doi:10.3390/BRAINSCI11111437

30. Palty R, Silverman WF, Hershfinkel M, et al. NCLX is an essential component of mitochondrial Na+/Ca 2+ exchange. *Proc Natl Acad Sci U S A*. 2010;107(1):436-441. doi:10.1073/PNAS.0908099107/SUPPL_FILE/PNAS.200908099SI.PDF

31. Boyman L, Williams GSB, Khananshvili D, Sekler I, Lederer WJ. NCLX: The Mitochondrial Sodium Calcium Exchanger. *J Mol Cell Cardiol*. 2013;59:205. doi:10.1016/J.YJMCC.2013.03.012

32. Alvarez B V., Villa-Abrille MC. Mitochondrial NHE1: a newly identified target to prevent heart

disease. *Front Physiol*. 2013;4. doi:10.3389/FPHYS.2013.00152

33. Assali EA, Jones AE, Veliova M, et al. NCLX prevents cell death during adrenergic activation of the brown adipose tissue. *Nat Commun*. 2020;11(1). doi:10.1038/S41467-020-16572-3

34. Luongo TS, Lambert JP, Gross P, et al. The mitochondrial Na+/Ca2+exchanger is essential for Ca2+ homeostasis andviability. *Nature*. 2017;545(7652):93. doi:10.1038/NATURE22082

35. Pan X, Liu J, Nguyen T, et al. The physiological role of mitochondrial calcium revealed by mice lacking the mitochondrial calcium uniporter. *Nat Cell Biol*. 2013;15(12):1464-1472. doi:10.1038/NCB2868

36. Jiang D, Zhao L, Clapham DE. Genome-wide RNAi screen identifies Letm1 as a mitochondrial Ca2+/H+ antiporter. *Science*. 2009;326(5949):144-147. doi:10.1126/science.1175145

37. Waldeck-Weiermair M, Jean-Quartier C, Rost R, et al. Leucine Zipper EF Hand-containing Transmembrane Protein 1 (Letm1) and Uncoupling Proteins 2 and 3 (UCP2/3) Contribute to Two Distinct Mitochondrial Ca2+ Uptake Pathways. *J Biol Chem*. 2011;286(32):28444-28455. doi:10.1074/jbc.m111.244517

38. Austin S, Nowikovsky K. LETM1: Essential for Mitochondrial Biology and Cation Homeostasis? *Trends Biochem Sci*. Published online 2019. doi:10.1016/j.tibs.2019.04.002

39. Prakriya M, Feske S, Gwack Y, Srikanth S, Rao A, Hogan PG. Orai1 is an essential pore subunit of the CRAC channel. *Nat 2006 4437108*. 2006;443(7108):230-233. doi:10.1038/nature05122

40. Zhang SL, Yu Y, Roos J, et al. STIM1 is a Ca2+ sensor that activates CRAC channels and migrates from the Ca2+ store to the plasma membrane. *Nature*. 2005;437(7060):902-905. doi:10.1038/NATURE04147

41. Liou J, Kim ML, Won DH, et al. STIM is a Ca2+ sensor essential for Ca2+-store-depletion-triggered Ca2+ influx. *Curr Biol*. 2005;15(13):1235-1241. doi:10.1016/J.CUB.2005.05.055

42. Roos J, DiGregorio PJ, Yeromin A V., et al. STIM1, an essential and conserved component of store-operated Ca2+ channel function. *J Cell Biol*. 2005;169(3):435-445. doi:10.1083/JCB.200502019

43. Naghdi S, Waldeck-Weiermair M, Fertschai I, Poteser M, Graier WF, Malli R. Mitochondrial Ca2+ uptake and not mitochondrial motility is required for STIM1-Orai1-dependent store-operated Ca2+ entry. *J Cell Sci*. 2010;123(15):2553-2564. doi:10.1242/jcs.070151

44. Trenker M, Malli R, Fertschai I, Levak-Frank S, Graier WF. Uncoupling proteins 2 and 3 are fundamental for mitochondrial Ca2+ uniport. *Nat Cell Biol*. 2007;9(4):445-452. https://pubmed.ncbi.nlm.nih.gov/17351641

45. Madreiter-Sokolowski CT, Klec C, Parichatikanond W, et al. PRMT1-mediated methylation of MICU1 determines the UCP2/3 dependency of mitochondrial Ca2+ uptake in immortalized cells. *Nat Commun*. 2016;7(1):12897. doi:10.1038/ncomms12897

46. Koshenov Z, Oflaz FE, Hirtl M, et al. The contribution of uncoupling protein 2 to mitochondrial Ca2+ homeostasis in health and disease – A short revisit. *Mitochondrion*. Published online 2020. doi:10.1016/j.mito.2020.10.003

47. MITCHELL P. Coupling of Phosphorylation to Electron and Hydrogen Transfer by a Chemi-Osmotic type of Mechanism. *Nature*. 1961;191(4784):144-148. doi:10.1038/191144a0

48. Brand MD, Brindle KM, Buckingham JA, Harper JA, Rolfe DFS, Stuart JA. The significance and mechanism of mitochondrial proton conductance. *Int J Obes*. 1999;23(S6):S4--S11. doi:10.1038/sj.ijo.0800936

49. Ježek P, Holendová B, Garlid KD, Jabůrek M. Mitochondrial Uncoupling Proteins: Subtle Regulators of Cellular Redox Signaling. *Antioxid Redox Signal*. 2018;29(7):667-714. doi:10.1089/ars.2017.7225

50. Palou A, Picó C, Bonet ML, Oliver P. The uncoupling protein, thermogenin. *Int J Biochem Cell Biol*. Published online 1998. doi:10.1016/S1357-2725(97)00065-4

51. Couplan E, Gonzalez-Barroso M del M, Alves-Guerra MC, Ricquier D, Goubern M, Bouillaud F. No Evidence for a Basal, Retinoic, or Superoxide-induced Uncoupling Activity of the Uncoupling Protein 2 Present in Spleen or Lung Mitochondria. *J Biol Chem*. 2002;277(29):26268-26275. doi:10.1074/jbc.m202535200

52. Waldeck-Weiermair M, Duan X, Naghdi S, et al. Uncoupling protein 3 adjusts mitochondrial Ca2+ uptake to high and low Ca2+ signals. *Cell Calcium*. 2010;48(5):288-301. doi:10.1016/j.ceca.2010.10.004

53. Waldeck-Weiermair M, Malli R, Naghdi S, Trenker M, Kahn MJ, Graier WF. The contribution of UCP2 and UCP3 to mitochondrial Ca2+ uptake is differentially determined by the source of supplied Ca2+. *Cell Calcium*. 2010;47(5):433-440. http://www.sciencedirect.com/science/article/pii/S0143416010000485

54. Madreiter-Sokolowski CT, Győrffy B, Klec C, et al. UCP2 and PRMT1 are key prognostic markers for lung carcinoma patients. *Oncotarget*. 2017;8(46):80278-80285. doi:10.18632/oncotarget.20571

55. Madreiter-Sokolowski CT, Waldeck-Weiermair M, Bourguignon M-P, et al. Enhanced inter-compartmental Ca2+ flux modulates mitochondrial metabolism and apoptotic threshold during aging. *Redox Biol*. 2019;20:458-466. doi:10.1016/j.redox.2018.11.003

56. DeBerardinis RJ, Mancuso A, Daikhin E, et al. Beyond aerobic glycolysis: Transformed cells can engage in glutamine metabolism that exceeds the requirement for protein and nucleotide synthesis. *Proc Natl Acad Sci U S A*. 2007;104(49):19345-19350. doi:10.1073/pnas.0709747104

57. Madreiter-Sokolowski CT, Gottschalk B, Parichatikanond W, et al. Resveratrol Specifically Kills Cancer Cells by a Devastating Increase in the Ca2+ Coupling Between the Greatly Tethered Endoplasmic Reticulum and Mitochondria. *Cell Physiol Biochem*. 2016;39(4):1404-1420. doi:10.1159/000447844

58. Rossi A, Pizzo P, Filadi R. Calcium, mitochondria and cell metabolism: A functional triangle in bioenergetics. *Biochim Biophys Acta - Mol Cell Res*. Published online 2019. doi:10.1016/j.bbamcr.2018.10.016

59. Porporato PE, Filigheddu N, Pedro JMB-S, Kroemer G, Galluzzi L. Mitochondrial metabolism and cancer. *Cell Res*. 2018;28(3):265-280. doi:10.1038/cr.2017.155

60. Madreiter-Sokolowski CT, Gottschalk B, Sokolowski AA, Malli R, Graier WF. Dynamic Control of Mitochondrial Ca2+ Levels as a Survival Strategy of Cancer Cells. *Front Cell Dev Biol*. 2021;9(February):1-14. doi:10.3389/fcell.2021.614668

61. Krebs HA. The citric acid cycle: A reply to the criticisms of F. L. Breusch and of J. Thomas. *Biochem J*. 1940;34(3):460. doi:10.1042/BJ0340460

62. Denton RM, McCormack JG, Edgell NJ. Role of calcium ions in the regulation of intramitochondrial metabolism. Effects of Na+, Mg2+ and ruthenium red on the Ca2+-stimulated oxidation of oxoglutarate and on pyruvate dehydrogenase activity in intact rat heart mitochondria. *Biochem J*. 1980;190(1):107-117. doi:10.1042/bj1900107

63. Denton RM. Regulation of mitochondrial dehydrogenases by calcium ions. *Biochim Biophys Acta - Bioenerg*. 2009;1787(11):1309-1316. doi:10.1016/j.bbabio.2009.01.005

64. Denton RM, Randle PJ, Martin BR. Stimulation by calcium ions of pyruvate dehydrogenase phosphate phosphatase. *Biochem J*. 1972;128(1):161-163. doi:10.1042/bj1280161

65. Denton RM, McCormack JG, Rutter GA, et al. The hormonal regulation of pyruvate dehydrogenase complex. *Adv Enzyme Regul*. 1996;36:183-198. doi:10.1016/0065-2571(95)00020-8

66. Golic I, Aleksic M, Lazarevic A, Bogdanovic M, Jonic S, Korac A. Methods for studying the localization of mitochondrial complexes III and IV by immunofluorescent and immunogold microscopy. *Arch Biol Sci*. 2016;68(4):767-772. doi:10.2298/abs150618061g

67. Cogliati S, Enriquez JA, Scorrano L. Mitochondrial Cristae: Where Beauty Meets Functionality. *Trends Biochem Sci*. 2016;41(3):261-273. doi:10.1016/j.tibs.2016.01.001

68. Palmieri L, Pardo B, Lasorsa FM, et al. Citrin and aralar1 are Ca2+-stimulated aspartate/glutamate transporters in mitochondria. *EMBO J*. 2001;20(18):5060-5069. doi:10.1093/emboj/20.18.5060

69. Borst P. The malate–aspartate shuttle (Borst cycle): How it started and developed into a major metabolic pathway. In: *IUBMB Life*. ; 2020. doi:10.1002/iub.2367

70. Pardo B, Contreras L, Serrano A, et al. Essential Role of Aralar in the Transduction of Small Ca + Signals to Neuronal Mitochondria. *J Biol Chem*. 2005;281(2):1039-1047. doi:10.1074/jbc.m507270200

71. Greenhouse WV V., Lehninger AL. Magnitude of Malate-Aspartate Reduced Nicotinamide Adenine Dinucleotide Shuttle Activity in Intact Respiring Tumor Cells. *Cancer Res*. 1977;37(11).

72. Greenhouse WV V., Lehninger AL. Occurrence of the Malate-Aspartate Shuttle in Various Tumor Types. *Cancer Res*. 1976;36(4).

73. Del Arco A, Agudo M, Satrústegui J. Characterization of a second member of the subfamily of calcium-binding mitochondrial carriers expressed in human non-excitable tissues. *Biochem J*. Published online 2000. doi:10.1042/0264-6021:3450725

74. Del Arco A, Satrústegui J. Molecular cloning of aralar, a new member of the mitochondrial carrier superfamily that binds calcium and is present in human muscle and brain. *J Biol Chem*. Published online 1998. doi:10.1074/jbc.273.36.23327

75. Contreras L, Gomez-Puertas P, Iijima M, Kobayashi K, Saheki T, Satrústegui J. Ca 2+ Activation

Kinetics of the Two Aspartate-Glutamate Mitochondrial Carriers, Aralar and Citrin. *J Biol Chem*. 2007;282(10):7098-7106. doi:10.1074/jbc.m610491200

76. Indiveri C, Palmieri F, Bisaccia F, Krämer R. Kinetics of the reconstituted 2-oxoglutarate carrier from bovine heart mitochondria. *Biochim Biophys Acta*. 1987;890(3):310-318. doi:10.1016/0005-2728(87)90158-7

77. Szibor M, Gizatullina Z, Gainutdinov T, et al. Cytosolic, but not matrix, calcium is essential for adjustment of mitochondrial pyruvate supply. *J Biol Chem*. 2020;295(14):4383-4397. doi:10.1074/jbc.ra119.011902

78. MacDonald MJ, Brown LJ. Calcium Activation of Mitochondrial Glycerol Phosphate Dehydrogenase Restudied. *Arch Biochem Biophys*. 1996;326(1):79-84. doi:10.1006/ABBI.1996.0049

79. Mráček T, Drahota Z, Houštěk J. The function and the role of the mitochondrial glycerol-3-phosphate dehydrogenase in mammalian tissues. *Biochim Biophys Acta - Bioenerg*. Published online 2013. doi:10.1016/j.bbabio.2012.11.014

80. Denton RM. Regulation of mitochondrial dehydrogenases by calcium ions. *Biochim Biophys Acta - Bioenerg*. Published online 2009. doi:10.1016/j.bbabio.2009.01.005

81. Hetz C, Saxena S. ER stress and the unfolded protein response in neurodegeneration. *Nat Rev Neurol*. 2017;13(8):477-491. doi:10.1038/nrneurol.2017.99

82. Madden E, Logue SE, Healy SJ, Manie S, Samali A. The role of the unfolded protein response in cancer progression: From oncogenesis to chemoresistance. *Biol Cell*. 2019;111(1):1-17. doi:10.1111/boc.201800050

83. Almanza A, Carlesso A, Chintha C, et al. Endoplasmic reticulum stress signalling – from basic mechanisms to clinical applications. *FEBS J*. 2019;286(2):241-278. doi:10.1111/febs.14608

84. Schwarz DS, Blower MD. The endoplasmic reticulum: structure, function and response to cellular signaling. *Cell Mol Life Sci*. 2016;73(1):79. doi:10.1007/S00018-015-2052-6

85. Travers KJ, Patil CK, Wodicka L, Lockhart DJ, Weissman JS, Walter P. Functional and genomic analyses reveal an essential coordination between the unfolded protein response and ER-associated degradation. *Cell*. 2000;101(3):249-258. doi:10.1016/S0092-8674(00)80835-1

86. Yong J, Bischof H, Burgstaller S, et al. Mitochondria supply ATP to the ER through a mechanism

antagonized by cytosolic Ca2+. *Elife*. 2019;8. doi:10.7554/eLife.49682

87. Wang WA, Groenendyk J, Michalak M. Calreticulin signaling in health and disease. *Int J Biochem Cell Biol*. 2012;44(6):842-846. doi:10.1016/J.BIOCEL.2012.02.009

88. Ellgaard L, Frickel EM. Calnexin, calreticulin, and ERp57. *Cell Biochem Biophys 2003 393*. 2003;39(3):223-247. doi:10.1385/CBB:39:3:223

89. Bergeron JJM, Brenner MB, Thomas DY, Williams DB. Calnexin: a membrane-bound chaperone of the endoplasmic reticulum. *Trends Biochem Sci*. 1994;19(3):124-128. doi:10.1016/0968-0004(94)90205-4

90. Lee AS. The ER chaperone and signaling regulator GRP78/BiP as a monitor of endoplasmic reticulum stress. *Methods*. 2005;35(4):373-381. doi:10.1016/J.YMETH.2004.10.010

91. Schröder M, Kaufman RJ. The mammalian unfolded protein response. *Annu Rev Biochem*. 2005;74:739-789. doi:10.1146/annurev.biochem.73.011303.074134

92. Bravo R, Vicencio JM, Parra V, et al. Increased ER-mitochondrial coupling promotes mitochondrial respiration and bioenergetics during early phases of ER stress. *J Cell Sci*. 2011;124(13):2143-2152. doi:10.1242/jcs.080762

93. Koshenov Z, Oflaz FE, Hirtl M, et al. Sigma-1 Receptor Promotes Mitochondrial Bioenergetics by Orchestrating ER Ca2+ Leak during Early ER Stress. *Metab 2021, Vol 11, Page 422*. 2021;11(7):422. doi:10.3390/METABO11070422

94. Deniaud A, Sharaf El Dein O, Maillier E, et al. Endoplasmic reticulum stress induces calcium-dependent permeability transition, mitochondrial outer membrane permeabilization and apoptosis. *Oncogene*. 2008;27(3):285-299. doi:10.1038/sj.onc.1210638

95. Hayashi T, Su TP. Sigma-1 Receptor Chaperones at the ER- Mitochondrion Interface Regulate Ca2+ Signaling and Cell Survival. *Cell*. 2007;131(3):596-610. doi:10.1016/j.cell.2007.08.036

96. Kekuda R, Prasad PD, Fei Y-J, Leibach FH, Ganapathy V. Cloning and Functional Expression of the Human Type 1 Sigma Receptor (hSigmaR1). *Biochem Biophys Res Commun*. 1996;229(2):553-558. doi:10.1006/bbrc.1996.1842

97. Hayashi T. The Sigma-1 Receptor in Cellular Stress Signaling. *Front Neurosci*. 2019;13(JUL):733. doi:10.3389/fnins.2019.00733

98. Hayashi T, Su T-P. Sigma-1 Receptor Chaperones at the ER- Mitochondrion Interface Regulate Ca2+ Signaling and Cell Survival. *Cell*. 2007;131(3):596-610. doi:10.1016/j.cell.2007.08.036

99. Mori T, Hayashi T, Hayashi E, Su T-P. Sigma-1 Receptor Chaperone at the ER-Mitochondrion Interface Mediates the Mitochondrion-ER-Nucleus Signaling for Cellular Survival. *PLoS One*. 2013;8(10):e76941. doi:10.1371/journal.pone.0076941

100. Srivats S, Balasuriya D, Pasche M, et al. Sigma1 receptors inhibit store-operated Ca2+ entry by attenuating coupling of STIM1 to Orai1. *J Cell Biol*. 2016;213(1):65-79. doi:10.1083/jcb.201506022

101. Weng T-Y, Tsai S-YA, Su T-P. Roles of sigma-1 receptors on mitochondrial functions relevant to neurodegenerative diseases. *J Biomed Sci*. 2017;24(1):74. doi:10.1186/s12929-017-0380-6

102. Crottés D, Guizouarn H, Martin P, Borgese F, Soriani O. The sigma-1 receptor: A regulator of cancer cell electrical plasticity? *Front Physiol*. 2013;4 JUL:175. doi:10.3389/fphys.2013.00175

103. Mazure M, Yan L-J, Oflaz FE, et al. Sigma-1 Receptor Modulation by Ligands Coordinates Cancer Cell Energy Metabolism. *Biomol 2022, Vol 12, Page 762*. 2022;12(6):762. doi:10.3390/BIOM12060762

104. Imamura H, Huynh Nhat KP, Togawa H, et al. Visualization of ATP levels inside single living cells with fluorescence resonance energy transfer-based genetically encoded indicators. *Proc Natl Acad Sci U S A*. Published online 2009. doi:10.1073/pnas.0904764106

105. San Martín A, Ceballo S, Baeza-Lehnert F, et al. Imaging mitochondrial flux in single cells with a FRET sensor for pyruvate. *PLoS One*. Published online 2014. doi:10.1371/journal.pone.0085780

106. Arce-Molina R, Cortés-Molina F, Sandoval PY, et al. A highly responsive pyruvate sensor reveals pathway-regulatory role of the mitochondrial pyruvate carrier MPC. *Elife*. Published online 2020. doi:10.7554/eLife.53917

107. Hung YP, Albeck JG, Tantama M, Yellen G. Imaging cytosolic NADH-NAD + redox state with a genetically encoded fluorescent biosensor. *Cell Metab*. Published online 2011. doi:10.1016/j.cmet.2011.08.012

108. Palmer AE, Giacomello M, Kortemme T, et al. Ca2+ Indicators Based on Computationally Redesigned Calmodulin-Peptide Pairs. *Chem Biol*. Published online 2006.

doi:10.1016/j.chembiol.2006.03.007

109. Palmer AE, Jin C, Reed JC, Tsien RY. Bcl-2-mediated alterations in endoplasmic reticulum Ca2+ analyzed with an improved genetically encoded fluorescent sensor. *Proc Natl Acad Sci U S A*. Published online 2004. doi:10.1073/pnas.0408030101

110. Zhao Y, Araki S, Wu J, et al. An expanded palette of genetically encoded Ca2+ indicators. *Science (80-)*. 2011;333(6051):1888-1891. doi:10.1126/science.1208592

111. Waldeck-Weiermair M, Gottschalk B, Madreiter-Sokolowski CT, et al. Development and Application of Sub-Mitochondrial Targeted Ca2 + Biosensors. *Front Cell Neurosci*. 2019;13:449. doi:10.3389/fncel.2019.00449

112. San Martín A, Ceballo S, Ruminot I, Lerchundi R, Frommer WB, Barros LF. A Genetically Encoded FRET Lactate Sensor and Its Use To Detect the Warburg Effect in Single Cancer Cells. *PLoS One*. Published online 2013. doi:10.1371/journal.pone.0057712

113. Pak V V, Ezerin¸a D, Ezerin¸a E, et al. Ultrasensitive Genetically Encoded Indicator for Hydrogen Peroxide Identifies Roles for the Oxidant in Cell Migration and Mitochondrial Function. Published online 2020. doi:10.1016/j.cmet.2020.02.003

114. Zhao Y, Shen Y, Wen Y, Campbell RE. High-Performance Intensiometric Direct- And Inverse-Response Genetically Encoded Biosensors for Citrate. *ACS Cent Sci*. Published online 2020. doi:10.1021/acscentsci.0c00518

115. Berardi MJ, Chou JJ. Fatty acid flippase activity of UCP2 is essential for its proton transport in mitochondria. *Cell Metab*. Published online 2014. doi:10.1016/j.cmet.2014.07.004

116. Saheki T, Moriyama M, Funahashi A, Kuroda E. AGC2 (Citrin) Deficiency—From Recognition of the Disease till Construction of Therapeutic Procedures. *Biomol 2020, Vol 10, Page 1100*. 2020;10(8):1100. doi:10.3390/BIOM10081100

117. Hayasaka K. Metabolic basis and treatment of citrin deficiency. *J Inherit Metab Dis*. 2021;44(1):110-117. doi:10.1002/JIMD.12294

118. Luengo A, Li Z, Gui DY, et al. Increased demand for NAD+ relative to ATP drives aerobic glycolysis. *Mol Cell*. 2021;81(4):691-707.e6. doi:10.1016/j.molcel.2020.12.012

119. Goodman RP, Markhard AL, Shah H, et al. Hepatic NADH reductive stress underlies common variation in metabolic traits. *Nature*. Published online 2020:1-5. doi:10.1038/s41586-020-

2337-2

120. Patgiri A, Skinner OS, Miyazaki Y, et al. An engineered enzyme that targets circulating lactate to alleviate intracellular NADH:NAD+ imbalance. *Nat Biotechnol*. 2020;38(3):309-313. doi:10.1038/s41587-019-0377-7

121. Pérez-Liébana I, Juaristi I, González-Sánchez P, et al. "A feed-forward Ca 2+-dependent mechanism boosting glycolysis and OXPHOS by activating Aralar-malate-aspartate shuttle, upon neuronal stimulation." doi:10.1101/2021.02.02.429391

122. Mármol P, Pardo B, Wiederkehr A, Arco A del, Wollheim CB, Satrústegui J. Requirement for Aralar and Its Ca 2+ -binding Sites in Ca 2+ Signal Transduction in Mitochondria from INS-1 Clonal β-Cells. *J Biol Chem*. 2008;284(1):515-524. doi:10.1074/jbc.m806729200

123. Gellerich FN, Gizatullina Z, Gainutdinov T, et al. The control of brain mitochondrial energization by cytosolic calcium: the mitochondrial gas pedal. *IUBMB Life*. 2013;65(3):180-190. doi:10.1002/IUB.1131

124. Gellerich FN, Gizatullina Z, Trumbekaite S, et al. Cytosolic Ca2+ regulates the energization of isolated brain mitochondria by formation of pyruvate through the malate-aspartate shuttle. *Biochem J*. 2012;443(3):747-755. doi:10.1042/BJ20110765

125. Rubi B, Arco A del, Bartley C, Satrustegui J, Maechler P. The Malate-Aspartate NADH Shuttle Member Aralar1 Determines Glucose Metabolic Fate, Mitochondrial Activity, and Insulin Secretion in Beta Cells. *J Biol Chem*. 2004;279(53):55659-55666. doi:10.1074/jbc.m409303200

126. Sekine N, Cirulli V, Regazzi R, et al. Low lactate dehydrogenase and high mitochondrial glycerol phosphate dehydrogenase in pancreatic beta-cells. Potential role in nutrient sensing. *J Biol Chem*. 1994;269(7):4895-4902. doi:10.1016/S0021-9258(17)37629-9

127. Malmgreh S, Nicholls DG, Taneera J, et al. Tight Coupling between Glucose and Mitochondrial Metabolism in Clonal β-Cells Is Required for Robust Insulin Secretion. *J Biol Chem*. 2009;284(47):32395-32404. doi:10.1074/JBC.M109.026708

128. Klec C, Madreiter-Sokolowski CT, Ziomek G, et al. Presenilin-1 Established ER-Ca(2+) Leak: a Follow Up on Its Importance for the Initial Insulin Secretion in Pancreatic Islets and beta-Cells upon Elevated Glucose. *Cell Physiol Biochem*. 2019;53:573-586. https://www.ncbi.nlm.nih.gov/pubmed/31529929

129. Waldeck-Weiermair M, Malli R, Parichatikanond W, et al. Rearrangement of MICU1 multimers for activation of MCU is solely controlled by cytosolic Ca(2.). *Sci Rep*. 2015;5(1):15602. doi:10.1038/srep15602

130. Basso V, Marchesan E, Ziviani E. A trio has turned into a quartet: DJ-1 interacts with the IP3R-Grp75-VDAC complex to control ER-mitochondria interaction. *Cell Calcium*. 2020;87:102186. doi:10.1016/j.ceca.2020.102186

131. Honrath B, Metz I, Bendridi N, Rieusset J, Culmsee C, Dolga AM. Glucose-regulated protein 75 determines ER–mitochondrial coupling and sensitivity to oxidative stress in neuronal cells. *Cell Death Discov*. 2017;3(1):17076. doi:10.1038/cddiscovery.2017.76